ABSTRACT

Title of Dissertation:	THE APPLICATION OF MICRODEVICES FOR INVESTIGATING BIOLOGICAL SYSTEMS
	Wu Shang, Doctor of Philosophy, 2018
Dissertation directed by:	Professor William E. Bentley, Fischell Department of Bioengineering

The gastrointestinal (GI) tract is a complex ecosystem with cells from different kingdoms organized within dynamically-changing structures and engaged in complex communication through a network of molecular signaling pathways. One challenge for researchers is that the GI tract is largely inaccessible to experimental investigation. Even animal models have limited capabilities for revealing the rich spatiotemporal variation in the intestine and fail to predict human responses due to genetic variation. Exciting recent advances in *in vitro* organ model (i.e., organ-on-chips (OOC)) based on microfluidics are offering new hope that these experimental systems may be capable of recapitulating the complexities in structure and context inherent to the intestine. A current limitation to OOC systems is that while they can recapitulate structure and context, they do not yet offer capabilities to observe or engage in the molecular based signaling integral to the functioning of this complex biological system.

This dissertation focuses on developing microfluidic tools that provide access to interrogating signaling events amongst populations in the GI tract (e.g., microbes and

enterocytes). First, a membrane-based gradient generator is built to establish linear and stable chemical gradients for investigating gradient-mediated behaviors of bacteria. Specifically, this platform enables the study of bacterial chemotaxis and potentially facilitates the development of genetically rewired lesion-targeted probiotics. Second, “electrobiofabrication” is coupled with microelectronics, for the first time, to create molecular-to-electronic (i.e., “molectronic”) sensors to observe and report the dynamic exchange of biochemical information in OOC systems. Last, to address the issue of poor compatibility between OOCs and sensors, we assemble OOCs with molectronic sensors in a modular format. The concept of modularity greatly reduces the system complexity and enables sensors to be built immediately before applications, avoiding functional decay of active biorecognition components after long-term device storage and use. We envision this work will “open” OOC systems for molecular measurement and interrogation, which, in turn, will expand the *in vitro* toolbox that researchers can use to design, build and test for the investigation of GI disease and drug discovery.

THE APPLICATION OF MICRODEVICES FOR INVESTIGATING BIOLOGICAL SYSTEMS

by

Wu Shang

Dissertation submitted to the Faculty of the Graduate School of the
University of Maryland, College Park, in partial fulfillment
of the requirements for the degree of
Doctor of Philosophy
2018

Advisory Committee:
Professor William E. Bentley, Chair
Professor Gregory F. Payne
Assistant Professor Kimberly Stroka
Assistant Professor Ryan D. Sochol
Professor Nam Sun Wang, Dean's Representative

Dedication

I dedicate this work to my parents, Dr. Shiqiang Shang and Dr. Zhihong Ye, whose unconditional love, unselfish support and example over 28 years have laid the foundations for the curiosity, discipline and diligence necessary to complete this work.

Acknowledgements

I would like to acknowledge my doctoral committee for their membership and support through my 4-year path in academia at the University of Maryland. Specifically, I wish to express my sincere appreciation to my Principal Supervisor, Dr. William Bentley, for his wise mentorship that make my doctoral achievement possible and shape me into an independent scholar with critical thinking. I would also like to thank my colleagues in the Bentley lab for their generous support and assistance in both research and daily life. I thank my collaborators for their contribution to help me succeed and make all academic publications possible. I would also like to appreciate my family for their unconditional love and support, and for fostering a correct outlook on life, values and world views of me. I thank my friends, especially my girlfriend, for their trust and encouragement during my depressed and anxious moments. Finally, I thank my motherland, China, for providing a peaceful and prosper environment during my growth so that I could have the opportunity to explore the world and pursue my dream.

Table of Contents

List of Figures

Chapter 1: Introduction

This chapter outlines the scope of this dissertation and the underlying motivation. Chapters 2, 3, and 4 describe three aims, which together build up the overarching goal of this work. Each of these chapters is representative of a manuscript published, submitted or prepared during the doctorate, and possesses their own abstracts and introductions, with accompanying results and conclusions. An overall summary, relevant contributions, and both performed and potential future work are detailed in Chapter 5. It should be noted that although this dissertation mainly focuses on investigating the gastrointestinal (GI) disorders, the methodologies developed in this work can be expanded to broader areas.

Background

Gastrointestinal (GI) ecological imbalance and associated disorders. The adult human body is colonized by microorganisms that are estimated to outnumber somatic cells by an order of magnitude.[1] The majority of these microbes reside in the GI tract in the form of microbiota (microbial community), where they form a stable alliance amongst the epithelial barrier, and the immune mediators (**Scheme 1.1**).[2,3] The three components of GI ecosystems have co-evolved to established a unique host-microbiota relationship termed a symbiosis.[4] This symbiosis relationship is essential for the maintenance of intestinal homeostasis and modulates vital functions of the healthy host[5], ranging from metabolism (e.g., food digestion and immunomodulation) to brain function[6,7] while at the same time provides a means to prevent pathogen outgrowth of commensal strains[8,9]. On the other hand, perturbation of microbial-host

symbiosis is implicated in many GI disorders. For example, inflammatory bowel disease (IBD), a chronic and relapsing inflammatory disorder, is characterized by gut dysbiosis including the reductions of beneficial bacteria (e.g., *Bifidobacteria*[10–12]) and increased number of species (e.g., *Pseudomonas*[13,14]) normally not found (or in low amount) in healthy controls.[15] Increased numbers of pathogenic gut microbial species may disrupt the epithelial barrier, resulting in aberrant immune responses against gut microbes. [16]

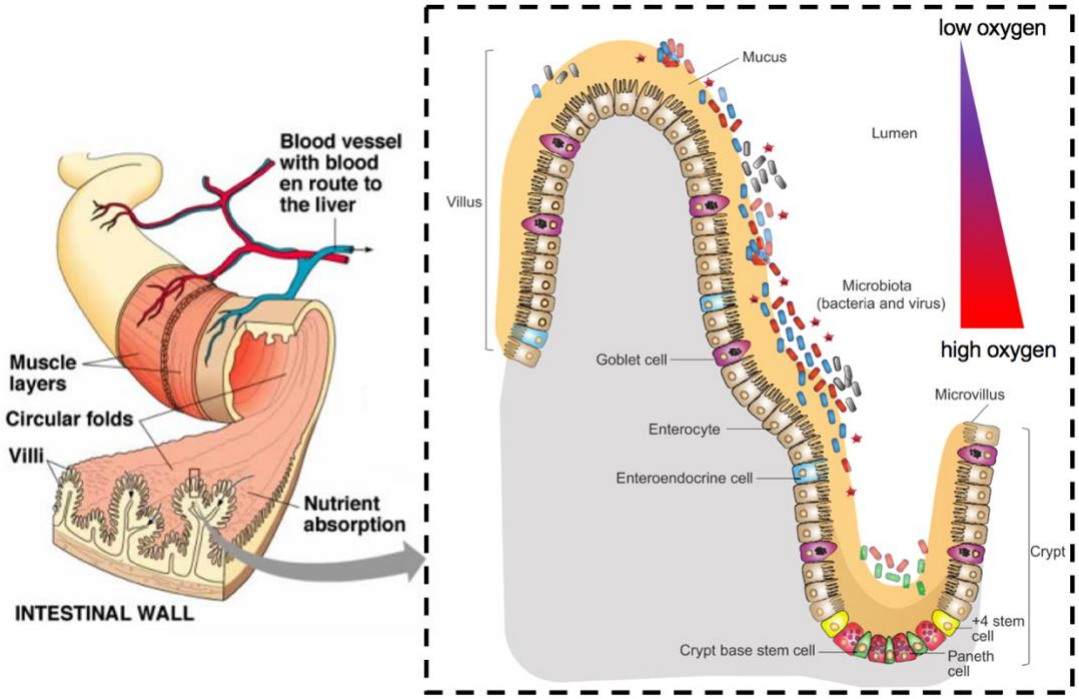

Scheme 1. 1. Schematic of GI tract. The villi (right) consist of a monolayer of absorptive enterocytes that have migrated to the tip during maturation. The resident commensal microbiota is found within and on top of the mucus layer. Paneth cells and Enteroendocrine cells are found in crypts to secrete antimicrobial peptides and small bioactive peptides in response to signals from commensal bacteria, respectively. The redox environment shifts from fully oxygenated in the vasculature and lymphatic system to anaerobic in the intestinal lumen. Figure adapted from Wong et al (2016).[17]

Probiotics as therapeutic agents in GI disorders. Because of the evidence implicating the importance of microbial-host interplay in the gut and its relevance in GI disorders, various attempts have been made to modify the gut flora using probiotics.[18–23]

Different from conventional medications, such as immunomodulator drugs (e.g., azathioprine[24]) and biologics (e.g., anti-TNFα antibodies[25,26]), probiotics are defined as living microorganisms that upon ingestion, can exert health benefits beyond those inherent in basic nutrition.[27] Although the exact molecular mechanisms remain still elusive, studies have shown beneficial effects of ingesting various probiotic strains. Among these are the ability to fight infections.[28] By virtue of developments in synthetic biology, commensal bacteria (e.g., *Escherichia coli*) have also been genetically rewired to target lesion sites and serve as vectors for drug delivery.[19,20,29,30] Because of their origin in the GI tract, these engineered probiotics withstand the harsh conditions of the GI tract, including the effect of gastric acid and bile secretion. Such engineered strains retain their ability to survive competition with other enteric microorganisms.[31,32] We note, however, that the design of such probiotics requires platforms that are sophisticated, enabling recapitulation of GI biology using *in vitro* systems.

In vitro GI models and their applications in preclinical studies. Preclinical studies are used to estimate the efficacy and toxicity of a drug (e.g., probiotics) before it moves into clinical trials. Conventional preclinical studies rely heavily on the use of animal models, which are expensive, highly variable, and difficult to manipulate. Besides these disadvantages, most animal models fail to predict human responses due to their inability to accurately mimic the critical features of human physiology.[33] Over the past decade, microfluidics technologies have emerged that establish many benefits to *in vitro* analysis, they are gaining wider acceptance as the next-generation *tools* for drug testing. That is, microfluidics-based biomimetic *in vitro* models that simulate

human organ microenvironments have made progress in providing critical insight into the cellular and molecular basis for pathophysiology. Further, researchers have incorporated many organs into microsystems that help to reduce the high costs and complexity of *in vivo* studies. These systems, also named as organ-on-chips (OOCs), yield significant advantages in re-creating *in vivo* microenvironments: i) they provide comparable dimensions for *in vivo* organ representation; ii) they enable defined chemical and physical culture conditions that are controlled with the appropriate spatial resolution for cell and tissue culture; and iii) the resulting tissue systems recapitulate many aspects of the native *in vivo* tissue.[34] That is, several notable proof-of-concept studies have demonstrated that recapitulating the key environmental factors contribute to restoring essential functions of human organs. For example, *in vitro* GI models (i.e., gut-on-a-chip) have successfully recreated many aspects of the intestine, the frontline of most orally administrated drugs[35], including the incorporation of oxygen gradients, peristalsis, invading pathogens, and various epithelial or lymphatic cells[36–45]. Layered configurations of epithelial cells were also shown to promote native-like redox gradients that enable enterocyte polarization and differentiation along the villus.[46–51]

Bio-based redox capacitor for information acquisition from biology.

Oxidation/reduction (Redox) reactions can bridge bio-device communication because they shares features of the molecular modalities of biology and the electronic modality of devices.[52] Biologically, redox is a globally-acting signaling modality independent from molecularly-specific receptor based modalities (e.g., kinase signaling) and from the molecularly-nonspecific electrical modality associated with

ion gradients across membranes. Biological redox signals are simple diffusible molecules (e.g., H_2O_2) that are recognized through atomically-specific mechanisms (e.g., sulfur switches) and engage multiple cell signaling pathways with pleiotropic responses. From a technological perspective, redox-based signals are accessible to electrochemical instruments that are simple and portable, and provide inputs/outputs in a convenient format for signal processing and wireless transmission.[53–57]

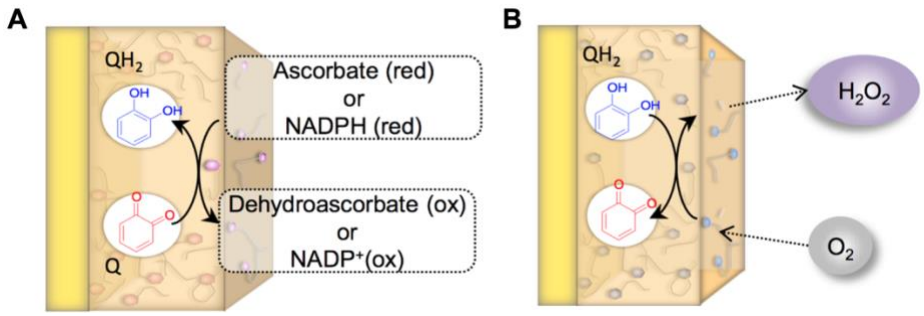

Scheme 1. 2. Schematic of catechol-modified chitosan film. Catechol-modified chitosan film (i.e., bio-based redox capacitor, BBRC) can exchange electrons with common biological (A) reductants and (B) oxidants. Q: quinone; QH_2: catechol

Both Chapter 3 and 4 of this dissertation utilize bio-based redox capacitor (BBRC) developed by Payne's group and ours to facilitate redox-based signal processing within microfluidic devices (**Scheme. 1.2**).[54,58,59] BBRC is a catechol-modified chitosan wherein catechols are readily oxidized to o-quinones which are reactive electrophiles. We electrochemically generate quinones which react with the nucleophilic amines of chitosan. Electrodeposited BBRC films are non-conducting as they cannot exchange electrons directly with the underlying electrode.[60] They are hydrogels, however, that allow the diffusion of ions and small molecules (i.e., the films are ionically conducting) and are also redox-active. The films can be switched between oxidized (Q; o-quinone moieties) and reduced (QH_2; catechol moieties)

states by exchanging electrons with diffusible mediators that interact with an electrode. In essence, the film is a redox-capacitor because it can accept electrons (by reductive redox-cycling), store electrons (as a reduced QH_2 state) and donate electrons (by oxidative redox-cycling).[54,56] Importantly, the BBRC films can exchange electrons with biologically-relevant oxidants and reductants[53]. **Scheme. 1.2** illustrates that we initially tested two common biological reductants: ascorbate which can be found extracellularly (e.g., in lumen)[56], and NADPH which is a common intracellular reducing agent. In both cases, these reductants were observed to donate their electrons to charge the BBRC film[53]. Molecular oxygen is the common biological oxidant, and initial studies demonstrated that the BBRC film can donate electrons to partially reduce O_2 to generate reactive oxygen species (ROS).[53]

Motivation

Besides the role for digestion, the GI tract is also the frontline to most orally administrated drugs, and its complexity and importance in human health and disease has been well-accepted. While the intestine's villi structure provides a large surface area for nutrient/drug absorption, it is also composed of a dynamically-changing spatially organized array of cells that are embedded within a complex biological context.[61,62] One challenge for researchers is that the intestine is largely inaccessible to experimental investigation. Even animal studies have limited capabilities for revealing the rich spatiotemporal variation in the intestine.[36] Exciting recent advances in microfluidics are offering new hope that these *in vitro* experimental platforms may be capable of recapitulating the complexities in structure and context inherent to the

intestine.[34,36–38,44,63–68] However, current microfluidic devices are often complicated in device design and fabrication which in turn, hampers the translation of these technologies from lab to industry.[69–73] Moreover, while existing on-chip biomimetic *in vitro* systems can recapitulate structure and context, it is still difficult to access the molecular communication networks, the human intestinal microbiota composition and the signaling activities that are critical factors during the drug development.[8,9,42,43,74,75]

Research goals

The overarching goal of this work is to develop user-friendly microfluidic devices to expand the *in vitro* "toolbox" that researchers can use to design, build and test for the investigation of GI disease and drug discovery. The study builds upon our expertise in microfabrication, thin-film electrobiofabrication and electrochemistry. Because of the comparable contributions of microbes and intestinal epithelia in gut health, devices will be developed for studying both species. In this dissertation, I have subdivided my work into three major thrusts:

1) Development of a gradient generator to study bacterial chemotactic behavior. This is potentially useful for discovering probiotics (Chapter 2);

2) Development of a "molectronic" sensor to access biochemical information from gut pathogens and enterocytes (Chapter 3); and

3) Development of a modular assembled system to facilitate information access from organ-on-chips with quality control (Chapter 4).

Chapter 2: The state-of-the-art study in bridging microdevice to biological systems

This chapter delineates the state-of-the-art research on connecting microdevices to biological systems. Extended from current studies, Chapter 3, 4 and 5 will deliver innovative works developed in this dissertation. The future directions described in Chapter 6 are also built upon work described here.

Background

Biology and electronics are both expert at processing information and many people dream of coupling the molecular-specificity of biology with the speed, computational power and convenience of electronics. Such capabilities could extend molecular sensing from individual sensors to distributed networks (i.e., internet of things [76]) and portable systems (i.e., wearable electronics [77]). Extensions to enable molecular actuation could have an even greater impact. For instance, integration of molecular sensing and actuation capabilities into capsular endoscopes could allow the detection of pathological signatures to be coupled to the generation of molecular cues (i.e., quorum sensing molecules [78,79]). Such technologies could be used to guide the resident microbiome away from pathological trajectories [80]. However, there are many challenges to integrating the molecular capabilities of biology into electronics and we propose three key innovations toward this dream.

Synthetic biology (synbio). Beyond its more typical translational goal of providing alternative pathways for synthesis, synbio allows living components to be designed to process molecularly-based information. In particular, synbio provides access to

biology's capabilities for: (i) molecularly-specific recognition to receive molecular information; (ii), intracellular signal transduction to process information; and (iii) biosynthetic capabilities to generate molecular transmissions. Here we will use synbio constructs for communication in two directions: to receive device-imposed inputs and transmit molecular outputs [81]; and to receive molecular inputs and transmit device compatible outputs [82,83]. Over the long term, we imagine that a population of living synbio information processors could be "networked" into complex systems with even greater "computational" capabilities (e.g., learning).

Oxidation/reduction (Redox) reactions. Redox can bridge bio-device communication because it shares features of the molecular modalities of biology and the electronic modality of devices.[52] Biologically, redox is a globally-acting signaling modality independent from molecularly-specific receptor based modalities (e.g., kinase signaling) and from the molecularly-nonspecific electrical modality associated with ion gradients across membranes. Biological redox signals are simple diffusible molecules (e.g., H_2O_2) that are recognized through atomically-specific mechanisms (e.g., sulfur switches) and engage multiple cell signaling pathways with pleiotropic responses. From a technological perspective, redox-based signals are accessible to electrochemical instruments that are simple and portable, and provide inputs/outputs in a convenient format for signal processing and wireless transmission.[53,54,57,58,60] Our synbio constructs , that are deployed in Chapter 3, will ultimately communicate with the electronics through this redox modality.[81,82,84] Thus, our approach for

"connecting" biological components into electronic circuitry should be generic with impacts extending well beyond OOC systems.

Biofabrication. Biofabrication, and especially the electrodeposition of stimuli-responsive self-assembling biopolymers (e.g., chitosan and alginate), will be used to build our bio-device interface.[53,85–88] The programmability of electrodeposition mechanisms enables electrode addresses to be independently functionalized in closed OOC systems (i.e., electrodeposition does not require line-of-sight or direct access like photolithographic or printing methods). The biocompatible nature of the hydrogels employed preserves the activities of labile biological components (i.e., maintains cell viability).[89,90] The organic nature of these hydrogel films allows them to be removed after use allowing the OOC modules to be re-used. Finally, the versatility of these thin-film biofabrication technologies is enabling the generation of increasingly complex multilayer assemblies that can perform increasingly complex cellular and signaling functions.

Chapter 3: Development of a gradient generator to study bacterial chemotactic behavior

The majority of this section is adapted with permission from the following publications: i) Shang, W., et al. (2017) A simple and reusable bilayer membrane-based microfluidic device for the study of gradient-mediated bacterial behaviors. *Biomicrofluidics* **11**, 044114, ii) McKay, R., et al. (2017) Controlling Localization of *E. coli* Populations Using a Two-Part Synthetic Motility Circuit: An Accelerator and Brake. *Biotechnol. Bioeng.* 1–13, and iii) Virgil, C., et al (2018) Engineering bacterial motility towards hydrogen-peroxide. *PloS One* 13(5): e0196999. This Chapter describes the development, characterization and application of a membrane-based microfluidic gradient generator for studying the gradient-sensing behavior of planktonic cells. This user-friendly device is capable of establishing linear and stable chemical gradient. Here, this platform is used to investigate the chemotactic response of wildtype *E. coli* towards glucose, and the pseudotactic response (an ability that allows engineered cells to accumulate towards an inducer of choice) of genetically rewired *E. coli* towards pyocyanin. Overall, microfluidic tool for the research of bacterial gradient-sensing behavior is constructed here to facilitate the advance of lesion-targeted probiotic therapy.

Abstract

We have developed a user-friendly microfluidic device for the study of gradient-mediated bacterial behaviors, including chemotaxis. This device rapidly establishes

linear concentration gradients by exploiting solute diffusion through porous membranes in the absence of convective flows. As such, the gradients are created rapidly and can be sustained for long time periods (e.g., hours), sufficient to evaluate cell phenotype. The device exploits a unique simple bilayer configuration that enables rapid setup and quick reproducible introduction of cells. Its reusability represents an additional advantage in that it need not be limited to settings with microfluidics expertise. We have successfully demonstrated the applicability of this tool in studying the chemotactic response of Escherichia coli to glucose. When coupled with our recent Python program, quantified metrics such as speed, ratio of tumble to run, and effective diffusivity can be obtained from slow frame rate videos. Moreover, we introduce a chemotaxis partition coefficient that conveniently scores swimming behavior on the single-cell level.

Introduction

Concentration gradients of biomolecules are found throughout the human body and play pivotal roles in regulating biological activities, including wound healing, immune responses, and cancer metastasis.[91–95] Microorganisms inside the human body can produce, sense, and react to these chemical gradients in multiple ways, some involved in pathogenicity. For instance, biofilm growth of pathogenic bacteria often results in infections. Bacteria within a biofilm exhibit distinct gene expression profiles and metabolic activities in response to concentration gradients of nutrients, signaling compounds, and bacterial wastes within the biofilm.[96] This heterogeneity protects cells inside the biofilm from environmental stresses and attacks from the

immune system or antimicrobials, thus decreasing therapeutic efficacy.[97] While often considered from the perspective of pathogenicity, some gradient-sensing behaviors could be also harnessed for therapeutic purposes. Bacteria can move up or down a chemical gradient in response to a natural attractant or repellent, which is referred to as chemotaxis.[98] Leveraging this character, genetically rewired *Escherichia coli* (*E. coli*) were attracted to cancer cell lines[29,30] and could serve as vectors for drug delivery. Therefore, developing a robust platform for investigation of gradient-mediated bacterial behaviors would be essential.

Over the last several decades, numerous platforms have been devised, such as the Boyden chamber,[99] the Dunn slide chamber,[100] and the Zigmond chamber,[101] which generate chemical gradients mimicking physiological conditions. However, the reproducibility, controllability, and stability of these approaches are limited.[92,102,103] To address these issues, researchers have turned to advanced microfluidic systems based on high resolution lithography and soft lithography. Because fabrication methods are programmable, precise, and facile, these approaches have enabled more detailed study of biological phenomena (e.g., morphogen-mediated development,[103,104] tumor cell migration,[105,106] drug delivery and distribution[67]). Gradient generators built within microfluidic platforms offer greater resolution and provide well-controlled hydrodynamic and mass transfer conditions.[107] Additionally, microfluidics facilitate the integration and manipulation of multiple design spaces, predominately time, chemical species, and chemical concentrations into a single platform.[71]

Due to the length scales and well-defined stream functions, the majority of microfluidic gradient generators apply laminar flows to establish gradients.[108–113] As such, parallel flows of incompressible and miscible fluids mix only by diffusion. By appropriately designing the spatial configurations and the solute concentrations in multiple adjacent streams, gradients can be established across a channel.[114] This methodology is particularly suitable for surface-adherent cells as they can be exposed to a steady state gradient with small shear forces. However, these flow-based platforms are unsuitable for many bacterial studies due to two major limitations: (i) bacteria are often non-adherent (planktonic) and thus would experience unsteady concentration gradients as they are transported along the channel by the flow[114] and (ii) cells in the device would experience both chemical gradients and shear forces, and because of this, it is challenging to discern the independent effects of each on cell movement.[115,116] As a result, flow-free gradient generators have been proposed.[98,114,116–123]

A common strategy to form chemical gradients within a flow-free device relies on chemical exchange between source and sink reservoirs through flow resistive elements, such as hydrogels[116–118,124] or membranes.[98,119–123] Submicron-sized pores in these elements generate large hydrodynamic resistances that minimize convective flows and shear forces, leaving diffusive transport unperturbed. Subsequently, concentration gradients can be established without disturbance from flows. Compared to hydrogel-based gradient generators that require in situ fabrication, membrane-based devices are rapidly assembled from uniform components and are easily sealed and integrated with ancillary flow and analytical systems.[123,124] We have found that

many membrane-based gradient generators facilitate the study of mammalian cells and tissues, with their designs taking advantage of the larger length scales of cell, organoid, and/or tissue morphologies and relatively long time constants. These systems are not ideal, however, for studying motile bacteria and are generally non-reusable.[119–123]

Previously, Wang et al. developed a bilayer microfluidic gradient generator for bacterial study, which established linear gradients of chemicals by balancing the pressure between source and sink inlets.[118] Introduction of bacteria or solutions into their device was based on diffusion, which increased experimental time (>1 h) and washing difficulty. Here, we describe a next generation bilayer membrane-based microfluidic gradient generator (**Scheme 2.1**) behavior that can be easily operated in laboratories not specialized in microfluidics. It has the following features: (1) the concentration gradient is formed by diffusion and is steady, sharp, and homogenous for accurate experimental performance; (2) the experimental setup and washing procedures are facile; (3) the device can be coupled to analytical software (e.g., similar to Mohari et al. for non-gradient systems[125]); and (4) it is reusable. Herein, we describe its design and assembly as well as its performance by illustrating the gradient generation and the tracking of *E. coli* chemotactic responses.

Materials and Methods

Device fabrication. The device consists a top layer and a bottom layer (**Scheme 2.1**). The top layer (**Scheme 2.1A**) contains two parallel channels that deliver either an attractant/repellent (i.e., the source channel) or a buffer solution (i.e., the sink

channel). These two channels have a convergence (i.e., the pressure balance) that is structurally similar to a previous work by Irimia et al.[126] This convergence dissipates pressure differences between the channels and stabilizes the concentration gradient formed downstream. The length of the convergence and the flow rates of both sink and source channels are optimized in order to avoid chemical diffusion from the source channel to the sink channel when the flow is fully developed. The bottom layer contains a single channel. All channels are 50 μm tall and 500 μm wide. From a top-down view (**Scheme 2.1B**), the three channels in both layers form two intersections. At each intersection, a polycarbonate membrane is sandwiched between the top and the bottom layers and is large enough to separate channels on both sides (see side views, **Schemes 2.1C&1D**). The membrane is porous with each pore being 1μm in diameter and generates high hydrodynamic resistance ($R_h=\delta\mu L/\pi r^4$, r = pore radius). Convective flows transmitting through the membrane are thus negligible, and

diffusive transport becomes the dominating communication between solutions in the top and the bottom channels.

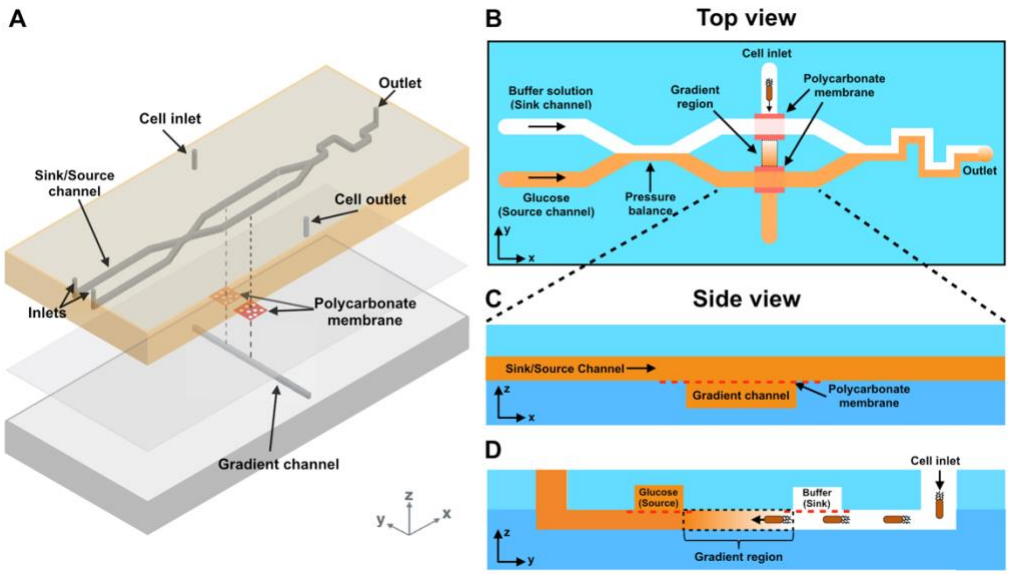

Scheme 2. 1. Schematic of gradient generator. (A) A 3D rendering of a membrane-based bilayer gradient generator. (B)–(D) Schematic top and side representations of the device. Solution of a fixed concentration flows in the source channel while blank buffer flows in the sink channel. The axis that is parallel to the source and sink channels is denoted as the x axis. The convergence of these flows balances the pressure between the two channels. The top and bottom channels are separated by polycarbonate membranes. Small biomolecules and other chemicals diffuse downward through the membrane, forming an orthogonal linear gradient within the bottom channel. The cells are introduced into the cell inlet in the bottom channel. All channels are 50 μm in height and 500 μm in width.

All layers were made from polydimethylsiloxane (PDMS) (Sylgard 184, Dow Corning Co., Midland, MI) cast on an SU-8 master. The SU-8 master was fabricated using standard soft lithography techniques performed in the Maryland Micro and Nano Fabrication Center. Patterns on both layers were designed on AutoCAD (Autodesk, Inc., Mill Valley, CA), converted, exposed, and developed onto a Mylar mask. A 4-in. silicon wafer was cleaned with Piranha solution (concentrated H_2SO_4 and 30% H_2O_2, 3:1, v/v) and spin coated with 5ml SU-8 3050 photoresists (MicroChem, Westborough, MA) at 3000 rpm for 30 s followed by 15 min baking at 95 C. The pattern was then transferred from the mask to the wafer by exposing the wafer to UV light (405nm wavelength) at 23.4 mW cm^2 using an EVG 620 mask

aligner (Electronic Visions Inc., Phoenix, AZ). The wafer was subsequently developed for 8 min in an SU-8 developer (MicroChem, Westborough, MA). The residual photoresist was removed by rinsing with isopropanol and deionized (DI) water followed by air-drying. The resulting SU-8 master can be reused almost indefinitely.

The device fabrication involved three steps (**Fig. 2.1**). First, the SU-8 master was surrounded with aluminum foil to prevent leakage. PDMS was prepared by mixing the base and the curing agent (10:1, w/w) and cast over the SU-8 master followed by baking at 60 ^{o}C for 2h. The cured PDMS was peeled from the SU-8 master. Inlets and outlets were perforated using a 1 mm biopsy punch (Miltex, York, PA). The last step was the sandwiching of porous polycarbonate membranes (cut from CorningVR transwell) between the top and the bottom PDMS layers. The membranes were first attached to the top PDMS layer at the desired positions. Then, both layers were treated with oxygen plasma (IPC 4000 series plasma system) (Branson, Philadelphia, PA). After the treatment, both layers were bonded with proper alignment.

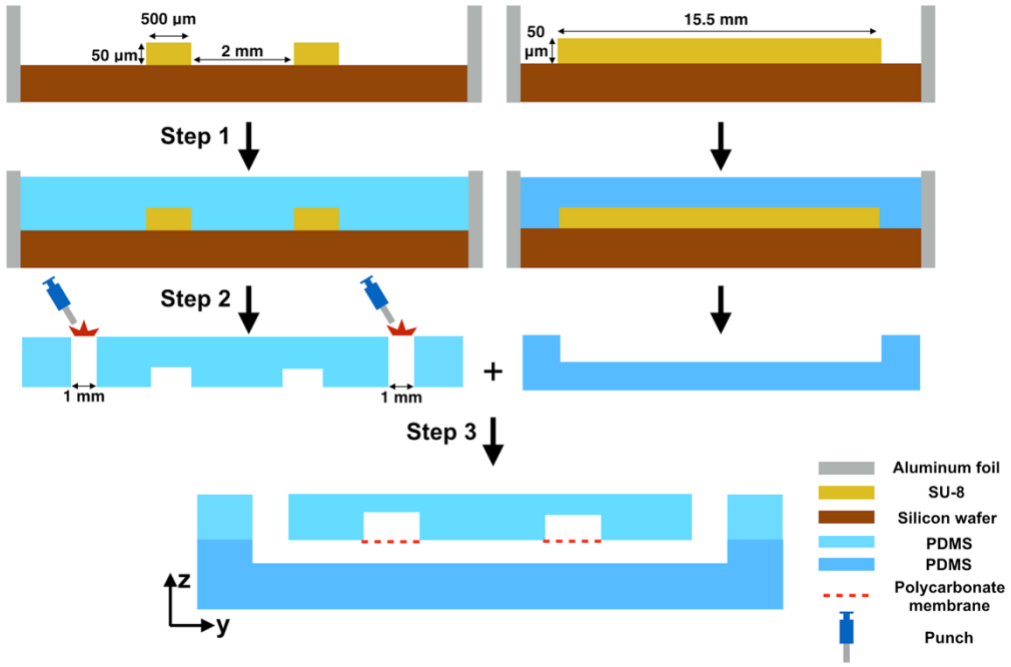

Figure 2. 1. Step-by-step device fabrication. (i) The SU-8 master on a silicon wafer is surrounded by aluminum foil. Freshly mixed PDMS (base and curing agent, 10:1 w/w) is cast onto the SU-8 master. (ii) After baking at 60 ºC for 2 h, the PDMS is cooled at room temperature and then peeled from the SU-8 master. (iii) Inlets and outlets are perforated at the positions indicated. The polycarbonate membranes are then sandwiched between the top and bottom PDMS layers.

Gradient profile characterization. The device was characterized using fluorescein isothiocyanate (FITC) (Thermo Fisher Scientific, Rockville, MD). Initially, the device was filled with DI water using 1ml syringes. Outlets of the bottom channel were taped to prevent flow. Flows in the top channels were driven by two independent syringe pumps (Kent Scientific, Genie Plus; Fisher Scientific, Single Syringe Pump), each at a rate of 120 µl h^{-1}. Subsequently, buffer solution in the source channel was replaced with 1.5 x 10^{-5} M FITC. To avoid FITC diffusion to the sink channel at the convergent site, the pumping rate of FITC was set to a rate of 50 µl h^{-1}. Excess solution at outlet was wiped away. The time was set to be t = 0 when FITC was loaded. A CCD camera, an inverted fluorescence microscope, a FITC filter cube, and a 20X Olympus objective lens were used to image both bright-field and

fluorescent images. Images were taken every minute for a total of 100 min. ImageJ (shareware: https://imagej.nih.gov/ij/download.html) was used to analyze fluorescence intensity. The fluorescence intensity was normalized using equation (1)[119]:

$$I_{norm}(t) = (I(t) - I_0)/(I_{max} - I_0) \quad (1)$$

where I(t) is the intensity of pixels along the gradient at each time point, I_0 is the intensity of a pixel across the gradient channel before the introduction of fluorescein, and I_{max} is the intensity of a pixel across the gradient channel with the highest fluorescein concentration (close to the source channel) at 100 min after starting the gradient generation. Another full characterization of the same device was repeated after 50 times of experiments/washing cycles, demonstrating reusability.

Bacterial chemotaxis. *E. coli* K-12 strain W3110 was used in all chemotaxis experiments. Cells were inoculated and grown overnight in Luria-Bertani (LB) media (Fisher, Pittsburgh, PA) with 50 µg/ml each of ampicillin and kanamycin (Sigma-Aldrich, St. Louis, MO). Cells were reinoculated from the overnight culture and grew to an OD_{600} of 0.45 at 37 C, shaking at 250 rpm. Following, samples were spun at 400 g for 5 min and resuspended in freshly made chemotaxis buffer solution (CB) (1 PBS with 0.1 mM EDTA, 0.01 mM L-methionine, and 10 mM sodium DL-lactate).

Prior to bacteria introduction, the bottom channel was primed with Pluronic F-127 (1% w/v, Sigma-Aldrich, St. Louis, MO) for 1 h before replacing with CB. This minimized nonspecific retention of cells to channel walls. Chemotaxis buffer was perfused through both the source and sink channels using 1 mL syringes and syringe

pumps. The pumping rate was 120 µl h^{-1} for both channels. *E. coli* at an OD_{600} between 0.7 and 1.0 (in the late exponential growth phase) was introduced into the bottom channel with the same volume for each test. Both ends of the bottom channel were then taped to stop flow. Glucose solution (1 mM D-glucose (Sigma) in CB) was then introduced at a rate of 50 µl h^{-1} to replace CB in the source channel. The time when glucose was added was set to be $t = 0$. Bright-field images were taken at 0, 10, 20, and 30 min by a 20X Olympus objective. Cell numbers in each image were counted using ImageJ. The device was washed by manually pumping buffer solution through the system.

Single-cell analysis. Twelve-second videos were taken in the center of the bottom channel (350 µm wide in the y-axis/ 300 µm wide in the x-axis) at 0, 10, 20, and 30 min by a 20X Olympus objective. Bacteria in each video were detected and tracked using a single-cell, analytic program developed in Python by our group (freely available under request), which was a modified version of the Trackpy code.[120] We used Trackpy's core modules for finding and tracking bacteria, whereas the analysis of the measurements was performed using custom-built modules developed specifically to the purposes of this work. The detection of features using Trackpy depended essentially on two parameters: brightness and size. In order to detect as many features as possible in each frame of the dataset, we tested different values and combinations for both parameters and then visually inspected the results until most of the features present in the frame were detected (including artifacts created by the optical system). We found the best results when adopting values of 500 and 15 (in Trackpy's units) for the brightness and size, respectively, and no significant

improvement could be achieved by varying these parameters. Based on the displacement of the features between each pair of frames, we were able to filter the results and classify the features into two categories: artifacts (no significant displacement between frames) and bacteria (displacement larger than 1.5 μm between frames). The latter was further divided into two classes: bacteria that were moving and bacteria that were not (stuck in the same place). For the results presented in this paper, we only took into consideration bacteria that were actually moving and tracked for more than 1 s (or about 10 frames with our instrumental setup). The directionality of each bacterium was determined based on the displacement direction along the y-axis comparing the initial and the final time points. The chemotaxis partition coefficient (CPC) was calculated using equation (2):

$$CPC = (N_{y+} - N_{y-})/(N_{y+} + N_{y-}) \quad (2)$$

where N_{y+} is the total number of cells moving towards the positive y direction (towards glucose), while N_{y-} is the total number of cells moving towards the negative y direction (away from glucose). In the control groups for all time points, both delivering channels were loaded with CB.

Statistical analysis. The goodness of fit of regression models was determined based on the coefficient of determination. The level to accept a model was set at $R^2 \geq 0.95$. One-way ANOVA was used to determine significant differences between groups. The level of significance was set at $\alpha = 0.05$.

Results and Discussion

Device characterization. The device was characterized using FITC. This method was based on the observation that the fluorescent light intensity emitted by fluorescein solutions in a microfluidic channel (depth 100 μm) was linearly proportional to the fluorescein concentration. This linearity held when the fluorescein concentration was less than 10^{-3} M.[116] Based on this information, we chose a stock 1.5 x 10^{-5} M FITC solution for all experiments. **Figure 2.2A** is a representative bright-field image of both delivery channels in the top layer aligned perpendicularly to the channel in the bottom layer. Two polycarbonate membranes are readily visualized at both intersections. **Figure 2.2B** depicts a fluorescence image (ex/em: 490/525nm) in which DI water and FITC were perfused in parallel in the x direction. A FITC gradient is readily seen emanating from the bottom channel, as indicated in the red box.

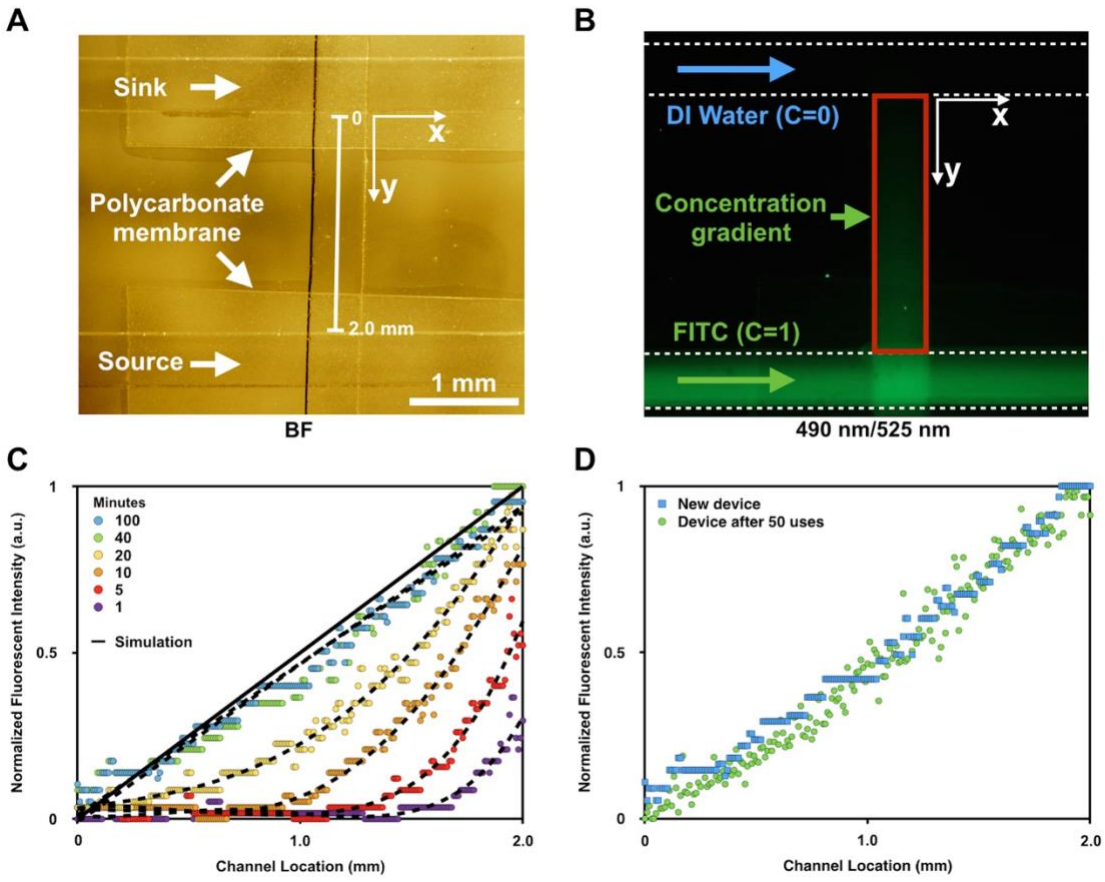

Figure 2. 2. Fluorescence characterization of the concentration gradient within the lower channel. Bright-field (A) and fluorescence (B) images show the bottom channel flanked by parallel sink (c = 0) and source (c = 1) channels. FITC and DI water are flowed into each channel at a constant rate (B). The FITC is detected using an excitation wavelength of 490 nm and an emission filter of 525 nm. The red box (B) marks the region over which the gradient is established. (C) Fluorescence intensity profiles are plotted along the y-axis, the length indicated in (A), for 100 minutes at various increments as noted. A finite element simulated steady state profile is also included. (d) Fluorescence intensity profiles of a freshly made device and an old device (used 50 times) are overlaid. C: Concentration of FITC.

Figure 2.2C depicts the quantified fluorescence intensity of FITC as a function of distance from the sink channel to the source channel (2 mm apart). All data were normalized to the fluorescence intensity at the source (i.e., a scale from 0 to 1). All datasets were least squares fitted by 4th-order polynomial functions. It was not until 40 minutes that the gradient profile could be interpreted as a linear and steady function ($R^2 = 0.95$). We evaluated the long-term stability of the gradient and found that it was maintained at least until 100 min, a period long beyond our need. The

steady state gradient profiles displayed no significant differences with results from finite element modeling (Comsol Multiphysics). Due to the linear relationship between fluorescence and fluorescein concentration and the similarity between diffusion coefficients of FITC in water ($D = 0.64 \times 10^{-9}\ m^2\ s^{-1}$)[121] and glucose in buffer solution ($D = 0.72 \times 10^{-9}\ m^2\ s^{-1}$)[122], we surmised that glucose concentration gradients at different time points could be estimated based on the already measured FITC fluorescent gradient profiles. Also, after 50 repetitions of chemotaxis experiments, the device was re-evaluated and characterized using the same gradient protocols. The profile after 50 uses was not significantly different than that from the freshly made device (**Fig. 2.2D**).

Chemo/pseudotaxis demonstration. We next demonstrated the chemotactic response of *E. coli* on both population and single-cell levels. We first examined the bacteria's spatial population distribution under glucose stimuli. Bright-field images of cells in the channel were taken every 10 min at two positions along the bottom channel: position *a* was close to the sink channel, whereas position *b* was close to the source channel (**Fig. 2.3A**). It should be noticed that the polycarbonate membrane blocked cells beneath from being observed visually. Therefore, positions *a* and *b* were not chosen at exactly C = 0 (sink) or C = 1 (source). Instead, they were shifted slightly towards the channel center (1.36 mm apart) to ensure that cells were properly viewed. As a result, the glucose concentration at position *a* was higher than 0 and that at position *b* was lower than 1 mM at steady state. Cell numbers in *a* and *b* were normalized as

$$N_{a\_norm} = N_a/(N_a + N_b) \quad (3)$$

$$N_{b\_norm} = N_b/(N_a + N_b) \quad (4)$$

where N_a and N_b are the total number of cells in *a* and *b*, respectively.

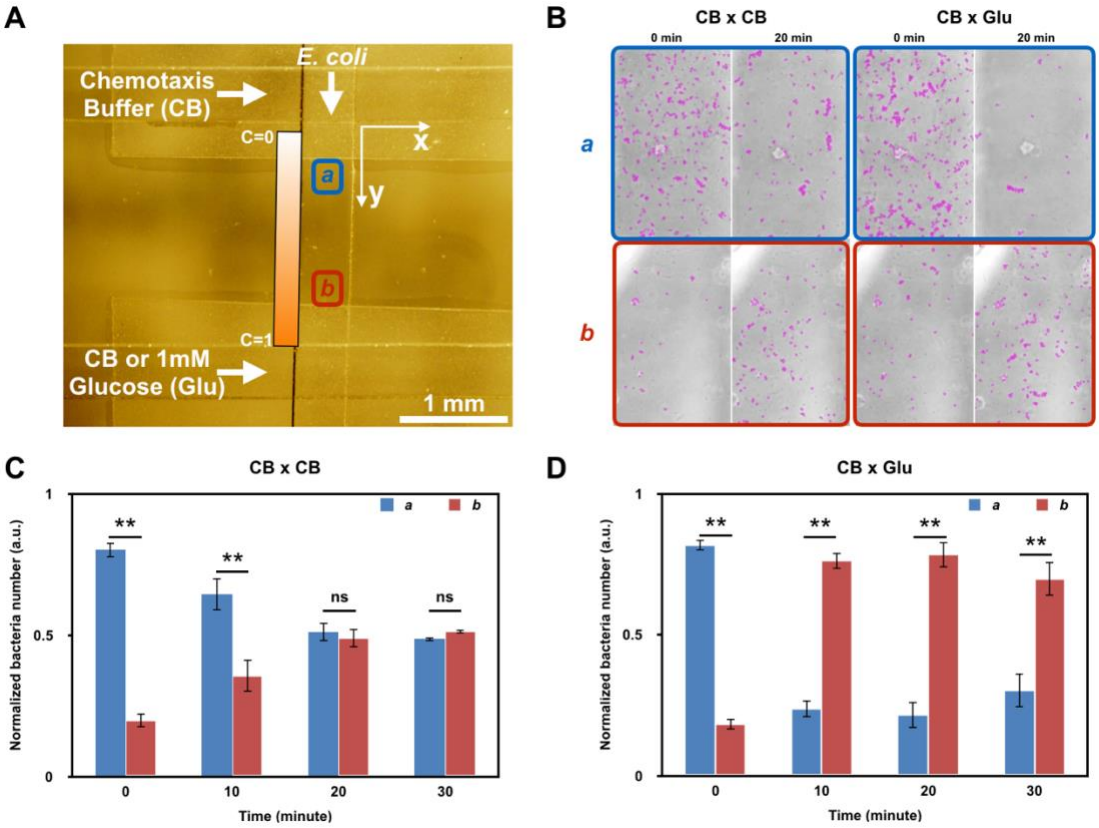

Figure 2. 3. Bacterial chemotaxis experiment. (A) Bright-field image indicating the bottom channel (top to bottom) flanked by parallel sink and source channels (horizontally aligned). Imaging positions *a* and *b* are selected along the bottom channel but outside the region of the permeable polycarbonate membrane. Position *a* is closer to the sink channel (CB), while position *b* is closer to the source channel (Glu). (B) Bright-field images of positions a and b at 0 and 20 min. Cells are marked with purple circles using Imagej TrackMate software. CB x CB: the control group in which chemotaxis buffer (CB) is flowed in both sink and source channels. CB x Glu: the experimental group in which CB in the source channel is replaced with 1 mM glucose in CB. Quantitative results of (B) are shown in (C) and (D). The cell number is normalized to the total cell number in both imaging areas. Data are collected at 0, 10, 20, and 30 min. ns, not significant; *, $p < 0.05$; **, $p < 0.01$. CB: chemotaxis buffer. Glu: glucose. C: concentration of glucose.

Before glucose addition, cells were unevenly distributed in the channel: the initial cell concentration was much higher at position *a* than at position *b* (**Fig. 2.3B**). This was

due to the loading procedure and importantly can be accommodated in our design. In the control group where both sink and source channels were loaded with chemotaxis buffer, the cell numbers at positions *a* and *b* became closer at 10 min and were nearly equal at 20–30 min (**Fig. 2.3C**). This result was due to the cell's random dispersion from high cell density areas to low-density areas in the absence of a chemoattractant so that the cell concentration eventually became homogeneous throughout the channel. In contrast, in the experimental group where glucose was introduced at the source, the population distribution changed dramatically, as noticed in the first sample just 10 min into the experiment. The number of bacteria at position *b* reached nearly three times that of position *a*. This was remarkable and statistically significant. Interestingly, this population distribution remained the same for the full 30 minutes (**Fig. 2.3D**). This result was in accord with the expectation that in the presence of a chemoattractant gradient, cells sensed stimuli and altered the direction of rotation of their flagella to improve their chances of migrating towards the higher concentration of attractant.[123] The fact that chemotaxis occurred quicker than the time required for establishing a steady state was due to the minimum glucose concentrations necessary to induce chemotaxis (1×10^{-6} M) being less than the concentrations available to cells in a steady state gradient.[125]

Using the same manner, we further studied pseudotaxic response of genetically engineered bacteria. Pseudotaxis is the phenomenon whereby a cell's motility is controlled by a chemical such that it results in the engineered cells swimming up a gradient of the chosen molecule. Here, two strains of engineered bacteria were studied: 1) engineered *E. coli* that accumulate within a gradient of pyocyanin

(PYO),[19] and 2) engineered *E. coli* that migrate towards a gradient of H_2O_2.[20] Both strains originate from *E. coli* K-12 W3110-*ΔcheZ* strain (lacking running capability) and were engineered to incorporate plasmids with promoters that response to either PYO (*soxRS* promoter) or H_2O_2 (*oxyRS* promoter) to restore their motility (by inducing CheZ expression). Engineered cells were tested using the gradient generator and all experimental steps were the same as aforementioned except PYO or H_2O_2 was introduced at the source instead of glucose. In **Figure 2.4**, we observed the restoration of motility (at ~ 90 min) drove engineered cells to directionally accumulate towards PYO comparing to the control group (motile cells with no directionality). Similarly, **Figure 2.5** depicted that when engineered cells were exposed to increasing amounts of H_2O_2, an increase in the number of bacteria was found at the source. Both results demonstrated the application of the gradient generator in studying pseudotaxis of engineered bacteria.

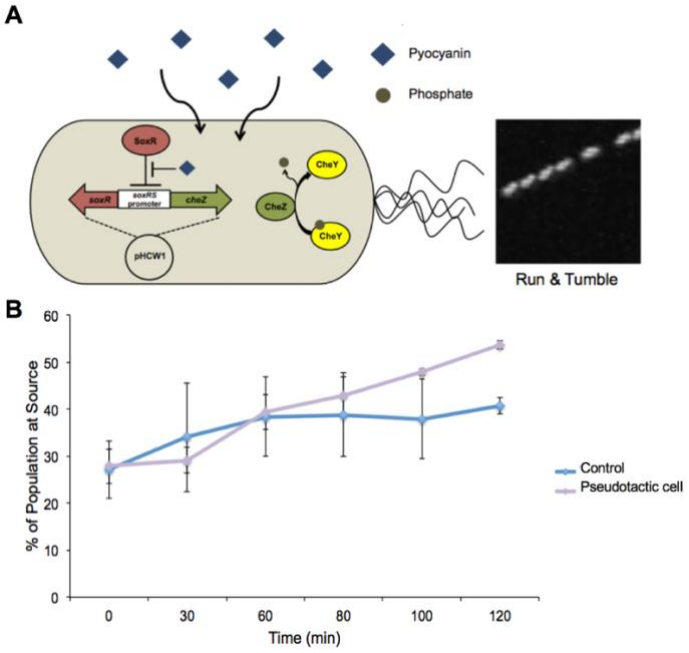

Figure 2. 4. Pseudotaxis assay of engineered *E. coli* towards pyocyanin. (A) Cells are engineered to "pseudotaxis" to pyocyanin. (B) Cells are grown to an OD_{600} of 0.45, resuspended in chemotaxis buffer and introduced at the sink. Pyocyanin is present at the source to form a gradient of 0µM to 5µM along the channel. The cell number is normalized to the total cell number in both imaging areas (i.e., position *a* and *b*). Error bars are standard error. Data adapted from Mckay et al (2017) with permission.[19]

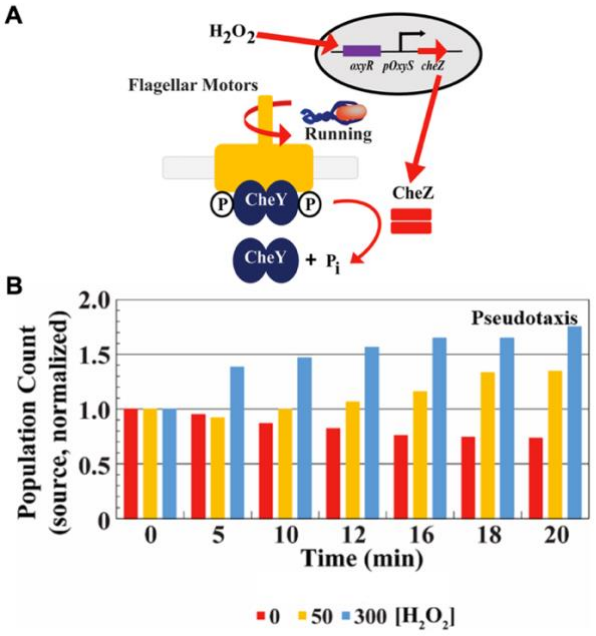

Figure 2. 5. Pseudotaxis assay of engineered *E. coli* towards H_2O_2. (A) Cells are engineered to "pseudotaxis" to H_2O_2. (B) Engineered cells demonstrated pseudotaxis to H_2O_2 of various concentrations that were introduced into the source channel. All population counts are normalized to time 0 population counts at the respective positions (i.e., position *a* and *b*). Data adapted from Virgile et al (2018) with permission.[20]

Single-cell analysis. In addition to observing changes in the overall population distribution, we analyzed bacterial chemotactic behavior on the single-cell level by video tracking cells in the center of the bottom channel (**Figs. 2.6A&B**). At every 10 min increment, 12 s videos were recorded and analyzed, as described above. The trajectory of every moving target in a video was marked by a white tail (**Fig. 2.6C**). To further quantify the degree of chemotaxis, we calculated a chemo- taxis partition coefficient (CPC), a parameter that represented the difference between cell populations that moved towards the chemoattractant and the opposite direction, for each video.[109] A CPC of 1 or -1 suggested an absolute net directionality towards or away from the chemoattractant, while a CPC of 0 indicated no net directionality. In both control and experimental groups, bacteria showed small directionalities (CPC<0.05) at $t = 0$ (**Fig. 2.6D**). After 10 min, however, bacteria in the experimental groups exhibited nearly 10 times stronger directionalities towards glucose than the control groups. This difference remained at this level for 20 min and eventually grew to 15 by 30min. These results were in agreement with the regional concentration gradient profiles exhibiting over these time domains within the video, as depicted in the time resolved gradient profiles in **Fig. 2.6B**. That is, at $t = 0$, there was no concentration gradient within the experiment during the course of the video. Thus, at early times (e.g., 1 and 5 min) bacteria swam randomly and barely exhibited net directionality. As the glucose concentration gradient gradually became established (concentration profiles transitioned to gold, yellow, and green in **Fig. 2.6B**), bacteria presumably upregulated chemotaxis machinery and moved towards the source, as demonstrated by significantly increased net directionalities. We observe increased

CPC values at 10 minutes when the maximum glucose concentration in the video scope reached 1 x 10^{-4} M (not shown). These results are consistent with a minimum D-glucose concentration needed to trigger a chemotactic response of E. coli (1 x 10^{-6} M).[127]

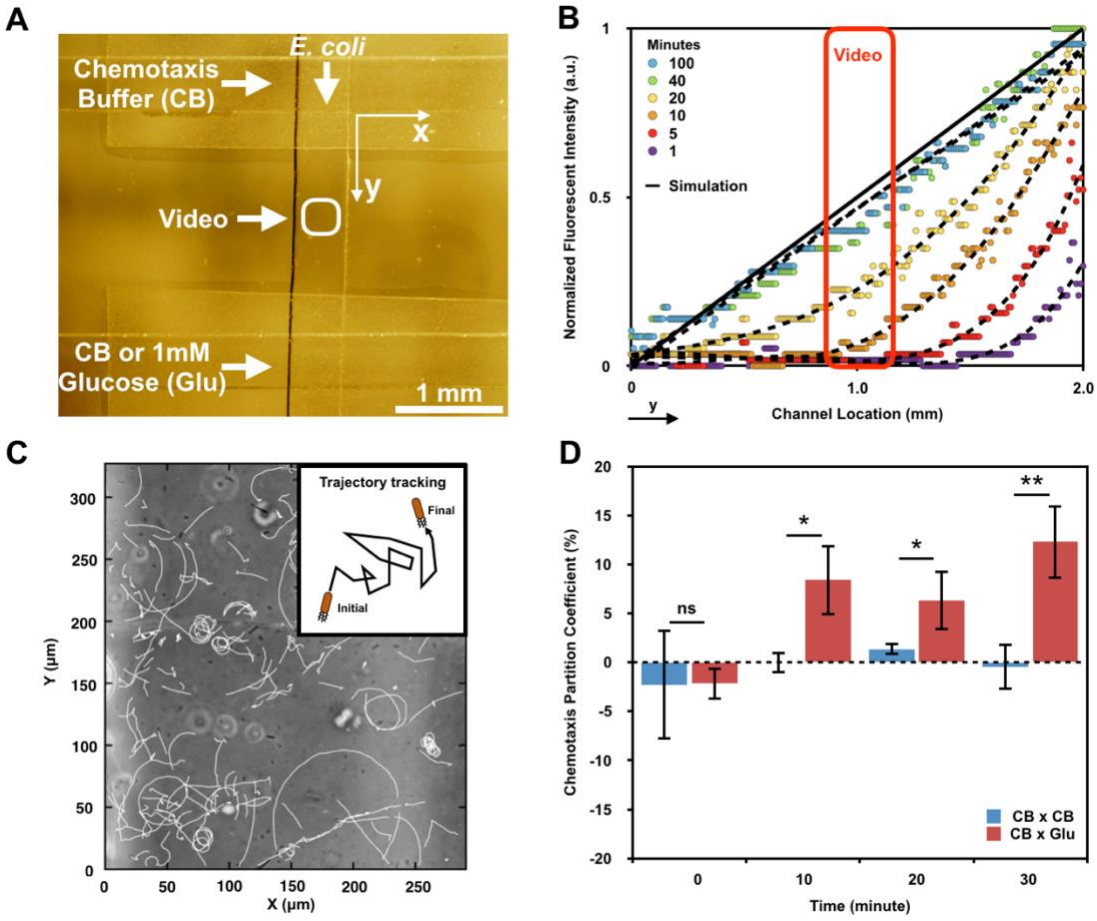

Figure 2. 6. Single cell analysis. (A) Bright-field image indicating the bottom channel (top to bottom) flanked by parallel sink and source channels (horizontally aligned). Videos are taken at the center of the gradient channel as indicated. Each video scope is about 350 μm wide on the y-axis and 300 μm wide on the x-axis. (B) Fluorescence intensity profiles of FITC are used to predict glucose concentration gradient profiles. The data inside the red box indicate the regional glucose gradient profiles within the video scope. (C) Cells in the video are tracked by a Python single cell analytics program, which generates a trajectory tail after each captured cell in a 11.7 s tracking. (D) The chemotaxis partition coefficient (CPC) of both experimental (CB Glu) and control (CB CB) groups is calculated at 0, 10, 20, 30 min. ns, not significant; *, $p < 0.05$; **, $p < 0.01$. CB: chemotaxis buffer. Glu: glucose.

Conclusions

In summary, we have demonstrated that this bilayer membrane-based gradient generator is able to establish stable and sharp concentration gradients in a user-friendly manner. In this device, bacterial introduction and experimental setup can be completed in a simple and quick manner. Furthermore, the device can be reused for at least 50 experiments or as long as the polycarbonate membranes remain intact. Therefore, multiple experiments can be conducted continuously within a short time period. Based on our fluorescence characterization, the gradient evolves to a steady state in less than 40min and lasts for at least 100 min. Using this device, we have studied the *E. coli* chemotactic response on both population and single-cell levels. We envision that this gradient generator will be amenable for use in microbiological laboratories with only limited access to microfluidics (just need a microscope and a syringe pump).

We envision this device can also be reconfigured to suit various purposes owing to its unique bilayer structure. For instance, the bottom channel could be replaced by modalities that immobilize planktonic bacteria, thereby resembling biofilms. Such a modification would enable the study of bacterial genetic responses to signal molecules of various concentrations (e.g., autoinducer[29]) and broaden the range of possible biofilm studies. Also, by including an accessible cell reservoir adjacent to the lower channel, one could subject cells to a steady gradient (e.g., by exposing cells after 30 min). Further, by integrating modalities that enable co-culture of bacteria with mammalian cells in the bottom channel, this device could find utility in investigating inter-kingdom communication under various chemical stimuli. These, in

turn, will enable a more detailed study of human disease. Electrochemical and other biosensors may also be integrated into the system to interrogate biochemical information and otherwise monitor cellular metabolic activities in situ and in real-time.[54,60] Overall, these contributions advancing both microfluidic technology and in vitro gradient generation will prove beneficial to further investigations of cell and tissue biology.

Chapter 4: Development of a "molectronic" sensor to access biochemical information from gut pathogens and enterocytes

This section is adapted from a manuscript that has been submitted to *Lab on a Chip* with the title "Selective assembly and functionalization of miniaturized redox capacitor inside microdevices for microbial toxin and mammalian cell cytotoxicity analyses". In this Chapter, microelectronics is integrated with our "electrobiofabrication" toolbox to develop a "molecular-electronic" (molectronic) sensor that facilitates information access from biology via electronics. The key component of the sensor is a miniaturized bio-based redox capacitor (BBRC) film which can exchange electrons with soluble redox-active species and amplify electrochemical signal. We demonstrated applying the molectronic sensor to interrogate bacteria-secreted toxin and cell death biomarker released from mammalian cell culture. Chapter 4 will describe the assembly of this device to organ-on-a-chip systems to enable molecular measurement and interrogation within microfluidic organ models.

Abstract

We report a novel strategy for bridging information transfer between electronics and biological systems within microdevices. This strategy relies on our "electrobiofabrication" toolbox that uses electrode-induced signals to assemble biopolymer films at spatially defined sites and then electrochemically "activates" the films for signal processing capabilities. Compared to conventional electrode surface modification approaches, our signal-guided assembly and activation strategy provides on-demand electrode functionalization, and greatly simplifies microfluidic sensor

design and fabrication. Specifically, a chitosan film is selectively localized in a microdevice and is covalently modified with phenolic species. The redox active properties of the phenolic species enable the film to transduce molecular to electronic signals (i.e., "molectronic"). The resulting "molectronic" sensors are shown to facilitate the electrochemical analysis in real time of biomolecules, including small molecules and enzymes, to cell-based measurements such as cytotoxicity. We believe this strategy provides an alternative, simple, and promising avenue for connecting electronics to biological systems within microfluidic platforms, and eventually will enrich our abilities to study biology in a variety of contexts.

Introduction

Integrating electronics with microfluidics for biochemical analysis has drawn significant attention.[72,128–132] However, electronics are not inherently favorable for acquiring information from biological systems due to its poor molecular and biological specificity.[54] Several approaches have been developed to improve the connection between electronics and biological systems. The most common approach relies on using biorecognition components such as nucleic acids[133], enzymes[72,134], and antibodies[132,135]. Yet, functionalizing electrodes to include biomolecular species with spatial selectivity within microdevices remains a challenge. Extra cumbersome steps (e.g., photolithography) are usually required during device fabrication,[128,135–137] which raises the complexity and cost in device manufacturing. Additionally, biorecognition components that are enclosed within microdevices are often not assembled in the best configuration, they undergo degradation and denaturing, and these lead to short

device shelf-life (typically less than 7 days[133]). Both factors limit biodevice dissemination and use. Here, we propose a novel concept to bridge information transfer between electronics and biological systems inside microdevices. This concept is based on our "electrobiofabrication" toolbox.[138–142] Such an electrobiofabrication toolbox simplifies the design and fabrication of biosensors by uncoupling electrode functionalization from device manufacturing. That is, biosensors can be stored as "inactivated" versions (i.e., plain electronics) that are "activated" (i.e., functionalized) immediately before use. "Inactivated" devices can be stored for long periods of time without concern for the decay of biological components. Electrobiofabrication makes use of the stimuli-responsive and self-assembling properties of several biological polymers. These biological polymers are natural or engineered materials that recognize and respond to electrode-imposed signals in order to undergo hierarchical assembly. Previous studies have focused on using self-assembly to localize biological components (e.g., enzymes, cells) that could be used for recognition. Here we are extending electrobiofabrication from physical self-assembly mechanisms to electrode-induced covalent modification of the films for the purpose of creating functionality for signal transduction.

To demonstrate this concept, we functionalize microelectronics with a bio-based redox capacitor (BBRC) film within microchannels.[58,60] This functionalization involves two electrochemical steps: electrodepositing a thin film of aminopolysaccharide, chitosan, and then grafting phenol molecules into the chitosan film.[143,144] That is, at low pH, chitosan is a soluble cationic polyelectrolyte, as its primary amines are protonated. At even slightly basic pH, the amines get

deprotonated and chitosan becomes insoluble. Instead of precipitating as insoluble particles, when in proximity to an electrode-generated pH gradient, chitosan can form a three-dimensional hydrogel film.[145] **Scheme 3.1A** depicts this electrodeposition mechanism onto a standard gold electrode. By controlling the intensity and the time of the applied electric signal, chitosan films of different thickness can be established.[146] It is interesting that the nucleophilic property of the deposited chitosan film also allows the film to be "activated". For instance, phenols can readily diffuse through the chitosan film and be anodically oxidized at the underlying electrode. The oxidized products undergo rapid grafting to the nucleophilic primary amines of the chitosan (**Scheme 3.1B**).[147,148] The resulting film is referred to as a BBRC film (**Scheme 3.1C**) as it is prepared from biological compounds and possesses redox-capacitor properties (endowed by the addition of the phenol, catechol), including accepting, storing and donating electrons in a controllable fashion.[149] Importantly, BBRC films can be removed with a strong acid wash and the underlying electrode is reusable.[140,150] BBRC films are non-conducting (i.e., unable to exchange electrons directly with the underlying electrodes) but redox-active and can repeatedly exchange electrons with soluble redox-active species. That is, the presence of catechol in the chitosan films enables redox cycling, a process by which the initial transfer of electrons can be cycled repeatedly under an applied voltage in the presence of a redox mediator, providing amplified signal from the initial electron transfer. **Scheme 3.1D&E** illustrate the mechanisms of reductive- and oxidative-redox cycling of the film that serve to amplify an initial signal from a biological redox-active molecule and an electrochemical mediator, 1,1'-ferrocenedimethanol (Fc), respectively. During

reduction, biological reductants can diffuse from the bulk solution into the BBRC film and quickly donate electrons to the phenolic moieties grafted in the film and convert quinone (Q) to catechol (QH_2). During oxidation, a reducing mediator, Fc, diffuses through the film and is electrochemically converted to its oxidized state, Fc^+, at the electrode. The oxidized Fc^+ can diffuse into the BBRC film to accept electrons from the film and convert QH_2 to Q moieties. **Scheme 3.1F** illustrates the thermodynamics that control electron transfer to/from the film. Through these redox-cycling mechanisms, BBRC films can be reversibly switched between two redox states, during which electrons can be stored or extracted. Based on the direction of electron flow, reductive- and oxidative-redox cycling are also referred to as "charging" and "discharging" the film, respectively. Importantly, the discharging process can be performed after film charging to extract (or "titrate") the charged state of BBRC films. This mechanism provides a unique means to measure the level of biological reductants during film charging.

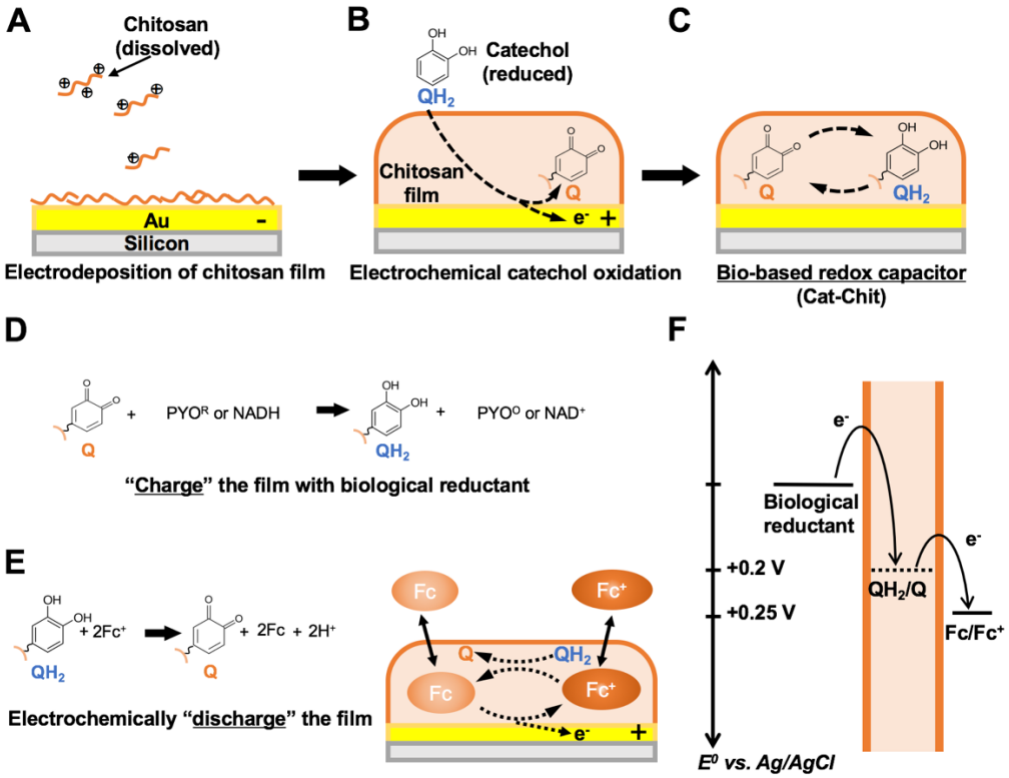

Scheme 3. 1. Schematic of bio-based redox capacitor (BBRC). (A) Electrodeposition of chitosan film on a gold electrode. Dissolved chitosan responds to the pH change induced by a cathode initiating the formation of a three-dimensional hydrogel film on its surface. (B) Catechol grafting to the chitosan film is enabled by an anodic voltage. (C) A catechol molecule conjugated to the nucleophilic amino group of the chitosan can undergo oxidation and reduction reactions in the assembled bio-based redox capacitor (BBRC). (D) Reductive redox-cycling between biological reductants and the BBRC film. (E) Oxidative redox-recycling between Fc^+/Fc and the BBRC film. (F) Thermodynamics of electron transfer. Q: quinone; QH_2: catechol.

In this paper, we integrate BBRC films into an enclosed microchannel to build a "molecular to electronic" ("molectronic") sensor for measuring analytes in biological samples ranging from small molecules (e.g., pyocyanin, a bacteria secreted toxin[151–153]), to enzymatic activity (e.g., lactate dehydrogenase (LDH), a biomarker for mammalian cell viability[154–156]). We note that electrochemical measurement of LDH activity, to our knowledge, is realized here for the first time within a microdevice. We further extend the application to assay the cytotoxicity of a drug mimic (e.g., Triton X-100) on cultures of mammalian cells.

Material and Methods

Chemicals and materials. The following materials were purchased from Sigma-Aldrich (St. Louis, MO): chitosan (85% deacetylated), pyrocatechol, sodium L-lactate, β-nicotinamide adenine dinucleotide sodium salt (NAD^+), pyocyanin (PYO) and hexaammineruthenium chloride (Ru^{3+}). 1,1'Ferrocenedimethonal (Fc) was purchased from Acros Organics (New Jersey, NJ). All mammalian cell culture media, LIVE-DEAD viability/cytotoxicity kit and Pierce LDH cytotoxicity assay kits were obtained from Thermo Fisher Scientific (Waltham, MA).

Device fabrication. The molectronic sensor consists of an electrode layer and a microchannel layer (**Figure 3.2A**), both layers were made in the Maryland Micro and Nano Fabrication Center. The pattern of three-electrode system was custom designed on AutoCAD (Autodesk, Inc., Mill Valley, CA), converted, exposed, and developed onto a stainless-steel shadow mask. The pattern was transferred from the mask to circular glass coverslips by depositing 5 µm chromium and 50 µm gold sequentially using Metra Thermal Evaporator (Telemark, Battle Ground, WA). The pattern of the microchannel was designed on AutoCAD, converted, exposed, and developed onto a mylar mask. The pattern was transferred from the mask to a 4-inch silicon wafer covered with SU-8 3050 photoresist (MicroChem, Westborough, MA) by exposing the wafer to UV light (405 nm wavelength) at 23.4 mW cm^{-2} using an EVG 620 mask aligner (Electronic Visions Inc., Phoenix, AZ). The wafer was subsequently developed for 8 min in an SU-8 developer (MicroChem, Westborough, MA). The resulting SU-8 master can be reused almost indefinitely. The microchannel layer was

made from polydimethylsiloxane (PDMS) (Sylgard 184, Dow Corning Co., Midland, MI) cast on the SU-8 master. Both electrode layer and microchannel layers were treated with oxygen plasma (IPC 4000 series plasma system) (Branson, Philadelphia, PA) and bonded with proper alignment. The device was equipped with a holder and rod electrodes for simple and stable connection to the external electrical source. The holder was 3D printed using a Connex 3 Object500 printer and MED610 ink (Stratasys, Eden Prairie, MN).

Selective functionalization of microelectrodes in microchannels with bio-based redox capacitor (BBRC) films. The working electrode in a three-electrode system was selectively functionalized with BBRC films in two steps.[54,59,60] First, the target working electrode was connected to an external electrical power supply (2400 Sourcemeter, Keithley, Cleveland, OH) and set as the cathode. A nearby electrode was set as the anode. The microchannel (3 mm x 3 mm x 100 μm) was filled with 1% chitosan solution (dissolved in water and adjusted pH to 5.6 using 1.0 M HCl) to immerse both electrodes. Chitosan film was electrodeposited on the cathode by applying a constant current of 3 A/m^2 for 30 s. Films deposited using these parameters are estimated to be 50 μm thick[146], which is about half of the channel height (100 μm). Second, the device was connected to a potentiostat for catechol grafting. The channel was filled with catechol solution (5 mM in 0.1 M phosphate buffer (PB), pH 7.0), and a constant anodic potential of + 0.6 V (vs Au) was applied for 3 min to oxidize the catechol. The oxidized catechol (i.e., o-quinone) undergoes grafting reactions to the chitosan film.[56,58,149] All BBRC films were freshly prepared before each experiment. Fluorescein (FITC) labeled chitosan was used to assist film

observation. In order to confirm the signal amplification capabilities of the film, the channel was filled with 50 µM Fc and 50 µM Ru^{3+} in PB (pH 7.0). Both the device and the Fc/Ru^{3+} solution was deoxidized with N_2 gas for 30 minutes. Cyclic voltammetry (CV, from -0.4 V to 0.4 V) was applied for analysis. All experiments were conducted in a custom designed anaerobic chamber with constant N_2 renewal. Results were compared between devices with the BBRC films and chitosan films only.

On-chip pyocyanin (PYO) measurement of conditioned medium (CM).

Pseudomonas aeruginosa (PAO1) and *Salmonella typhimurium* were obtained from American Type Culture Collection (Manassas, VA); *Escherichia coli* (W3110) was obtained from the Genetic Stock Center, Yale University (New Haven, CT). All were cultured in Luria broth (LB) medium at 37 ℃ with shaking (250 rpm). The conditioned media (CM) from overnight cultures were used for on-chip analysis of pyocyanin (PYO), a signal molecule secreted from PAO1. A standard curve for PYO measurement was generated using solutions with known PYO concentrations. The PYO samples of 0 µM, 5 µM, 10 µM, 15 µM and 20 µM were prepared in PB containing 50 µM Fc. Before each experiment, samples were deoxidized with N_2 gas for 30 min. Samples were introduced into the device inlet via syringe. CV was performed on each sample for analysis. The device was washed with PB between each test. The supernatants (CM) of overnight bacterial cultures were collected and deoxidized with N_2 gas. The deoxidized samples were introduced into the device for CV analysis. All experiments were conducted in a custom designed anaerobic

chamber with constant N_2 replacement. Results were compared between devices with BBRC films and with chitosan films only.

On-chip lactate dehydrogenase (LDH) measurement. Before experiments, the devices were filled with 50 µM Fc and BBRC films were discharged by applying anodic voltage of 0.4 V for 120 s. This discharging process was repeated until the film was fully discharged (i.e., no further change in chronocoulometry (CC) data, the film's catechols were all in oxidized =O form). LDH stock solution (2750 unit/L, 1 unit of LDH produces 1 µM of NADH in 1 minute) was prepared in PB containing 50 µM Fc. LDH substrate solution was prepared with 20 mM L-lactate and 10 mM NAD^+ in PB containing 50 µM Fc. For standard curve preparations, LDH stock solutions were spiked into the substrate solution to make samples with LDH concentrations of 0 unit/L, 15 unit/L, 30 unit/L, 45 unit/L, 60 unit/L, 90 unit/L and 120 unit/L. Time was set as t0 when the sample was mixed. Each sample was then immediately introduced into the device via syringe. At t = 10 min, CC was performed. Results were compared between the devices with BBRC films and with chitosan films (negative controls).

On-chip cytotoxicity - Effects of Triton X-100 on Caco-2 cell viability. Caco-2 cells were obtained from American Type Culture Collection (Manassas, VA). Cells were maintained using Dulbecco's Modified Eagle Media (DMEM) supplied with 10% fetal bovine serum (FBS) in T75 flasks under 37 ^oC and 5% CO_2 level and passaged every three days. At passage number 18, cells (~ $1.5x10^5$ cell/cm^2) were transferred to 35 mm petri dishes. All petri dishes were pre-sterilized with 70%

ethanol and UV (40 min), and treated with 50 µg/ml type I collagen (Corning, Corning, NY) for 2 hours. Cells were cultured under 37 ^{o}C and 5% CO_2 overlay. Caco-2 cell cultures at confluency were treated with Triton X-100 at levels of 0%, 0.001%, 0.01%, 0.015%, 0.02% and 0.1% (positive control) in DMEM for 2 hours. Then, the viability of each culture was assayed and visualized with a LIVE-DEAD viability/cytotoxicity kit. In parallel, the viability was quantified using the molectronic sensor and the Pierce LDH cytotoxicity assay kit. The supernatant of each culture was collected and diluted 10 times in the LDH substrate solution (this optimized dilution factor ensured that all measurements fell within the linear range of the calibration curve[157,158]). Time was set as t_0 when the sample and the substrate were mixed. The mixture was introduced into the device via syringe. For all experiments, BBRC films were fully discharged before use as aforementioned. At t = 10 min, CC was applied. Based on our in vitro assays, the samples treated with 0.1% of Triton X-100 were set as the positive controls (i.e., 100% cytotoxicity) and the samples treated with DMEM served as negative controls. The cytotoxicity of each sample was calculated using equation (1):

$$\text{Cytotoxicity (\%)} = ([\text{LDH}])/([\text{LDH}]_{\text{Max}} \times 100\%), \quad (1)$$

Where [LDH] referred to the LDH level measured in each sample and $[\text{LDH}]_{\text{Max}}$ referred the LDH level in the positive control.

Instrumentation. All electrochemical measurements were performed using a CHI 420a electrochemical analyzer (CH instruments, Austin, TX). Optical detection of LDH was performed with a SpectraMax® M2e plate reader (Molecular Devices, San

Jose, CA). Caco-2 cell cultures were imaged using a fluorescence microscopy (BX 60 microscope; Olympus) and a digital camera (Olympus DP72).

Statistical analysis. All assays were performed in triplicate. Results were expressed as mean ± standard error. One-way ANOVA was used to determine significant differences between groups. The level of significance was set at $\alpha = 0.05$. The Pearson product-moment correlation coefficient was applied to measure the strength of linear correlation between groups. The level of significant correlation was set at $r = 0.95$.

Results and Discussion

Selectively functionalizing microelectronics in microchannels for amplified electrochemical signals. Functionalizing electronics with BBRC films has previously been reported using standard electrochemical cells (**Fig. 3.1A**).[54,59,60] That is, standard electrochemical cells containing a gold working electrode (gold/chromium deposited on silicon wafer), a platinum counter electrode and a Ag/AgCl reference electrode have been routinely deployed.[57,58,159] We customized our electrochemical cell so that the gold working electrode can be properly placed and connected to an external power source. All three electrodes were connected to the same potentiostat and their working parts were immersed in the same solution. The signal amplification capability of the functionalized electrode was characterized using standard redox mediators, Ru^{3+} and Fc dissolved in 0.1 M PB. During CV, owing to the catechol in the BBRC, the electrochemical reduction of Ru^{3+} initiates reductive redox-cycling of the film through a similar mechanism described in **Scheme 3.1D** and the

electrochemical oxidation of Fc initiates oxidative redox-cycling of the film as described in **Scheme 3.1E**. Specifically, redox cycling yields amplified Ru^{3+} reduction currents and Fc oxidation currents (**Fig. 3.1B**). Electrodes coated with unmodified chitosan serve as our negative control because chitosan by itself is non-conducting.[149] It should also be noted that the BBRC films reversibly exchange electrons with these mediators although the film's redox-capacity is very large, but finite.

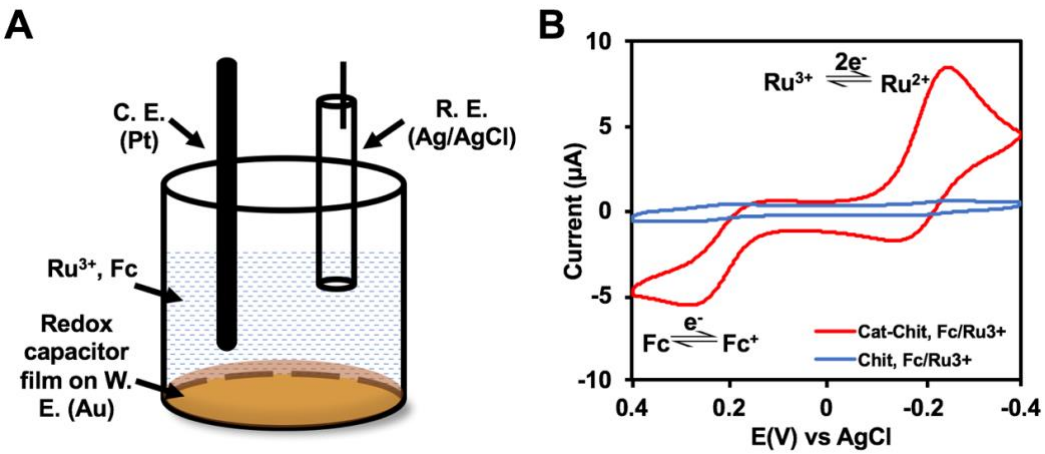

Figure 3. 1. BBRC film assembled on macroscale electrode. (A) Setup of a standard three-electrode electrochemical cell. The BBRC film is deposited on the working electrode. The system is characterized in a solution of Ru^{3+} and Fc. (B) Cyclic voltammogram (CV) comparing standard gold electrode modified with BBRC film (Cat-Chit) and chitosan film (Chit) using chamber in (A). W. E.: working electrode, C. E.: counter electrode, R. E.: reference electrode.

Here, we extended this technique to a microfluidic platform for the first time. Microfluidics enables precise and automated fluid control[107] and is envisioned to potentially enlarge the application scope of the molectronic sensor. Instead of inserting $Ag/AgCl_2$ reference electrode through channel inlets[88], we embedded a miniaturized three-electrode system in a simply designed microdevice (**Fig. 3.2A**). The device was stabilized in a 3D printed chip holder, through which the external power supply was connected. The three-electrode system was covered by a PDMS

layer containing a reaction chamber. Through "electrobiofabrication", we selectively functionalized the circular working electrode in situ with BBRC films, that is, via electroassembled chitosan and then grafted catechol, forming the BBRC. The entire functionalization procedure took 5.5 minutes to complete (30 seconds of chitosan deposition and 5 minutes of catechol grafting). Once functionalized, sensors were used within 24 hours. In **Fig. 3.2B**, fluorescein labeled chitosan was used enabling visualization of the BBRC film on the electrode. Then, functionalized electronics (i.e., the "molectronic" sensors) were tested to amplify electrochemical signals with standard redox mediators, Fc and Ru^{3+} (**Fig. 3.2C**). CVs taken of the microsensing system showed that peak currents of the molectronic sensors were about 10 times higher than those of the control group. Since the CVs of **Fig. 3.1B** (immersed macroscale electrodes) and the **Fig. 3.2C** (the molectronic sensor) were nearly identical (only slight peak shifts owing largely to varied film thicknesses and different reference electrodes), our results indicate that BBRC films for the first time, were able to reveal redox activities from miniature samples (i.e., 2 µL) within a microdevice.

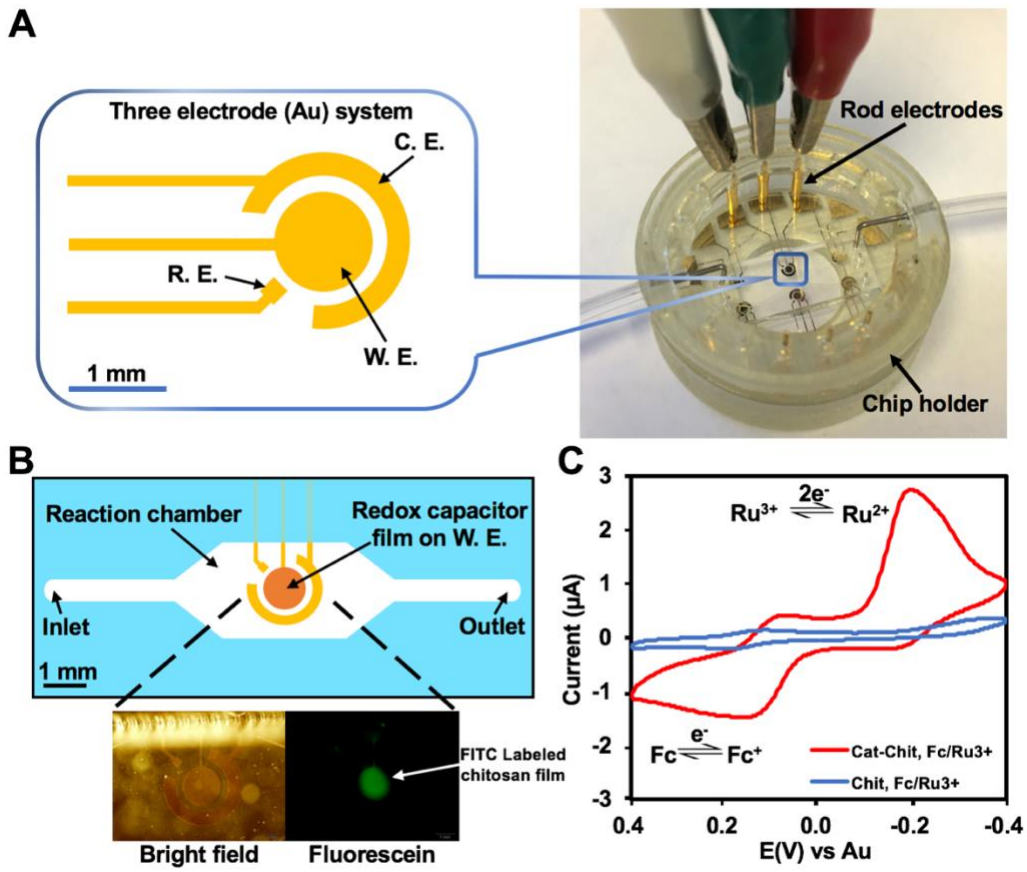

Figure 3. 2. Miniaturized BBRC film inside microdevice. (A) A miniaturized three-electrode electrochemical system designed and built inside a microdevice that is enclosed in a 3D printed chip holder. (B) Schematics showing the configuration of the molectronic sensor. The three-electrode system is contained within a reaction chamber. Lower panels depict bright field (BF) and fluorescent microscopic images of the functionalized electronics. (C) CV comparing the molectronic biosensor (Cat-Chit) and the control device (Chit) using electrode system in (B). W. E.: working electrode, C. E.: counter electrode, R. E.: reference electrode.

On-chip pyocyanin (PYO) measurement and bacterial sample analysis. The molectronic sensor was first leveraged in analyzing microbiological cell culture by magnifying the electrochemical signal of pyocyanin (PYO), a redox-active small molecule toxin produced by *P. aeruginosa* (**Fig. 3.3A**).[151–153] **Figure 3.3B&C** illustrate the mechanisms of redox-recycling involved in PYO measurement. When secreted by *P. aeruginosa*, PYO is in its oxidative state (PYO^{O}). Acting like an oxidizing mediator (e.g., Ru^{3+}), PYO^{O} can accept electrons from the cathode and be

electrochemically measured. With the presence of the BBRC film, the reduced PYO (PYO^R) can "charge" the redox capacitor film and be returned to its oxidative state (PYO^O) (**Fig. 3.3B**). The reductive redox cycling reaction amplifies the reduction current of PYO^O. However, as noted, the "charged" film (QH_2) can return to its oxidative state (Q) via the oxidative redox-cycling with Fc/Fc^+ in **Figure 3.3C**. The thermodynamics of electron transfer are depicted in **Fig. 3.3D**. Using CV, we found the reduction peak current of PYO^O corresponded to -0.3V and its magnitude was linearly proportional to PYO^O concentration (**Fig. 3.4A&B**). It should also be noted that increased PYO^O proportionally "charged" the BBRC film, which in turn, raised the oxidation peak current of Fc.[58]

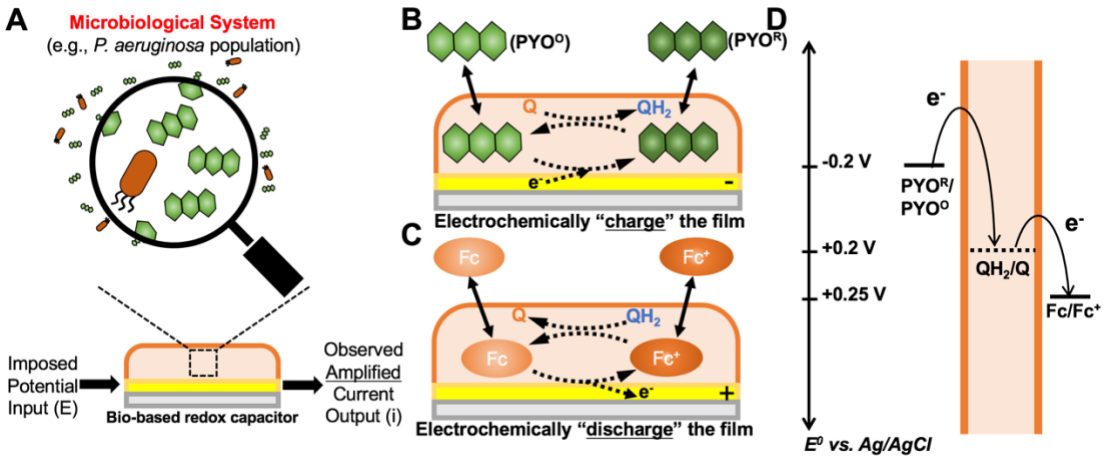

Figure 3. 3. Schematic of bacterial toxin analysis using the molectronic sensor. (A) Schematic illustrating the microbiological analysis using BBRC films made possible by amplifying electrochemical signals in the bacterial secretome. (B) Reductive redox-cycling between PYO^O/PYO^R and the BBRC film. (C) Oxidative redox-recycling between Fc^+/Fc and the BBRC film. (D) Thermodynamics of electron transfer. Q: quinone; QH_2: catechol

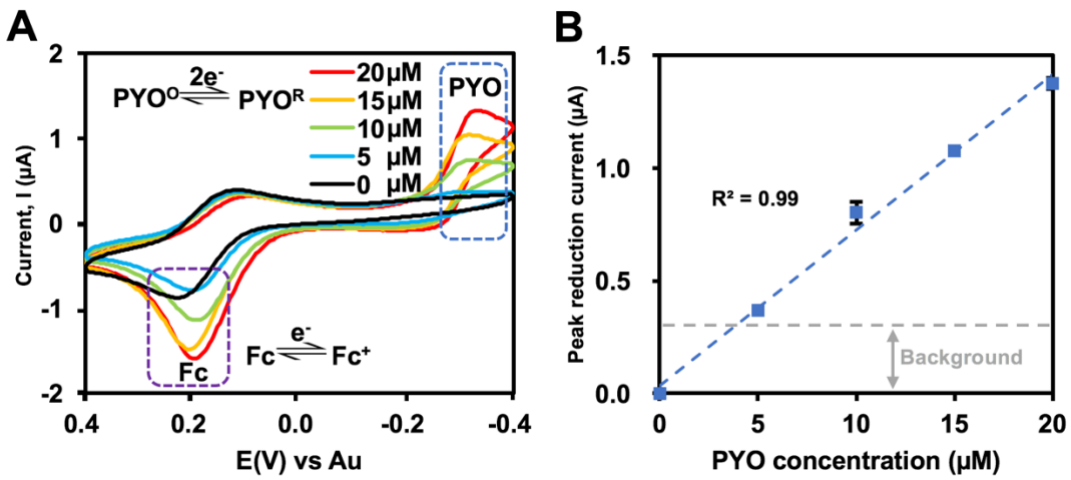

Figure 3. 4. Cyclic voltammogram (CV) results of PYO spiked PB samples. (A) CV of PYO^O in PB with concentrations from 0 µM to 20 µM. (B) Calibration curve of PYO measurement.

To test the selectivity of the molectronic sensor towards bacterial identification, CM from several overnight cultures were collected and analyzed. The peak currents were measured at - 0.3 V; CM from *P. aeruginosa* in the chitosan-only sensor control increased ~2-fold relative to uncultured LB media. When the molectronic sensor was used, the peak current increased nearly 8-fold for the case of *P. aeruginosa* ($p < 0.01$) (**Figure 3.5**). This result confirmed the signal amplification capability of BBRC films (i.e., catechol modified chitosan films). Neither *E. coli* nor *S. Typhimurium* had secreted redox active metabolites during the preceding cultures. Interestingly, the absolute values of the reduction peak current in all cases reported in **Figure 3.5** were lower than those in **Figure 3.4B**. This was presumably due to the complex components in LB media and bacterial CM that alter the electron flow between electrodes. In the case of LB alone, a non-zero current was obtained and in all cases the potential for redox cycling due to the presence of catechol was found to increase current. In sum, our results indicate that the molectronic sensor can selectively distinguish the presence

of *P. aeruginosa* among other bacteria owing to the pyocyanin that it secretes during growth.

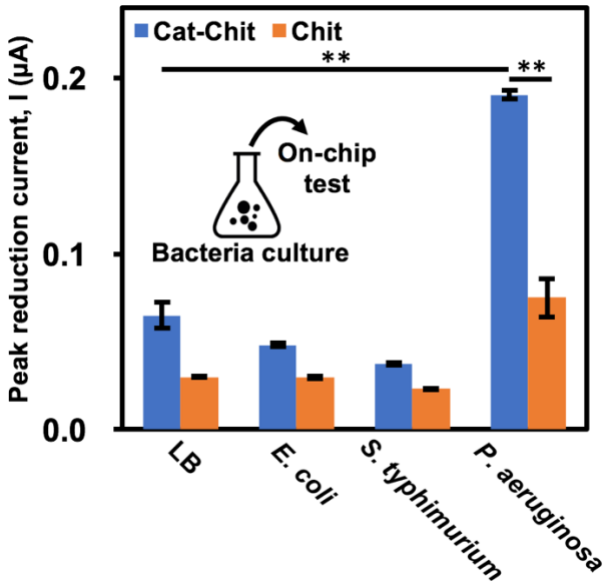

Figure 3. 5. On-chip PYO measurements within LB and conditioned media (CM) from *E. coli*, *S. Typhimurium* and *P. aeruginosa* overnight cultures (**, $p < 0.01$). Results are compared between the molectronic sensor (Cat-Chit) and the control device (Chit).

On-chip lactate dehydrogenase (LDH) measurement. In addition to small molecule analysis noted above, we evaluated the molectronic sensor's ability to measure enzymatic activity, specifically, LDH. LDH is an enzyme abundant in the cytosol of mammalian cells. When cell membranes are damaged, LDH is often released into the surrounding media (**Fig. 3.6A**), consequently, measurement of LDH enzymatic activity in cell culture media is a standard method for evaluating cytotoxicity and is widely utilized in drug screening.[154–156] An often used LDH-catalyzed reaction involves a coenzyme (NAD^+/NADH) which acts as an electron-shuttle mediator.[160] During electrochemical measurements, this mediator functions to shuttle the electrons between the enzyme and electrode.[161] Current LDH activity measurements rely on oxidants that oxidize NADH (e.g., Formazan[162]) and accordingly, undergo colorimetric changes.

Here, we leveraged the capacitor feature of the molectronic sensor to electrochemically measure LDH activity in a microdevice (**Fig. 3.6A**). **Figure 3.6B&C** illustrates the mechanisms involved. Briefly, LDH catalyzes reversible reactions between lactate and pyruvate with NAD^+/NADH as the coenzyme. When the reaction proceeds from lactate to pyruvate, generated NADH serves to "charge" the BBRC film (i.e., reduce quinone to catechol) and is then returned to the oxidized (NAD^+) state. This cycling between NADH and the BBRC film thus facilitates signal processing by amplifying the signal output. It should be noted that the enzymatic film charging takes place without the need of electrical input. Importantly, the electrons stored in the charged film can be extracted (or "titrated") by the oxidative-redox cycling reaction of Fc (i.e., discharging) in **Figure 3.6C**. The thermodynamics of electron transfer are depicted in **Figure 3.6D**. To test this possibility, we prepared films for the fully charged state, where the film's catechols were all in reduced QH_2 form (positive control) and the fully discharged state, where the film's catechols were all in oxidized Q form (negative control) by the electrochemical redox-cycling reactions. **Figure 3.7** shows that more electrons can be titrated from the fully charged films, compared with fully discharged films, as expected. That is, the capability of amplifying electrochemical signals between two control films is attributed to the charging state of film (**Fig. 3.7**) and this difference is utilized to reflect the LDH activity in samples.

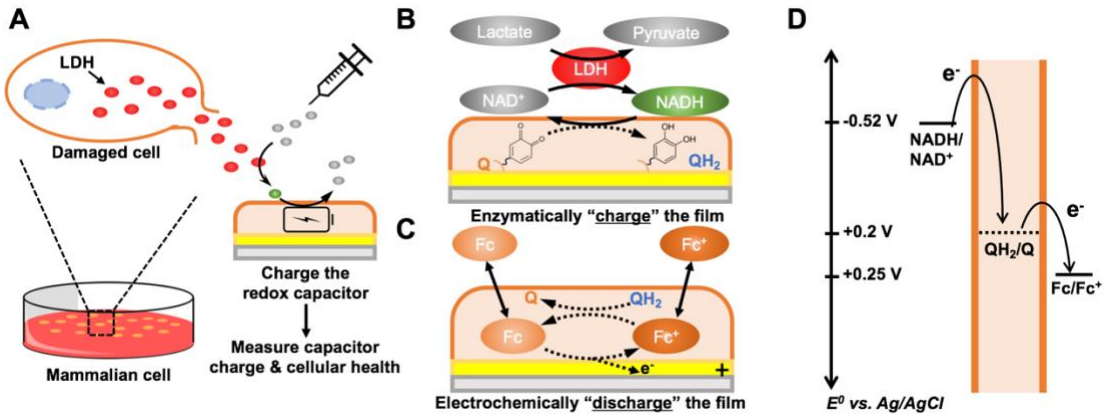

Figure 3. 6. Schematic of LDH analysis from mammalian culture. (A) Schematics showing that the membrane disruption of mammalian cells releases cytosolic lactate dehydrogenase (LDH) into surrounding environment. The released LDH can catalyze the added substrates (lactate & NAD^+) and in turn charge the molectronic sensor in an analogous manner to battery. The final charge of the molectronic sensor can be measured to reflect the health state of tested cell culture. (B) Reaction catalyzed by LDH. Reductive redox-cycling between NAD^+/NADH and the BBRC film. (C) Oxidative redox-recycling between Fc^+/Fc and the BBRC film. (D) Thermodynamics of electron transfer. Q: quinone; QH_2: catechol

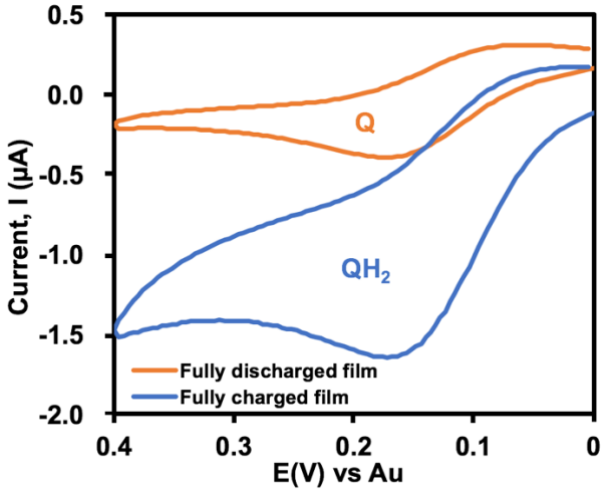

Figure 3. 7. Cyclic voltammogram (CV) of Fc oxidation at the surface of electrodes modified with fully discharged (Q) and fully charged (QH_2) BBRC films.

In order to accurately titrate the electrons in enzymatically charged films, chronocoulometry (CC) was employed. In **Figure 3.8A**, the fully discharged films were incubated in various solutions with no applied voltage and then each resulting film was titrated by the Fc-redox cycling reaction.[54] The red line in **Figure 3.8A** shows a large

oxidative charge curve of the film that has been incubated with LDH and substrate (lactate and NAD^+). However, when the film was incubated in solutions lacking LDH, the gray line in **Figure 3.8A** resulted. This shows a smaller oxidative charge transfer, and was more similar to the negative control that was fully discharged (dotted line). The results of **Figure 3.8A** indicate that the addition of LDH and the substrate enzymatically charged the BBRC film. Then, the charged film was titrated by measuring the amplified oxidative charge during Fc oxidation. The magnitude of this amplification is then dependent on the number of reduced catechols in the film, which, in turn, were found to be linearly proportional to the LDH activity (i.e., concentration) (**Fig. 3.8B**). That is, we found the response was linear up to 60 unit/L, where the signal was seen to saturate. The signal saturation was presumably due to the limited contact efficiency (confined space for diffusion) between NADH in the bulk solution and the film within microchannel.[160]

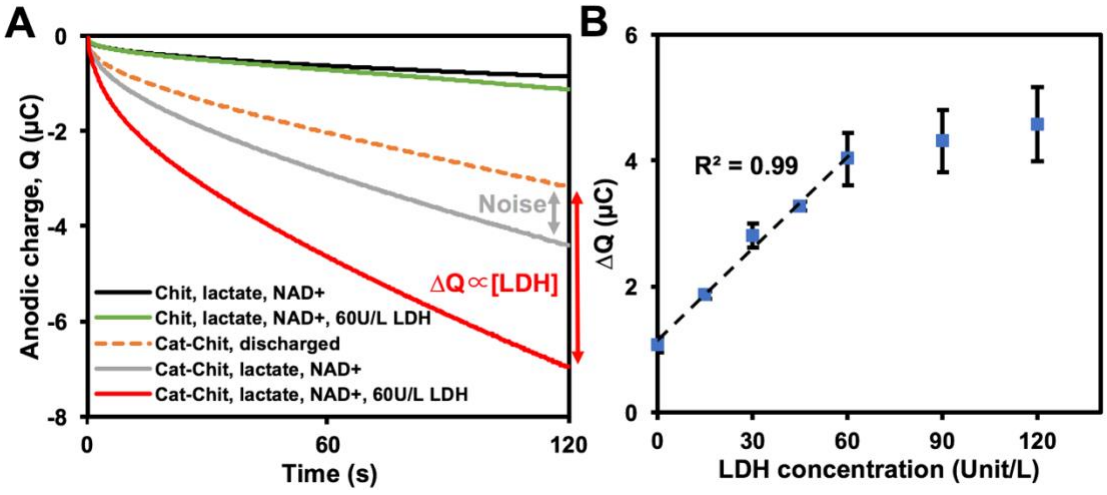

Figure 3. 8. (A) Chronocoulometry (CC) results comparing the molectronic sensor (Cat-Chit) and the control device (Chit) on LDH measurement. (B) Calibration curve of the molectronic sensor on LDH activity measurement.

On-chip cytotoxicity - Effects of Triton X-100 on Caco-2 cell viability. Since LDH activity can be used for determining cytotoxicity, we cultivated mammalian cells and challenged them with cytotoxic surfactant, Triton X-100, which permeabilizes cell membranes.[163] That is, a human epithelial colorectal adenocarcinoma cell line, Caco-2, was used as a model cell culture. Caco-2 cell is commonly used to resemble the enterocytes lining the human small intestine, which is pivotal in drug absorption.[164,165] Caco-2 cell cultures were exposed to Triton X-100 at various concentrations for 120 min, followed by on-chip viability measurements and LDH activity assays (**Fig. 3.9**).

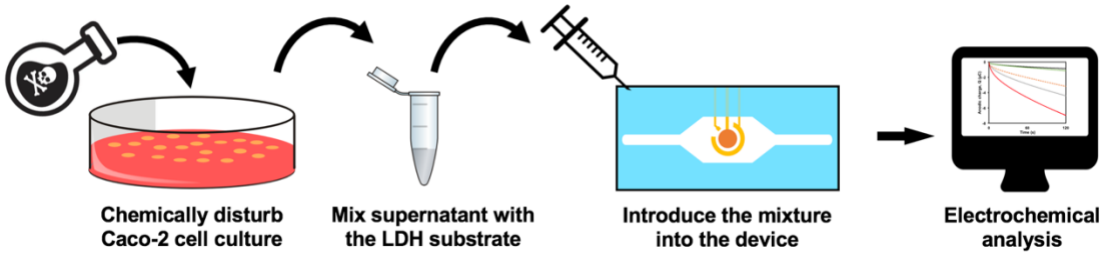

Figure 3. 9. Schematics demonstrating cytotoxicity assay steps using the molectronic sensor.

The viability of Caco-2 cells was examined using a commercial LIVE/DEAD viability kit (see Methods), while the LDH activity was measured using both the molectronic sensor and a commercialized cytotoxicity kit in parallel. The LIVE/DEAD viability kit stains live cells with green fluorescence (catalyzed by cytosolic esterase and retained intracellularly) while dead or permeabilized cells fluoresce red (generated by nucleic acid binding stain that only enters cells with damaged membrane). Microscopic images in **Fig. 3.10** reveal that cell viability was highest at the lowest Triton X-100 concentrations. In addition, it was evident in the bright field (BF) and green fluorescence images that as the Triton X-100 concentration increased, the Caco-2 cells

started to shrink and lyse. While the number of live cells decreased, the number of dead cells increased dramatically (sample treated with 0.02% Triton X-100 showed decreased cell number due to cell detachment from substrate). The qualitative results depicted in **Fig. 3.10** were quantified in **Fig. 3.11** using both the molectronic sensor and the commercial cytotoxicity kit, which measures LDH activity level via colorimetric means. All results were normalized to the positive control (cells treated with 0.1% Triton X-100, not shown). Both methods demonstrated similar values and patterns (r = 0.99, p = 0.94) that also corresponded to the microscopic results. In sum, these data demonstrate concordance between an electrobiofabricated molectronic sensor that can be assembled in situ within fluidic devices versus the commercialized kits that required pooled samples. Perhaps more importantly, the *in situ* measurement shown here is quantitative and augments visible fluorescence microscopy measurements that are difficult to quantify particularly at high cell densities.

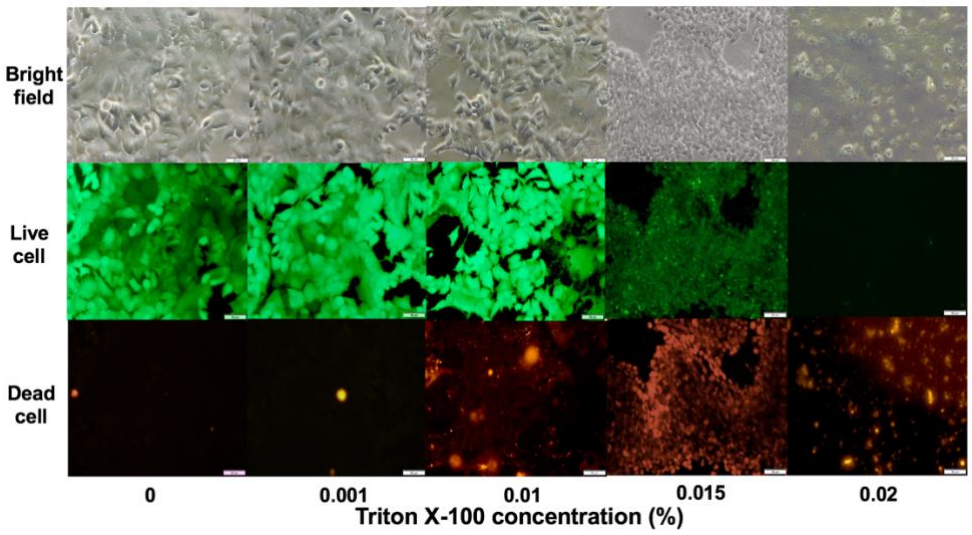

Figure 3. 10. Microscopic results of Caco-2 cell cultures treated with various concentration of Triton X-100. Green and red fluorescent images depict live and dead cells after 120 min, respectively. Scale bar = 50 µm. BF: bright field.

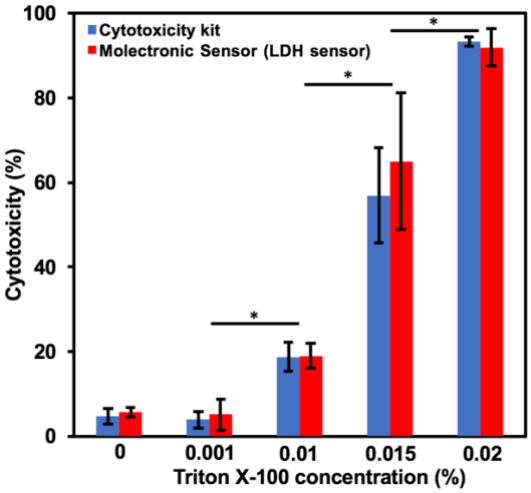

Figure 3. 11. Cytotoxicity measurements by the molectronic sensor and the commercialized cytotoxicity kit (*, $p < 0.05$). All results are normalized to data from the positive control, in which cell cultures are treated with 0.1% Triton X-100.

Conclusions

In this study, we proposed and developed a novel concept, based on our "electrobiofabrication" toolbox, to simplify the bridging between electronics and biological systems within microdevices. This concept permits biosensors to be assembled and functionalized on-demand and with minimal equipment – just the application of voltage in solutions for assembly of polysaccharide chitosan and then grafting of catechols to enable signal amplification via redox cycling. This process takes minutes and can be built into the experimental protocols instead of the chip design and manufacture processes. That is, this methodology avoids one of the most problematic issues of using biological components in biosensing: the decay of labile biorecognition components that occurs during manufacturing processes and long-term device storage. Specifically, we demonstrated three important advantages of the molectronic sensor. First, through "electrobiofabrication", target electrodes fabricated

inside completely packaged microdevices are functionalized with BBRC films with high spatial selectivity. Second, the molecular electronic properties of the BBRC films provide enhanced functional properties (e.g., signal amplification) that facilitate signal processing. Finally, the generic capacitor feature of BBRC film allows the molectronic sensor to accept electrons from biological reductants. We demonstrated the molectronic sensor in the analysis of several biological samples ranging from small molecules (e.g., PYO), to enzymatic activity (e.g., LDH), to monitoring the status of cellular health (e.g., cytotoxicity).

We believe such "electrobiofabrication" extends our means to develop microfluidic biosensors. We expect biosensors that are functionalized using this technique might be embedded in microfluidic platforms for broader applications. For instance, functionalized sensors with enhanced specificity and sensitivity can be incorporated in microfluidic cell culture systems (e.g., organ-on-a-chip[47,65,166,167]) for self-contained and automated drug screening and toxicity tests. The interrogated volumes using this system are on the order of nanoliters. Also, we have recently immobilized engineered bacteria onto BBRC films for expanded biological functions beyond biorecognition, such as signaling.[52] While we envision this work provides an alternative, simple, and promising avenue for bridging electronics to biological systems assembled within microfluidic platforms, we can envision many additional applications perhaps not confined by fluidics but equally as effective – the sum of these approaches will enrich our abilities to study biology in a variety of contexts.

Chapter 5: Development of a modularly assembled system to facilitate information access from organ-on-chips with quality control

This section is adapted from a manuscript submitted to *Nature Methods* with the title "Chip modularity enables molecular information access from organ-on-chips with quality control". This Chapter incorporates the molecular sensor developed in Chapter 3 to "open" organ-on-chip (OOC) system for direct molecular measurement and interrogation. Unique modular assembly between sensor and OOC system is designed to reduce the system complexity and enable quality control (QC) on each component, which, in turn, maintain assay consistency during long-term experiment.

Abstract

Organ-on-chips (OOCs) are envisioned to replace animal models in preclinical testing. Although significant progress has been made to improve the biofidelity of these devices, analyzing samples within miniaturized structures remains a challenge. Based on the concept of modularity, we developed accessorial modular functional units that facilitate information access from OOCs. Specifically, we developed three mutually independent microfluidic modules: a mixer, a "molecular-electronic" sensor, and a quality control unit. Each module can be interconnected/disconnected, multiplied or replaced as needed. As a proof of concept, we developed an autonomous programed cytotoxicity assay and linked this to a model OOC. Additionally, we developed design criteria for generic use, particularly for sensor measurements that require substrates and enzymes. We monitored sensor function during long-term experiments and, by design, maintained assay consistency by

switching at fouled sensors. Importantly, sensor assembly with biological components and its connection to the OOC requires only minutes and no bulky instrumentation. We believe a modular strategy where subsequent chips are interrogated could provide an alternative and promising path to enhance functionality, reproducibility, and will eventually enrich our repertoire, to access biological information in a variety of contexts.

Introduction

Organ-on-chips (OOCs) are gaining acceptance as *in vitro* models that would ultimately replace animal testing during drug development.[34,37,47,168–170] These miniaturized devices offer numerous advantages over traditional animal models, including reduced sample quantity and their integration of dynamic 3D microenvironment. Efforts have been devoted to recapitulate human tissue-/organ-level physiologies to improve the fidelity of OOCs which, in turn, alleviates the translational barrier from testbeds to *in vivo* expectations. Yet, information access from such miniaturized structures remains a challenge. Optical measurements are incorporated that often produce end-point data, their laborious labeling processes can be detrimental to cell cultures.[37,169,171,172] Recently, analytical interrogation using microelectronics-based sensors have opened an alternative pathway. With benefits of high detection sensitivity and high versatility, these sensors have been patterned into OOCs for analyzing tissue barrier integrity[173], cell migration[174], fluid pressure[175] and oxygen[41]. These integrated sensors can significantly increase the complexity of OOC design and fabrication and this can hamper the translation of these technologies from lab to industry.[134,176–182] In addition, chemicals involved in many sensors have

potential toxicity to cell cultures.[54,58,183] Short sensor shelf life and the lack of quality control further complicate assay inconsistency during long-term testing.[184,185]

Here, we propose to apply modularity to facilitate information access from OOCs while getting around the aforementioned concerns. Instead of monolithic OOCs with integrated sensors, we develop three categories of accessorial modular units, each with a unique functionality: input (e.g., medium/drug introduction), output (i.e., sample analysis), and quality control (QC) (**Scheme 4.1**). All modules are mutually independent and can be interconnected/disconnected, multiplied or replaced in an analogous manner to Lego™, but connected using microtubing. Upon being connected, the accessorial modules process information from the target OOC without increasing its complexity. To demonstrate this concept, the modular units are devised to evaluate culture cytotoxicity. Specifically, sample from a model OOC (cell culture in a simple 2D microdevice that contains a to-be-assayed enzyme) is first transferred into a mixer module, in parallel with enzyme substrate, and converted to final product that is then detected by a sensor module downstream. The entire process, with the exception of attaching modules with tubings, is entirely hands-free. Specifically, a redox-based sensor was developed to measure the activity of a cell death biomarker, lactate dehydrogenase. We show how this cytotoxicity assay works using a model cell line, human colorectal adenocarcinoma cells (Caco-2 cell), disturbed by a drug mimic (e.g., Triton X-100). The controlled fluidics within the modular system excludes entrée of detrimental chemicals within the sensor module (e.g., lactate[186–189] and catechol[190,191]) from interfering with the cell culture. By switching the OOC to a QC module, sensor function (normally exhibits declining sensitivity due to fouling[192]) is

repeatedly monitored during a long-term experiment (a typical and desired condition for cell and tissue culture). More importantly, we preserve assay consistency by replacing fouled sensors. Further, because electrochemical sensor can be assembled for assaying a variety of molecular species, we have developed design criteria for an enzyme/substrate assay. It should be noted that although this study focuses on a cytotoxicity assay, the concept of modularity and the design attributes described here can be extrapolated to broader studies and applications.

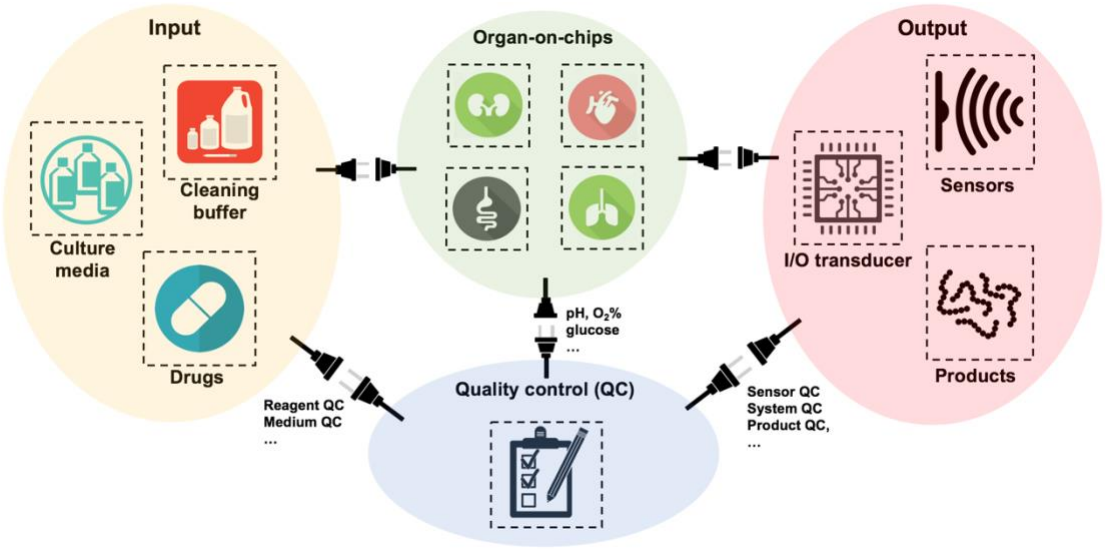

Scheme 4. 1. Schematic of modular connected organ-on-chips (OOC) system. Module in the system can be reversibly assembled in an analogous manner to Lego™, but connected using microtubing. "Input" modules can be placed upstream to OOCs to supply culture media for cell cultivation, introduce drug for screening, or even flush the system with cleaning buffer. Effluent from OOCs can be exported into "output" modules, wherein analytes of interest can be measured. In the case of bioreactor, cellular products can also be collected using output modules. Most importantly, the flexibility of modular assembly enables us to design unique modules to conduct quality control (QC) on each component in the system from input modules (e.g., medium quality, reagent activity), OOCs (e.g., pH, glucose, dissolved O_2 level), to output modules (e.g., sensor accuracy, transducer function).

Materials and Methods

Device fabrication. All microfluidic devices were created using standard soft lithography methods, performed in the Maryland Micro and Nano Fabrication Center.

Device designs were modelled on AutoCAD (Autodesk, Inc., Mill Valley, CA) and developed as a Mylar mask. SU-8 3050 photoresist (MicroChem, Westborough, MA) was deposited onto a sterilized 4 inch diameter silicon wafer. After spinning the wafer for 45 seconds at 2600 rpm, the wafer and photoresist were soft-baked at 95 ^{o}C for 15 minutes. The Mylar mask was aligned with the wafer to transfer the design onto the photoresist through UV light exposure (405 nm wavelength) using an EVG 620 mask aligner (Electronic Visions Inc., Phoenix, AZ) at an exposure energy of 23.4 mW cm^{-2}. After undergoing a post-exposure bake of 95 ^{o}C for 20 minutes, the wafer was submerged and agitated within SU-8 developer (MicroChem) for 8 minutes to create the final master structures. Isopropanol and deionized (DI) water was used to wash away residual photoresist.

The microchannel layer was made from polydimethylsiloxane (PDMS) (Sylgard 184, Dow Corning Co., Midland, MI) cast on an SU-8 master. PDMS was prepared by mixing the polymer material and curing agent (10:1 w/w) and deposited on the master structures followed by baking at 60 ^{o}C for 1 hour. Upon PDMS delamination from the mold, a 1 mm biopsy punch (Miltex, York, PA) created inlets and outlets. Cell culture devices were created by subjecting a PDMS layer and 30 mm glass coverslip (Bioptechs Inc., Butler, PA) with oxygen plasma using March Plasmod oxygen plasma cleaning system (Nordson Plasma Systems, Concord, CA). Microfluidic mixers were created in a similar fashion but used PDMS as the base layer instead of a glass surface. The base layer for the sensor contains a pattern of three-electrode system that was custom designed on AutoCAD, converted, exposed, and developed onto a stainless-steel shadow mask. The pattern was transferred from the mask to

circular glass coverslips by depositing 5 µm chromium and 50 µm gold sequentially using Metra Thermal Evaporator (Telemark, Battle Ground, WA). Sensors were fabricated by bonding the PDMS channel layer to the base layer with proper alignment. The sensor was equipped with a holder and rod electrodes for simple and stable connection to the external electrical source. Both sensor holder and modular chip holder were designed using Solidwork (Dassault System, Velizy-Villacoublay, France) and 3D printed by a Connex 3 Object500 and MED610 ink (Stratasys, Eden Prairie, MN).

Preparation of "molectronic" sensor with bio-based redox capacitor (BBRC) films. The sensors were functionalized with BBRC films in two steps.[54,59,60] First, the target working electrode was connected to an external electrical power supply (2400 Sourcemeter, Keithley, Cleveland, OH) and set as the cathode. A nearby electrode was set as the anode. The microchannel (3 mm x 3 mm x 100 µm) was filled with 1.1% chitosan solution (dissolved in water and adjusted pH to 5.6 using 1.0 M HCl) (Sigma-Aldrich, St. Louis, MO) to immerse both electrodes. A constant current of 3 A/m^2 was applied for 30s to selectively electrodeposit chitosan film (~ 50 µm thick[146]) on the cathode. Second, the device was connected to a potentiostat for catechol grafting. The channel was filled with catechol solution (5 mM in 0.1 M phosphate buffer (PB), pH 7.0) (Sigma-Aldrich), and a constant anodic potential of +0.6 V (vs Au) was applied for 3 min to oxidize the catechol. The oxidized catechol (i.e., o-quinone) undergoes grafting reactions to the chitosan film.[56,58,149] In order to confirm the signal amplification capabilities of the film, the channel was filled with 50 µM 1,1'Ferrocenedimethonal (Fc) (Acros Organics, New Jersey, NJ) and 50 µM

hexaammineruthenium chloride (Ru^{3+}) (Sigma-Aldrich, St. Louis, MO) in phosphate buffer (PB) (pH 7.0). Chronocoulometry (CC, 0.5 V, 120s) was applied to electrochemically charge and discharge BBRC films. Films at fully charged and fully discharged states were generated by the electrochemical redox-cycling reactions. The resulting sensor is name as "molectronic" (i.e., molecular to electronic) sensor.

Modular system dynamical characterization. The system was assembled by connecting the OOC, the mixer and the molectronic sensor sequentially via microtubings as depicted in **Fig. 4.1A**. The mixer was connected to both the OOC and a syringe filled with substrate solution for LDH catalyzed reaction (i.e., 20 mM L-lactate (Sigma-Aldrich), 10 mM β-nicotinamide adenine dinucleotide sodium salt (NAD+, Sigma-Aldrich), 50 µM Fc in PB). The system was driven by syringe pumps (Kent Scientific, Genie Plus; Fisher Scientific, Single Syringe Pump) propelling PB and LDH substrate at flow rates of 30 µl/hr and 270 µl/hr, respectively. To examine the fluidic dynamics in the system (mainly from OOC to sensor), Fc was used as an electrochemical tracer. Fc (500 µM in PB) was manually introduced into the OOC as sample. At time zero, the device was plugged into the system (**Fig. 4.1A**) when time was set as t_0. A constant chronoamperometry (CA) was applied to monitor Fc concentration in the molectronic sensor. In parallel, fluid dynamics and finite element simulation were respectively modeled using MATLAB software (The MathWorks, Natick, MA) and Comsol Multiphysics (COMSOL Inc., Stockholm, Sweden). In MATLAB, the axial dispersion model was applied based on Fick's law ($\partial C/\partial t = D \times \partial^2 C/\partial x^2$, D = diffusion coefficient). The minimal lengths for both the mixer and the connecting tubing (extender) between the mixer and the sensor were

calculated to accommodate the mixing molecules with different diffusion coefficients and enzymatic kinetics. The minimal detectable signal by the sensor was set as background noise level plus three times of standard deviation (σ). The minimal extender length is modeled based on equation $L = ((143.7 - 16.5 \times x)/x) \times 33.3$, where L is the minimal length of the extender for the LDH reaction to generator a minimal signal (143.7 μM of NADH), x is the maximal reaction rate (V_{max}) of LDH and 33.3 is the flow speed in unit of mm s^{-1}.

On-chip cell culture. The model cell line used in this study was Caco-2 cells obtained from American Type Culture Collection (Manassas, VA). Cells were maintained using Dulbecco's Modified Eagle Media (DMEM) (Gibco, Grand Island NY) supplied with 10% fetal bovine serum (FBS) and 1% pen-strep antibiotic (Gibco) in T75 flasks under 37 ºC and 5% CO_2 level and passaged every three days. The devices were sterilized with 70% (v/v) ethanol and 30 minutes of UV light exposure before cell introduction. Sterilized channels were coated with 50 μg/ml type I collagen and 300 μg/ml Matrigel matrix (Corning, Corning, NY) at 37 ºC for 2 hours. Caco-2 cells were then gently transferred to the device using 1 ml syringes at approximately 1.5 x 10^5 cells/cm^2/ml. Once the inlets and the outlets have been sealed, the device was incubated at 37 ºC in 5% CO_2 for 1 hr to allow cells to attach to substrate. Then, culture media was perfused through the channel at a constant flow rate of 30 μl/hr to replenish nutrients. The entire culture system was incubated at 37 ºC in 5% CO_2 for 24 hours before experiment. The viability of on-chip culture was assayed and visualized with a LIVE-DEAD viability/cytotoxicity kit (Thermo Fisher Scientific, Waltham, MA) and the molectronic sensor.

Microfluidic mixer characterization. The mixer was characterized using 1.5 x 10^{-5} M fluorescein isothiocyanate (FITC) (Thermo Fisher Scientific, Rockville, MD). This method was based on the observation that the intensity of fluorescence emission from fluorescein solutions in a microfluidic channel (depth 100 μm) was linearly proportional to the fluorescein concentration (not shown). This linearity held when the fluorescein concentration was less than 10^{-3} M.[116] FITC and deionized (DI) water were introduced into the mixer at flow rates of 30 μl/hr and 270 μl/hr, respectively. At steady state, fluorescent images were taken using a CCD camera, an inverted fluorescence microscope, a FITC filter cube, and a 10X Olympus objective lens. Fluorescence intensity was analyzed using ImageJ (shareware: https://imagej.nih.gov/ij/) and normalized to fluorescent intensity at the inlet.

Cytotoxicity testing. To chemically disturb cell cultures in microfluidic devices, a drug mimic, Triton X-100 was used. Triton X-100 was diluted in DMEM and pumped into devices at 40 μl/hr for 3 minutes. Then, the outlets were sealed to stop the flow and the device was incubated at 37 ^{o}C for 2 hours. After the incubation, the cell culture modules were "plugged" into the cytotoxicity testbed (i.e., the inlet and the outlet were connected to a syringe and the mixer, respectively). Time was set as t_0 when the device was plugged in. The molectronic sensor starts to discharge at t = 4 min (optimized time so that BBRC film can be fully discharged before contacting sample). The BBRC was fully discharged (i.e., no further change in CC, the film's catechols were all in oxidized =O form) at t = 12 min. Then, a 10-minute sensor charging was set to allow the BBRC films being enzymatically charged (i.e., the film's quinones were converted to catechols) by NADHs produced through LDH catalyzed reactions. At t = 22 min, CC

was applied to measure the electrons accepted and stored in the BBCR films. Based on the in vitro assays and data from previous work, cells treated with 0.1% of Triton X-100 were set as the positive controls (the viability of cells was near 0% as shown in Chapter 3). Cell-free DMEM was set as the negative controls. The cytotoxicity of each sample was calculated using equation (1):

$$\text{Cytotoxicity}\ (\%) = [\text{LDH}]/[\text{LDH}]_{\text{Max}} \times 100\%, \quad (1)$$

Where [LDH] referred to the normalized LDH level measured in each sample and $[LDH]_{Max}$ referred the normalized LDH level in the positive control. All [LDH] were normalized by subtracting the negative controls. For standard curve preparations, LDH stock solutions were spiked into the substrate solution to make samples with LDH concentrations of 0 unit/L, 15 unit/L, 30 unit/L, 45 unit/L, 60 unit/L, 90 unit/L and 120 unit/L (1 unit of LDH produces 1 μmol of NADH in 1 minute). After each experiment, the system was washed with PB thoroughly.

Long-term cell culture and quality control (QC). To evaluation sensor stability during long-term experiment, quality control (QC) units were connected to the mixer in replacement of the model OOC. The QC units have the same configuration as the model OOC but contains sensor characterization solution (50 μM Fc/Ru^{3+} in 0.1 M PB, pH 7.0) instead of cell culture. The sensor characterization solution was used to test the maximal electrochemical signal amplification capacity (i.e., charging the film with excess Ru^{3+} followed by titrating the film with excess Fc). Such measurement was conducted between every cytotoxicity testing. The sensor was replaced once lost its performance.

A five-day experiment initiated with two OOCs incubated simultaneously at 37 ^{o}C in 5% CO_2 with continuous perfusion of warm DMEM at flow rate of 30 µl/hr. After every 24 hours, cells were treated with 0.1% Triton X-100 followed by cytotoxicity testing. This experiment was repeated for five days. The cytotoxicity testing was conducted using two groups of sensors: 1) daily made and "modular" assembled sensors; and 2) long-term "built-in" OOC/sensor modules that were incubated with the OOCs. Cytotoxicity was calculated using equation (1), except results were normalized to the LDH level measured in day 1.

Instrumentation. All electrochemical measurements were performed using a CHI 6002e electrochemical analyzer (CH instruments, Austin, TX). Caco-2 cell cultures were imaged using a fluorescence microscopy (BX 60 microscope; Olympus) and a digital camera (Olympus DP72).

Statistical analysis. All assays were performed in triplicate. Results were expressed as mean ± standard error. One-way ANOVA was used to determine significant differences between groups. The level of significance was set at $\alpha = 0.05$. The Pearson product-moment correlation coefficient was applied to measure the strength of linear correlation between groups. The level of significant correlation was set at $r = 0.95$.

Results and Discussion

Modular assembly – design and characterization. The modular system demonstrated here consists four components: an OOC (2D on-chip cell culture) and three accessorial modular units including: (i) a mixer wherein the OOC sample

affluent is mixed with substrate and converted to an assayed biomarker; (ii) a "molecular-electronic (molectronic)" sensor that measures the biomarker quantity electrochemically; and (iii) a quality control (QC) module (see **Scheme 4.1**) that replaces the OOC to monitor sensor function. Each module is connected via microfluidic tubing wherein length is a design parameter; the system is controlled via syringe pumps and programmable electronics. Since the concept of modularity is envisioned to be generalized to expanded OOC applications, fluidic and enzymatic kinetic analyses were conducted to provide criteria for designing critical dimensions in the system. That is, the length of the mixer is designed according to the criteria that homogeneous mixing between sample and substrate is achieved at the outlet.

Figure 4.1 shows the configured device for this application. Recognizing that the length of the mixer is a function of the enzyme activity, substrate concentration, and fluid flow rate, we performed a modeling analysis to calculate the minimum time (hence distance) needed to accordingly determine analyte level in the sensor chip. **Figure 4.2A** plots the minimal length of the mixer as a function of the diffusion coefficient, for cell/protein and the small molecule substrate. It should be noted that the diffusion coefficient of enzyme (e.g., protein, LDH) is at least one order of magnitude less than chemicals in the substrate and is thus neglected during calculation. The mixer in this study was designed (length = 80 mm) to accommodate all analytes used in this study. Both finite element simulation and fluorescein isothiocyanate characterization revealed homogeneous mixing in the mixer with an expected dilution factor (**Fig. S4.1B-D**). As noted, the length of the extender (distance between the mixer outlet and the sensor inlet) was designed based on the criteria that

a minimal signal (i.e., background + 3σ) is generated when the sample reaches the sensor. Considering OOC samples with different initial enzyme concentrations yield distinct enzymatic kinetics within the mixer (**Fig. S4.2**), the extender length profile is adjusted accordingly (**Fig. 4.2B**). Theoretically, an infinitely long extender is required for sample with an infinite small enzyme activity. It should be noted that as enzyme activity increases, the required length for the extender becomes negative because a minimal signal is generated before leaving the mixer. For instantaneous reactions, the extender is defined by the diffusivity and flow rate. That is, the total reaction time needed is given by the point in the mixer where 100% of the OOC effluent is mixed with the reactants. The extender used in this study (90 mm) ensures that enzymatic reaction is sufficient for all samples and ease of use (spontaneous LDH release from the control group is 27.8 unit/L).

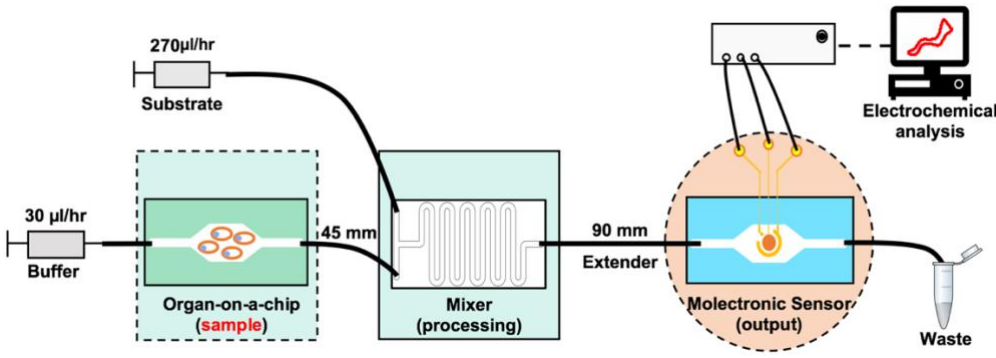

Figure 4. 1. Schematic diagram of the modular assay system.

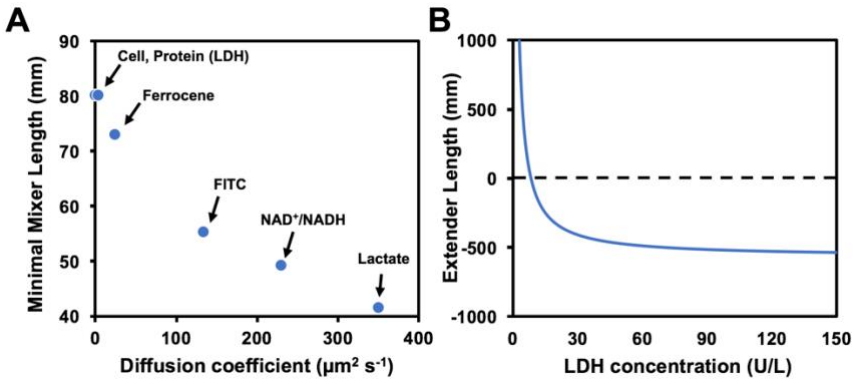

Figure 4. 2. Design criteria for the length of mixer and extender. (A) Minimal length of the mixer required for analytes of various diffusion coefficients to reach homogenous mixing. The diffusion coefficient of enzyme (e.g., LDH) is at least one order of magnitude less than chemicals in the substrate and is neglected during calculation. (B) Minimal length of the extender required to generate minimal signal (background + 3σ) for samples with various enzymatic kinetics. Data adjusted according to **Figure S4.2**.

The fluidic dynamics in the modular system was characterized using 1,1'Ferrocenedimethonal (Fc), an electrochemical mediator. Fc solution (500 µM in PB) was introduced to the OOC as a bolus and flowed downstream (30 µl/hr) to a mixer and a sensor. Chronoamperometry (CA) was continuously applied within the sensor to monitor the prevailing Fc concentration. A substrate solution (i.e., 20 mM L-lactate, 10 mM NAD^+ and 50 µM Fc in PB) was continuously introduced to the mixer at flow rate of 270 µl/hr. The entire system was operated under continuous flow. **Figure 4.3A** represents the concentration profile of Fc measured within the sensor (converted from the measured current). The measured Fc concentration matched our expectation (the final Fc concentration is a combination of 10 times diluted effluent from the OOC and 9/10 times diluted substrate). The result illustrates that after system assembly (t = 0 min), sample (Fc) reached the sensor at t = 13 min and completely exited at t = 25 min. The concentration profile was compared to a plug flow reactor model with axial dispersion. We matched the experimental results

with the model and found the best fit Peclet number (ratio of convective to dispersive flow) to characterize the system (Pe = 150). This high value demonstrates that the flow in the fluidic channels is near ideal and with minimal axial dispersion (i.e., convection-dominated).

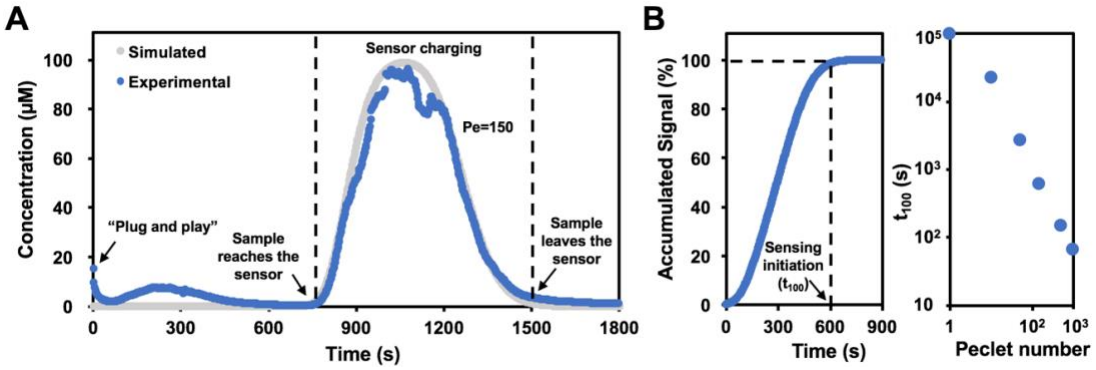

Figure 4. 3. System characterization using Fc. (A) Profile of model analyte (Fc) as it progresses from OOC through mixer and into sensor module. Overlayed with predicted quantity for Pe = 150. (B) Predicted signal accumulation in the sensor module after sample reaches the sensor (left). Time required to reach 100% signal accumulation (t_{100}) is dependent on Peclet numbers (right).

During testing with media and LDH (marker of cytotoxicity), signal (electron from NADH, biological reductant) is first accumulated in the sensor (i.e., sensor charging) before the total charge is measured. The level of accumulated signal is proportional to original biomarker concentration (i.e., NADH) in the sample. Accumulated signal was plotted as a function of time (**Fig. 4.3B**) by calculating the area under the concentration profile in **Figure 4.3A**. The x axis was normalized to the time when the sensor charging begins (i.e., t = 13 min). It should be noted that although enzymatic reaction initiates as soon as sample mix with substrate at the intersection, the product (NADH) has relatively low decomposition rate (6% per hour[193]) and can still be accumulatively measured at the sensor (for the entire duration of the assay is 22 minutes). According to the simulation, a minimum of 10 minutes of charging (t_{100}, see

the arrow in the left panel of **Fig. 4.3B**) is needed to ensure a sufficient signal (~100%) is accounted. We show that t_{100} is linearly dependent on Peclet number in the fluidic system (the right panel of **Fig. 4.3B)**. It should be noted that characterizations described here may not be necessary for assays that do not involved enzyme reaction (e.g., Fc, pyocyanin[55,59], glucose[88]).

Molecular information access from organ-on-chips - cytotoxicity testing using a "molectronic" sensor. We demonstrate a cytotoxicity assay to demonstrate "plug and play" modularity for OOC systems. A model OOC was constructed that contained a culture chamber (3 mm x 3 mm x 100 μm) flanked by two channels connecting both inlet and outlet (**Fig. 4.4**). A human epithelial colorectal adenocarcinoma cell line, Caco-2, was used as a model cell culture. Caco-2 cells are commonly used in drug delivery studies involving transport through the enterocytes lining the human small intestine.[164,165] Caco-2 cells (1.5×10^5 cells/cm^2/ml) were gently introduced into the OOC system using syringes. After 1 hour (cells attached to substrate), pre-warmed and oxygenated culture media was perfused through the channel at a constant flow rate of 30 μL/hr (which produces 0.02 dyne/cm^2 shear stress[37]). The entire cell culture system was incubated at 37 ^{o}C in 5% CO_2 for 24 hours before experiment. In **Fig. 4.4**, Caco-2 cell cultures are shown using microscopy (bright-filed and fluorescence). We used a fluorescence based viability kit in-end-of experiment samples to demonstrate highly viable cells as model inputs. In **Fig. 4.4**, "sample" refers to the supernatants exiting the OOC. That is, upon cell membrane damage, an enzymatic biomarker, lactate dehydrogenase (LDH), is released from cell cytosol to the surrounding environment. This solution contains

LDH and is flowed downstream to the mixer and then sensor modules. The LDH level indicates cytotoxicity of applied drugs or other factors.[154–156]

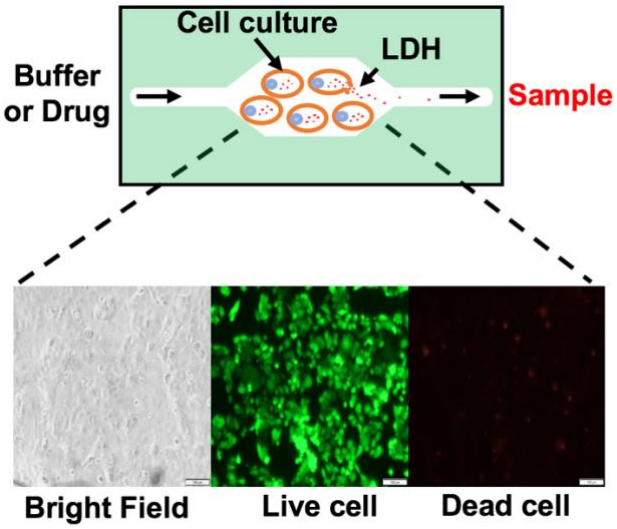

Figure 4. 4. Schematic of an organ-on-a-chip (OOC) module comprised of human intestinal epithelial cells, Caco-2 cells, grown in DMEM. Sample (culture supernatant) is pumped downstream after fluidically connecting to mixer and sensor modules. Microscopic images taken after 24-hr culture indicate coverage and viability (>90%). Scale bar = 100 µm.

The sensor module used in this work is a "molectronic" sensor developed in Chapter 3 (**Scheme 4.2**). A key aspect of the molectronic sensor is its enhanced sensitivity enabled by a catechol-modified chitosan film (i.e., bio-based redox capacitor (BBRC) film) electroassembled onto working electrode.[54,56] BBRC films are non-conducting (i.e., unable to exchange electrons directly with the underlying electrodes) but they are redox-active and can repeatedly exchange (i.e., accept, store and donate) electrons with soluble redox-active species, those either from the biological systems under study or added to the systems to infer biological information. Soluble biological reductants (e.g., NADH generated from LDH-catalyzed reaction) can donate electrons to the BBRC films through a reductive-redox cycling (converting quinone (Q) to catechol (QH_2)), which is also known as "enzymatic film charging" (**Scheme 4.2B**). The electrons stored in the charged film can then be "titrated" (i.e., extracted) by an

oxidative-redox cycling using Fc as mediator (**Scheme 4.2C**). We showed that through redox cycling mechanism, more electrons can be titrated from fully charged films (the film's catechols were all in the reduced QH_2 form), compared with fully discharged films (the film's catechols were all in the oxidized Q form) (**Fig. S4.3**). Hence, through redox cycling significant signal amplification is achieved.

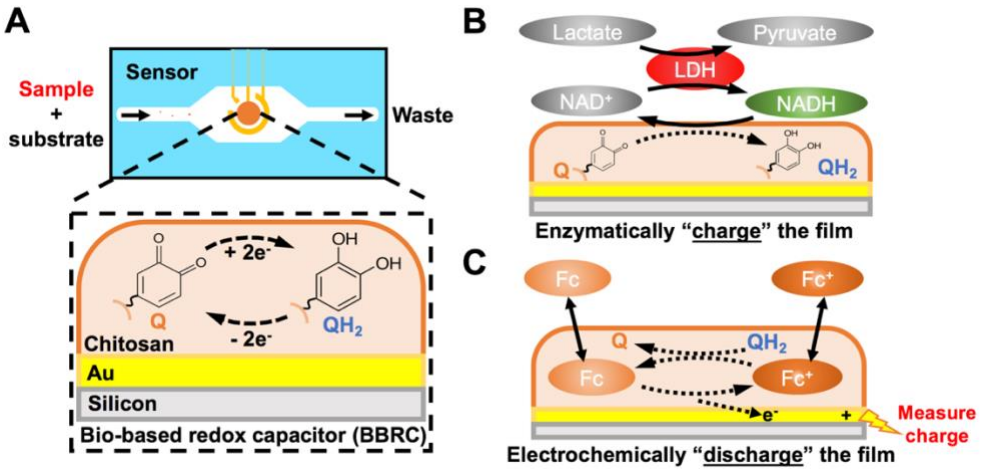

Scheme 4. 2. (A) Schematic of molectronic sensor module. Catechol is conjugated to an electroassembled chitosan film. The redox state of the quinone/catechol can be modulated using redox mediators and applied voltage. The catechol-modified chitosan is referred to as a bio-based redox capacitor (BBRC) owing to its ability to store and exchange electrons. (B) Lactate dehydrogenase (LDH) converts lactate (substrate) and NAD^+ (cofactor) to pyruvate and NADH, which, in turn, donates electrons to the quinone moieties in the BBRC film (i.e., enzymatic charging). (C) Oxidative redox-cycling between Fc^+/Fc and the BBRC film. Using this method, electrons stored in the BBRC film can be "titrated" and quantified as "charge" (current x time). Q: quinone; QH2: Catechol

To measure the cytotoxicity level within the OCC, the molectronic sensor module was connected to the outlet of the mixer module in the fluidic system. Importantly, the sensor module is easily fabricated and easily changed for simple use. Before every test, the sensor was fully discharged (using Fc) to the background level. The OOC module was connected to the inlet of the mixer and sample was assayed according to the protocol described in **Fig. 4.3A&B**. That is, in addition to the OOC outlet, the LDH activity assay is accomplished by introducing excess lactate and NAD^+ (with 50 µM Fc) as substrate that are introduced at defined rates in the feed to the mixer

module. In the sensor module, chronocoulometry (CC) was then employed to quantify titrated charge. In **Figure 4.5A**, the fully discharged BBRC film (the dotted line) was incubated with various solutions with no applied voltage and then each resulting film was titrated by the Fc-redox cycling reaction. Comparing to the control group where the film was incubated in solutions lacking LDH (the grey line), the red line indicates a large oxidative charge curve generated from a mixture of LDH spiked sample and substrate allowed to react during transport through the mixer and extender. These results confirmed that the products from LDH catalyzed reaction charge the BBRC film enabling signal measurement upon oxidative discharging. The magnitude of the signal is dependent on the number of reduced catechols in the film, which, in turn, are linearly proportional to the LDH concentration (**Fig. 4.5B**). Importantly, the response was found to be linear up to 60 unit/L, where the signal appeared to saturate. This signal saturation was presumably due to the limited contact efficiency (confined space for diffusion) between NADH in the bulk solution and the film within microchannel.[160] This size-based limitation should be relieved by either increasing the electrode size or by depositing more catechol-modified chitosan onto the electrode. In the latter case, this demonstrates the ease by which modifications can be made using this methodology. By applying voltage for a longer time drive the electroassembly period, more chitosan can be deposited increasing the number of catechols in the BBRC.

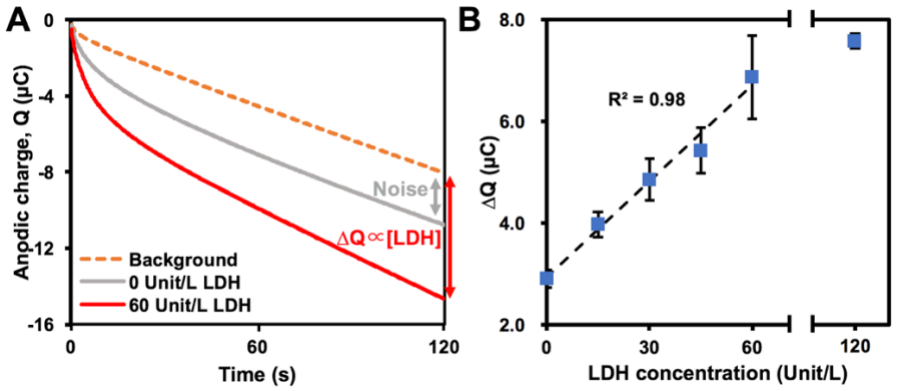

Figure 4. 5. (A) Chronocoulometry (CC) results comparing an LDH-spiked sample (with substrate in PB) to the negative control (film incubated with solution without LDH). The dotted line represents the background where the film is fully discharged using the Fc-oxidative cycling. (B) LDH activity titrated as charge in sensor module.

Using molectronic sensors, cytotoxicity levels of chemically disturbed OOCs were then measured. All results were normalized to the positive control (cells treated with 0.1% Triton X-100 are reported to be 17% viable[194], however in our case shown in Chapter 3, the viability was near 0%) and the negative control (cell-free culture media). Results in **Figure 4.6** corresponded with our expectations that cells treated with the drug mimics (Triton X-100) yielded a significantly higher cytotoxicity level (p = 0.016) than was otherwise observed for healthy cells. Moreover, increased triton X-100 resulted in more cell death (p = 0.001). We also note that the negative mimic case with cells did exhibit a viability of less than 100% (presumably due to spontaneous death).

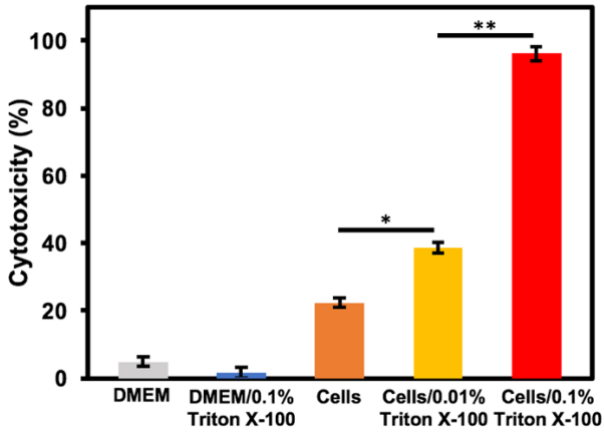

Figure 4. 6. Normalized cytotoxicity measurements on OOCs with various treatments (**, $p < 0.01$; *, $p < 0.05$).

Overall, these data demonstrate that appropriate placement of functional modules (e.g., sensor and mixer) enable the rapid assessment of cytotoxicity in OOC systems. Most importantly, the *in-situ* measurements showed here, are quantitative and require no pooling of sample (essential for samples with volume at sub-microliter scale) and are essentially real-time.

Introduction of a quality control (QC) module

One deficiency associated with current built-in sensors in OOCs is the lack of quality control to monitor sensor function during long-term cell culture. Repeated exposure to cell culture media increases the chance of sensor fouling, which leads to assay inconsistency. We developed modular QC units that contained control solutions (50 µM Fc/Ru^{3+} in 0.1 M PB, pH 7.0) for monitoring sensor function (**Fig. 4.7A**). In this configuration, the QC module replace the model OOC between cytotoxicity tests and enables continued examination of the signal amplification capacity (i.e., capacitance) of the BBRC film housed within the sensor module. Briefly, the BBRC film was electrochemically charged to its fully charged state using the Ru^{3+}-reductive cycling

(i.e., maximal capacitance). The charging state of the film was then titrated and measured by the Fc-redox cycling reaction. A daily decrease in maximal film capacitance was observed in a five-day experiment (**Fig. 4.7B**, data for day 2 and 4 not shown). This drop was presumably due to the fouling of BBRC films upon repeated contacting complex culture media, cell debris and substrate solution (exacerbated in miniaturized device).[192]

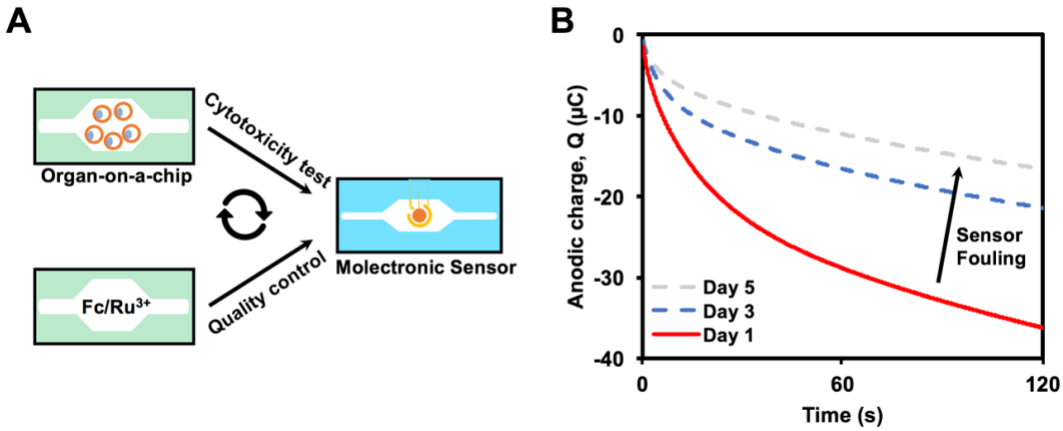

Figure 4. 7. (A) Conceptual scheme of QC module for sensor evaluation. The QC module is exchanged with OOC to conduct sensor quality control. (B) The quality of sensor module was controlled by measuring the maximal signal amplification capacity (fully charged by the Ru^{3+}-reductive cycling followed by titration using the Fc-redox cycling reaction) of the BBRC film within microchannel. CC results of a molectronic sensor at day 1, 3, and 5 were compared. Day 1 is the first day that the sensor is made. The sensor is reused and stored (filled with culture media) at 37 ^{o}C and 5% CO_2.

We tested whether the decrease in maximal film capacity would lead to a decrease in cytotoxicity measurement consistency. For this, we created a long-term exposure test and a plug-and-play modular format. In the long-term "built-in" format, a single sensor was incubated with an array OOCs at 37 ^{o}C and 5% CO_2 for five days. On each day, one OOC (prepared 24 hours beforehand) was chemically treated followed by cytotoxicity test. All tests in five days were conducted using the same "built-in" sensor. In the modular format, sensor function was monitored between assays and

fouled sensors were replaced (typically within 24 hours) (**Fig. 4.8A**). For every measurement, cells in OOCs were cultured and treated (0.1% Triton X-100 in DMEM) in the same manner. In the modular format, daily renewed sensors yielded nearly identical results with variation of less than 10% (**Fig. 4.8B**). By contrast, the measured value of cytotoxicity by the "built-in" sensor showed a constant drop, which was in accordance to the aforementioned decrease in BBRC film capacitance. Cytotoxicity results from these two groups showed a significant difference ($r = 0.603$, $p = 0.015$) even with similar inputs. In sum, our studies suggest that modularity enables us to monitor sensor function and thus maintain assay consistency by adding or replacing modules during long-term experiment.

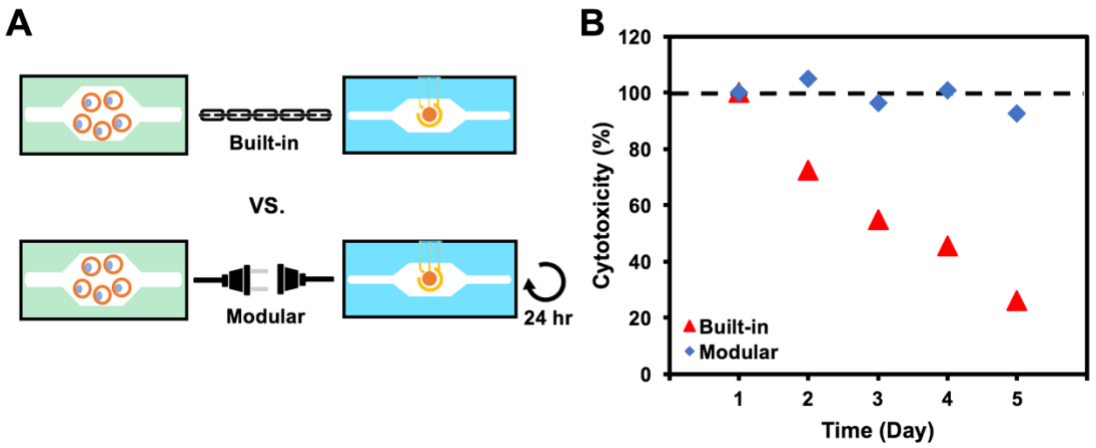

Figure 4. 8. (A) Conceptual scheme illustrating long-term "built-in" OOC/sensor modules (upper) and a "modular" assembly (lower) format. (B) Systems assembled in both "built-in" and "modular" formats were applied to measure the cytotoxicity level of OOCs for five days. For both systems, measured results from day 2 to day 5 were normalized to results from day 1 to compare assay consistency.

Conclusion

Many organ-on-chips (OOCs) utilize optically transparent microfluidic systems so that fluorophores, including those conjugated to antibodies and receptors that fluoresce based on biophysical microenvironments (pH, oxygen level, etc.), can be imaged enabling functional information from within the device. Ancillary MS or LS/MS and other omics based instruments augment fluorescence effect data while vitally important these are often end-of-experiment measures from pooled samples and they typically are not in real time. We have developed a methodology for electro-addressed sensors that provide easily accessed molecular information in near real time. In the present work, we show how various modules including a new quality control (QC) module, when assembled and incorporated into the modular system, provide accurate molecular information in near real time. Modules, including the main cell culture chip, can be assembled and dissembled based on their function and the design characteristics (rapidly assembled sensors, slowly assembled OOC, etc.) Such modular assembly vastly expands our capability to analyze/manipulate sample within miniaturized structure while keeping OOCs at their original designs. The entire process is hands-free after assembling. By controlling fluidics, the modular system prevents unwanted interaction between modules (e.g., deleterious biorecognition components affecting cell cultures). That is, the flexibility enabled by modularity permits all modules to be prepared on demand and, in turn, avoid many problematic issues pertaining to OOC design and use. Integrated sensors, for example, are also challenging due to increased chance of fouling inside OOCs and the decay of biorecognition components. Specifically, we demonstrate a proof-of-concept study by

conducting cytotoxicity measurements on model OOCs (intestinal epithelial cell cultures) using an interconnected microfluidic device consisting of mixers and redox-based "molectronic" sensors. Importantly, we also show how quality control modules could be designed to monitor sensor function (can be extended to other components in the system, see **Scheme 4.1**) and enabled us to maintain assay consistency by replacing fouled sensors.

We believe modularity vastly increases the "toolbox" by which investigators can design, build, and use OOC systems. Sensors, regardless of their biocompatibility and shelf-life, can be modularly incorporated into OOCs for broader information access. While we showed how the system is used to assay enzymatic activity, the same system can be used to assay small molecules that are detected using enzymes. Also, this can be extended to analytes that do not involve enzymatic reactions, such as redox-active molecules (Fc, pyocyanin[55,59]) that are measured directly. Non-redox active molecules can be converted to redox active analytes by enzymes (e.g., glucose[88]) or by cells (cell-based sensor[84]). Future work might incorporate control units (e.g., valves) to develop self-contained *in vitro* testbeds wherein module connection/disconnection is automated, and inputs (e.g., drug stimuli, signaling molecules) and outputs (e.g., cell metabolites, cell behavior) can be programmably controlled and monitored. Eventually, we envision this work provides a promising path to advance our preclinical models for drug development in the pharmaceutical industry.

Supplementary Information

Characterization of microfluidic mixer module. In order to initiate LDH-catalyzed reaction, a microfluidic mixer was designed and placed downstream to the model OOC while upstream to the sensor. The mixer contains a serpentine shaped channel (~80 mm x 0.5 mm x 0.05 mm), where sample and substrate solution merge at the intersection (**Fig. S4.1A**). The flow rates of sample and substrate were optimized to be 30 µl/hr and 270 µl/hr so that the mixing was homogenous. The sample was estimated to be 10 x diluted at the outlet. This expectation was proved by both simulation result and experiment data from FITC characterization (r = 0.99) (**Supplementary Fig. 4.1B-D**).

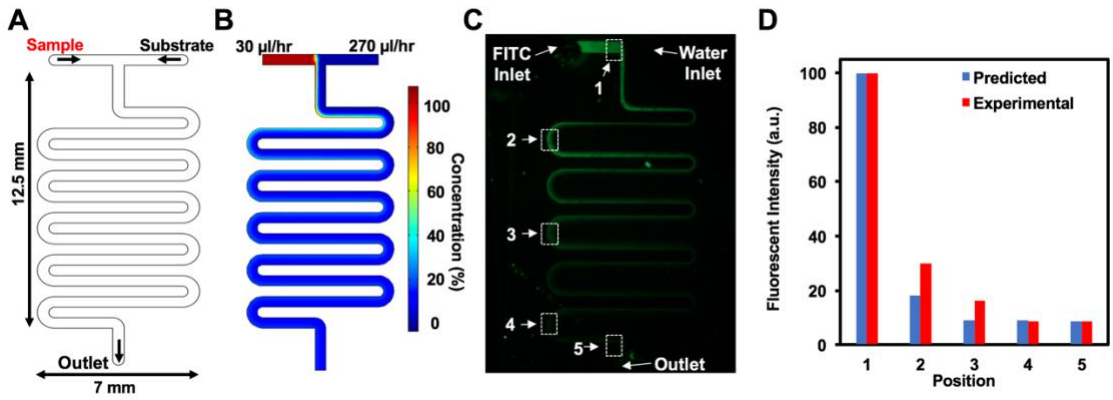

Figure S4. 1. (A) Design of the microfluidic mixer. Sample generated from the model OOC is introduced from one of the inlets at flow rate of 30 µl/hr. Substrate is pumped through the other inlet at flow rate of 270 µl/hr. (B) Finite element simulation of fluidic dynamics within the mixer. (C) Fluorescent microscopic image of the mixer characterized by FITC. Five positions along the mixer are highlighted and marked as position 1 to 5. (D) Transversal average fluorescent intensity of position 1 to 5. Experimental data are compared with simulated results.

Enzymatic kinetics within the mixer. Cytotoxicity measurement in this study relies on the measurement of NADH, a product from LDH-catalyzed reaction. This reaction initiates as soon as sample and substrate (always in excess amount) start mixing

within the mixer and the enzymatic kinetics is dependent on the initial enzyme level and the mixing. **Figure S4.2** plots the NADH concertation produced within the mixer module as a function of reaction time (reflected by position in the mixer as flow rate is constant). During mixing, the reaction rate (V) increases linearly as a function of time and thus, NADH concentration increases exponentially (i.e., the integral of "V vs. time"). The reaction rate becomes constant (maximal reaction rate, V_{max}) the reaction curve turns linear as mixing becomes homogeneous (~ 50 mm for NAD^+ and lactate, see **Fig. 4.2A**). Sample with higher initial LDH concentration (V_{max}) generates larger of NADH within the mixer. This data is used to adjust the extender length between the mixer and the sensor (see **Fig. 4.2B**).

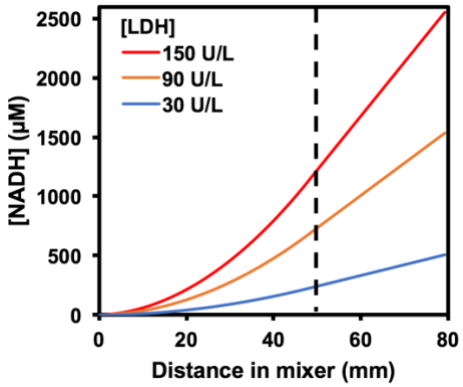

Figure S4. 2. Enzymatic kinetics of samples with various initial enzyme concentrations within the mixer. Distance in mixer starts from the place where sample and substrate starts to mix (0 mm) and ends at the outlet (80 mm). The exponential growth of NADH is due to the mixing between the substrate and LDH sample, which increases the number of activated LDH (i.e., increase the total reaction rate) as a function of mixing time. Dashed line indicates where mixing becomes homogeneous and the reaction rate becomes constant (i.e., V_{max}).

Characterization of molectronic sensor. The key part of the molectronic sensor is a bio-based redox capacitor (BBRC) film functionalized on the working electrode. This film consists catechol modified chitosan hydrogel. The redox-active catechols endow BBRC films with the ability to accept, store and donate electrons with soluble redox-active species. This ability was validated by electrochemically charging the films

(Ru^{3+}-reductive cycling, converting quinone (Q) to catechol (QH_2)) to different charging state followed by titrating (Fc-oxidative cycling, converting QH_2 to Q) the film for measurement. Using this method, CC analysis for fully charged (the film's catechols were all in the reduced QH_2 form) and fully discharged (the film's catechols were all in the oxidized Q form) films were demonstrated in **Fig. S4.3**.

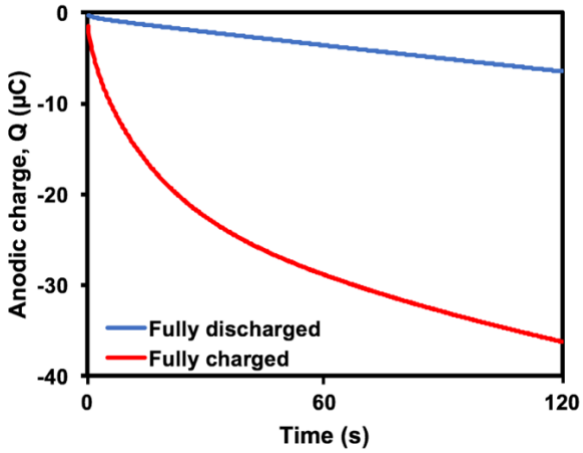

Figure S4. 3. Chronocoulometry (CC) of Fc oxidation at the surface of electrodes modified with fully discharged and fully charged BBRC films.

Chapter 6: Conclusions, contributions and future directions

Conclusions

In this study, we have developed microfluidic devices as *in vitro* tools for research and drug development for gastrointestinal (GI) disease. Due to the unique microbial-host interplay in the GI tract, devices were designed for studying both microbes and enterocytes. In Chapter 2, a bilayer membrane-based microfluidic gradient generator was built to establish long-lasting and linear chemical gradients for investigating gradient-sensing behaviors of non-adherent cells. Effectively, chemo/pseudotaxis of wildtype bacteria and engineered probiotics were validated on both population and single-cell levels (using a custom designed single-cell tracking program). In Chapter 3, we developed a novel "molectronic" sensor based on our "electrobiofabrication" toolbox. The key aspect of the sensor was a miniaturized redox capacitor (catechol-modified chitosan hydrogel film) assembled within microchannel with spatial selectivity. The redox capacitor was redox-active, endowing the sensor with the capability to facilitate electrochemical signal processing. We demonstrated the application of the molectronic sensor in assaying a microbial toxin (pyocyanin) as well as the cytotoxicity of a drug mimic (Triton X-100) on intestinal epithelial cells. In Chapter 4, we developed the concept of "modularity" to the OOC community. We interwove microelectronics-based sensors with organ-on-chips (OOCs) so as to facilitate information access the otherwise overly complex OOC systems. Specifically, we expanded the work from Chapter 3 and developed an assembled platform that consisted of four modules, each with a unique function. Using this

platform, the viabilities of intestinal epithelial cell cultures were examined. More importantly, the flexibility of modular assembly enabled us to monitor sensor function (by quality control modules) and maintain assay accuracy by switching fouled sensors, both of which were inaccessible to integrated sensors within OOCs, the more common approach. In sum, the microdevices and introduction of modular system design developed throughout this dissertation will enrich our ability to interrogate microbial and enterocytic phenotypes, and at the same time improve the drug development process for GI disorders (e.g., probiotics-mediated targeted therapy) and beyond.

Contributions

Cumulatively, this work helps to advance the prospect of *in vitro* testbeds for drug discovery. Specializing in GI disorders, the microdevices developed in this study highlight the optimal strategies to interrogate microbial and enterocytic phenotypes. Perhaps more importantly, we improve the underlying methodologies of the design and fabrication of current microfluidic devices, which further aids their exploitation and dissemination.

By improving upon existing microfluidic gradient generators, we optimized device configurations to accommodate the gradient-sensing study of non-adherent cells. While achieving linear and stable chemical gradients within short time, we simplified both device fabrication and handling. Additionally, we successfully coupled the device to a custom designed Python software (Trackpy) that selectively tracks the trajectory of target cells and quantitatively evaluates their movement. We have

uploaded this program online for free download. The underlying thoughts behind the user-friendly gradient generator and the Trackpy software were to provide amenable means for microbiological laboratories who are not specialized in microfluidics nor software programming, to investigate cell and tissue biology. While in this dissertation we have demonstrated chemo/pseudotaxis towards glucose, pyocyanin and H_2O_2, the platform established here can be reconfigured to suit a variety of chemo/pseudoattractants for an array of purposes.

Through the development of the "molectronic" sensor, we demonstrated functionalizing target electrodes contained inside completely packaged microdevices with spatial selectivity using our "electrobiofabrication" toolbox. Importantly, this effort uncouples device fabrication from sensor functionalization and may be useful to researchers and companies seeking to avoid the decay of labile biological components that often occurs during manufacturing processes and long-term device storage and use. For the ease of fabrication and use, the microelectronic systems were fabricated using gold (Au) instead of the more standard silver electrode. We showed, however, that the electrochemical cells made with the Au reference electrodes yielded quantitatively similar results to those with a standard silver reference electrodes. Offering additional electrode materials provides yet another option for researchers, depending on their device design. We also observed that the miniaturized catechol-modified chitosan film (BBRC film) possessed a nearly identical redox activity (signal amplification capability) to BBRC film fabricated at the macroscale; thus, effectively we have extended our electrobiofabrication toolbox from physical self-assembly mechanism to electrode-induced covalent modification of film within

microdevice, and interrogated miniature samples on the order of nanoliters. On the broadest level, this work further contributes an alternative modality to examine biological system, especially within microdevice, via a redox perspective.

In our efforts to install OOCs with the molectronic sensor for cytotoxicity test, we demonstrated that sensors can be modularly assembled to OOCs in an analogous manner to Lego™, but connected using microtubing. Compared to the prevalent "built-in" style, a modular assembly format was shown to possess prominent advantages: 1) OOCs were equipped with biosensing functionalities while retaining their original designs (i.e., systems were not complicated); 2) unwanted interactions between modules (e.g., deleterious sensor components affecting cell culture) were prevented by programmed fluidic control, and 3) the flexibility of modular assembly permitted module addition/subtraction, multiplication and replacement as needed. Taking advantage of the flexibility of the modular system, we designed Quality Control (QC) units to monitor sensor function, which allowed us to maintain assay consistency by switching fouled sensors during testing. To the best of our knowledge, this is the first work that enables QC evaluation of system components. Our concept of modularity provides an alternative and promising path to strengthen the current OOCs methodologies enabling more extensive functionalities which, we believe, will be broadly applicable. It is our hope that researchers or companies will find this method simple and useful so that they will examine its potential in their own applications.

We envision that the research performed in this dissertation will extend *in vitro* systems from recapitulating complex *in vivo* structures and contexts to be "opened" for molecular measurement and interrogation. These capabilities will enable an understanding of the richness of biology's molecular communication as well as the opportunity to enlist *in vitro* tools for discovering disease mechanisms and therapeutic interventions.

Future directions

Expanding upon the molectronic sensor described in Chapter 3 of this dissertation, we have already begun to construct cell-based molectronic devices by adding an additional layer of genetically rewired cells on top of the BBRC films for bidirectional "molecular-to-electronic" signal transduction. As described prior in this dissertation, the BBRC films enable real-time electrical sensing of redox active molecules. These, in turn, survey molecular space in an analogous manner to radar, but use electrochemistry. Then, engineered cells layered on top of the BBRC films, can potentially recognize a redox input and genetically synthesize a signaling molecule output (i.e., "electro-molecular" actuator) or, conversely recognize a vast array of signaling molecules and provide a redox output (i.e., "molecular-electro" sensor). (**Scheme 5.1**)

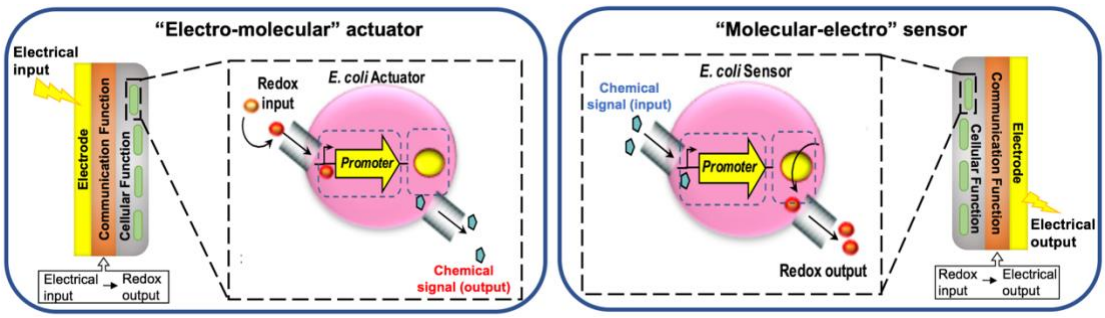

Scheme 5. 1. Schematic of "electro-molecular" actuator" and "molecular-electro" sensor assembled onto electrodes otherwise placed at the bottom (or side) of microfluidic channels. Both devices are comprised of an electrode, a redox-based "communication" function and a "cellular function" that together, mediate bidirectional "molecular-to-electronic" signal transduction.

Through synthetic biology, we are engineering *E. coli* cells as "translators" between signaling molecules and redox active molecules. In a recent study by Liu et al.[84], we demonstrated cell-based detection of non-redox active bacterial quorum sensing molecule, autoinducer-2 (AI-2), by making use of electrochemical measurement of β-gal, which converts 4-aminophenyl-D-galactopyranoside (PAPG) to redox-active p-aminophenol (PAP) (**Fig. 5.1**). We have generated preliminary data showing a linear correlation between measured CV result and AI-2 concentration (**Fig. 5.1C**). Using the same approach, cells can be engineered to translate a wide range of molecules. For example, our collaborator has developed *E. coli* strains expressing β-gal in response to IFNγ and TNFα, both important inflammatory GI-tract cytokines.[195]

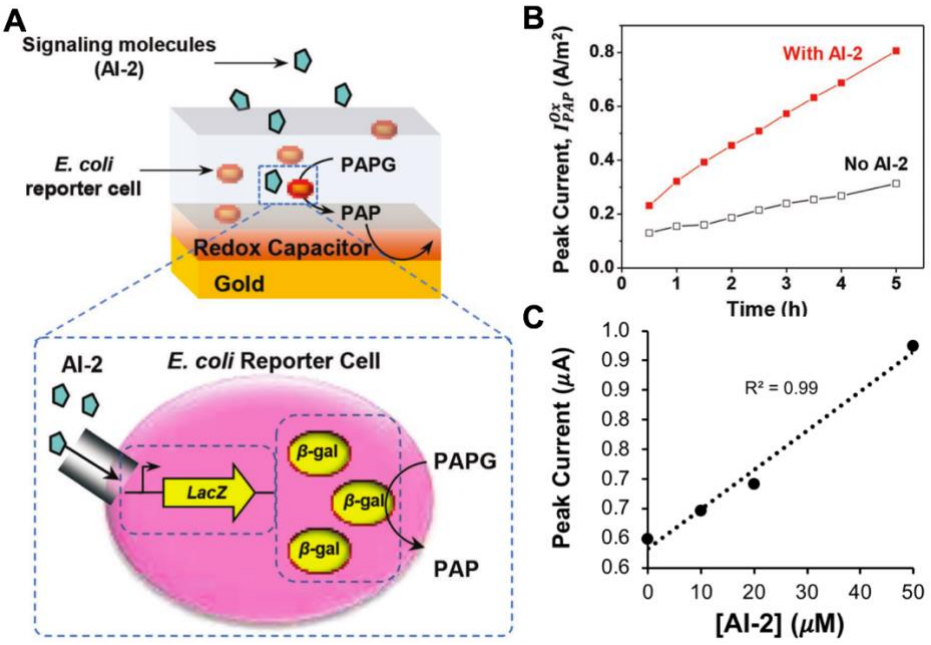

Figure 5. 1. AI-2 detection using cell-based molectronic sensor. (A) Schematic illustration showing signaling molecule AI-2 triggers β-gal expression in the engineered *E. coli* reporter cell; the enzyme β-gal converts PAPG to redox-active intermediate PAP; the redox-capacitor transduces PAP into amplified electrochemical output. (B) Peak current of cyclic voltammetry (CV) results from AI-2 measurement using the bilayer cell-based sensor as a function of AI-2 incubation time. (C) Peak current of CV results from AI-2 measurement using the bilayer cell-based sensor as a function of AI-2 concentration. Data presented in (A)&(B) are adapted from Liu et al, (2017) with permission.[84]

We also demonstrated electrode actuation of gene expression in *E. coli* (**Figure 5.2**).[81] Electrode-oxidized pyocyanin (PYO) initiates expression of fluorescent marker, phiLOV, from an engineered soxRS regulator. Supplementation with redox mediator, ferricyanide (FCN), amplifies expression 100-fold resulting in a linear relationship with applied charge. However, PYO is commonly known as a toxin and can disrupt the integrity of epithelial cells.[196] To obviate the need for PYO, we will develop an analogous H_2O_2 actuation system for *in-situ* electrode-based H_2O_2 generation and genetic actuation (via oxyRS). Because H_2O_2 is unstable, the bilayer configuration from **Scheme 5.1** which retains cells at the electrode surface is particularly well suited for this electrogenetic switch. That is, the H_2O_2 will be

surface generated, likely only diffusing to the outer reaches of the hydrogel. In the future work, the fluorescence marker used here can be replaced by a variety of genes that express protein of interest (e.g., signaling molecule, AI-2).

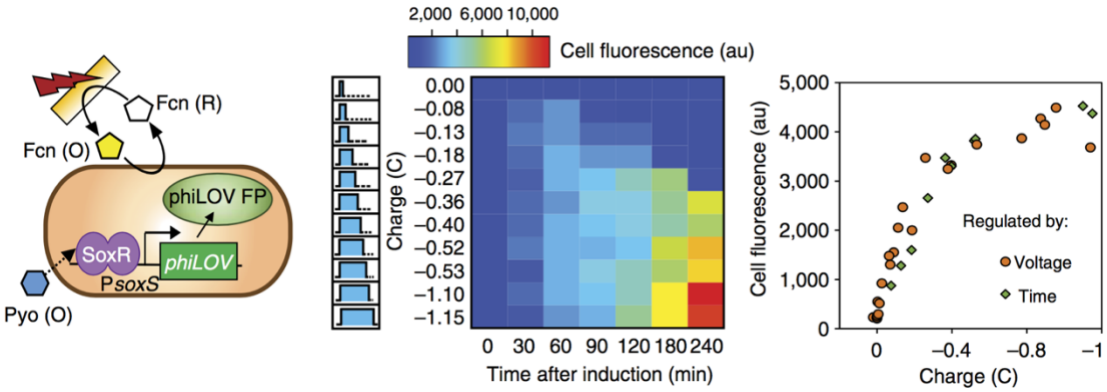

Figure 5. 2. Electrogenetic actuation of gene expression by oxidation of redox active signaling molecules, pyocyanin (PYO). Cell fluorescence (phiLOV expression) over time and as function of charge (current x time). Data adapted from Tschirhart et al, (2017) with permission[81]

In both configurations, we believe the integration of actuating cells or sensing cells engineered via synthetic biology greatly increases the molecular communication "bandwidth". Together, these next generation molectronic devices (cell-based) will further "open" the biological systems for not only interrogation but direct electrical control, greatly expanding "molecular communication".

Next steps include integrating the cell-based molectronic devices (i.e., "electro-molecular" actuator and "molecular-electro" sensor) with OOCs (here, *in vitro* GI model) in a modular format described in Chapter 4 for spatiotemporal control and reporting intra- and inter-kingdom signaling events (**Scheme 5.2**), which is currently unavailable in microsystems (or in macrosystems).

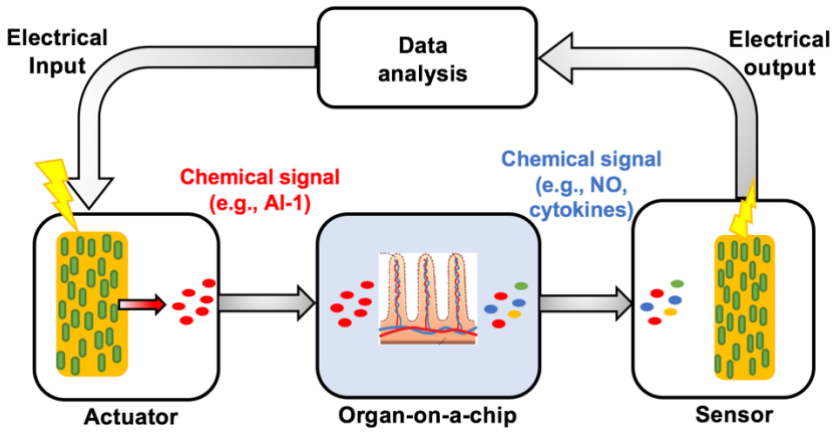

Scheme 5. 2. Schematic of a modular system for intra-/inter-kingdom signaling research. Both "electro-molecular" actuator and "molecular-electro" sensor devices are modularly connected to organ-on-a-chip (GI model) for evaluating stimulus and response dynamics of molecular signaling events within the system. Electrical output from the sensor can be analyzed outside the system to modulate electrical input to the actuator. Together, these signal transductions form a feedback loop that is essential in disease study and drug screening.

Our group has previously illustrated inter-kingdom communication between intestinal epithelial cells (IECs) and bacteria using *in vitro* systems and shown inflammatory response of IECs to quorum sensing (QS) molecules secreted from bacteria.[197,198] These results will be recapitulated utilizing modular systems spanning physiological relevant time scales with spatiotemporal control/reporting. Importantly, *in vitro* GI models will be built to improve biofidelity by recapitulating the 3D microenvironments of the villous structures. Epithelial cells grown in such 3D environments experience dynamically-changing gradients of growth factors [199] and oxygen supply[23] and others, which play key roles in cellular growth and differentiation. Recently, we have developed innovative top-down 3D printing methodologies using Nanoscribe™ (a high-resolution 3D printer) to assemble 3D porous villus structures directly within microchannel (**Fig 5.3)**. We believe that such 3D structures will provide excellent models to represent the gut microenvironment as proven by our collaborator, who has successfully demonstrated that IECs exhibit

physiological relevant features when co-cultured on villous scaffolds (on the lumen side) made in 3D with PLGA, but on a larger scale (**Fig. 5.4**) [48,49]. These results will be recreated on the 3D printed scaffolds within microchannels. We will then modularly assemble 3D printed *in vitro* gut model with molectronic devices for the interrogation of intra- and inter-kingdom signaling events.

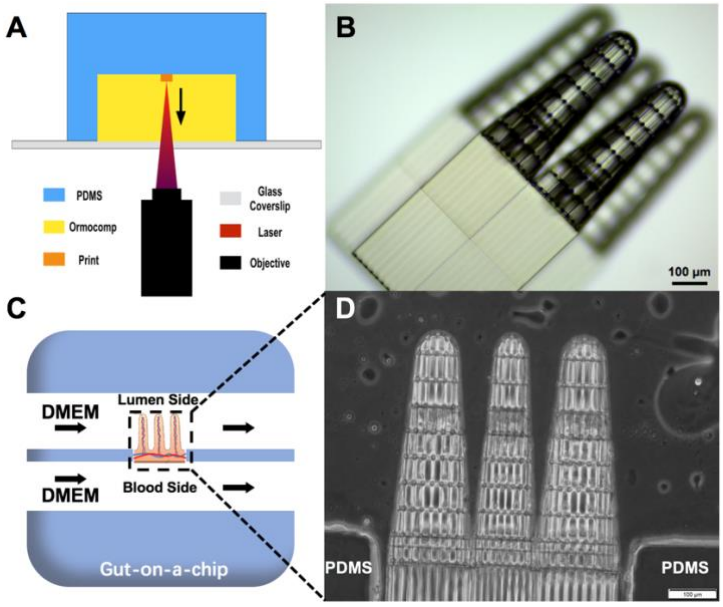

Figure 5. 3. 3D printed villi structure within microdevice. (A) Schematic of *in situ* laser writing within a microchannel. The print starts at the interface between PDMS and Ormocomp^{TM}, a biocompatible printing material. The structure is printed in a top-to-bottom sequence as indicated by the arrow. (B) A bilayered five-villus structure printed on a glass coverslip. (C) Gut-on-a-chip device with 3D villous structure printed in the center that separates two microchannels. (D) A three-villus structure printed in a microchannel.

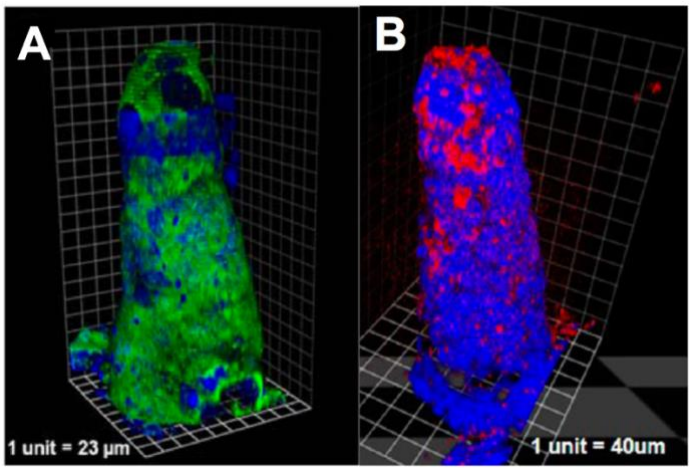

Figure 5. 4. Confocal microscopy of PLGA scaffold cultured for 21 days with (A) model intestinal cell lines (Caco-2 and HT29-MTX) with staining for nuclei (blue) and actin (green); (B) Caco-2 (blue), and 2h with *Salmonella typhimurium* (red). Data adapted from Costello et al, (2014)[48,49]

Successful completion of our work will enrich current OOC systems with molecular functions while minimizing system complexity. Owing to the dynamic and complex nature of the GI tract, which spans fully oxygenated to strictly anaerobic environments, where molecular autoinducers mediate dialogue among bacteria and between bacteria and the human epithelia, and where geometries *in vivo* are difficult to recapitulate *in vitro*, we envision a program that for the first time will enable direct control and interrogation of biological function at the length and time scales of the cells and tissues under study. While the application here focuses on GI tract biology, we envision far greater utility (e.g., diagnostic tools, such as endoscopic devices) and use in other biological systems.

Bibliography

1. Savage, D. C. Microbial Ecology of the Gastrointestinal Tract. *Annu. Rev. Microbiol.* **31,** 107–133 (1977).
2. McCracken, V. J., and Lorenz, R. G. The gastrointestinal ecosystem: a precarious alliance among epithelium, immunity and microbiota. *Microbiolgy* **3,** 1–11 (2001).
3. Camp, J. G., Kanther, M., Semova, I. & Rawls, J. F. Patterns and Scales in Gastrointestinal Microbial Ecology. *Gastroenterology* **136,** 87–92 (2016).
4. Eloe-Fadrosh, E. A. & Rasko, D. A. The Human Microbiome: From Symbiosis to Pathogenesis. *Annu. Rev. Med.* **64,** 145–163 (2013).
5. Schroeder, B. O. & Bäckhed, F. Signals from the gut microbiota to distant organs in physiology and disease. *Nat. Med.* **22,** 1079–1089 (2016).
6. Foster, J. A., Rinaman, L. & Cryan, J. F. Stress & the gut-brain axis: Regulation by the microbiome. *Neurobiol. Stress* **7,** 124–136 (2017).
7. Carabotti, M., Scirocco, A., Maselli, M. A. & Severi, C. The gut-brain axis: Interactions between enteric microbiota, central and enteric nervous systems. *Ann. Gastroenterol.* **28,** 203–209 (2015).
8. Backhed, F., Ley, R. E., Sonnenburg, J. L., Peterson, D. A. & Gordon, J. I. Host-Bacterial Mutualism in the Human Intestine. *Inn. Tube Life* **307,** 1915–1921 (2005).
9. Koropatkin, N. M., Cameron, E. A. & Martens, E. C. How glycan metabolism shapes the human gut microbiota. *Nat Rev Microbiol* **10,** 323–335 (2014).
10. Wensinck, F., Custers-van Lieshout, L. M. C., Poppelaars-Kustermans, P. A. J. & Schröder, A. M. The faecal flora of patients with Crohn's disease. *J. Hyg. (Lond).* **87,** 1–12 (1981).
11. Giaffer, M. H., Holdsworth, C. D. & Duerden, B. I. The Assessment of Fecal Flora in Patients with Inflammatory Bowel-Disease by a Simplified Bacteriological Technique. *J. Med. Microbiol.* **35,** 238–243 (1991).
12. Favier, C., Neut, C., Mizon, C., Cortot, A. & Colombel, J. F. Fecal beta-D-Galactosidase Production and Bi ® dobacteria Are Decreased in Crohn ' s Disease. *Dig. Dis.* **42,** 817–822 (1997).
13. Wei, B. *et al.* Pseudomonas fluorescens Encodes the Crohn' s Disease-Associated I2 Sequence Pseudomonas fluorescens Encodes the Crohn' s Disease-Associated I2 Sequence and T-Cell Superantigen. *Infect. Immun.* **70,** 6567–6575 (2002).
14. Wagner, J. *et al.* Identification and Characterisation of Pseudomonas 16S Ribosomal DNA from Ileal Biopsies of Children with Crohn's Disease. *PLoS One* **3,** (2008).
15. Tamboli, C. P. Dysbiosis in inflammatory bowel disease. *Gut* **53,** 1–4 (2004).
16. Chichlowski, M. & Hale, L. P. Bacterial-mucosal interactions in inflammatory bowel disease--an alliance gone bad. *AJP Gastrointest. Liver Physiol.* **295,** G1139–G1149 (2008).
17. Wong, A. C. N., Vanhove, A. S. & Watnick, P. I. The interplay between intestinal bacteria and host metabolism in health and disease: lessons from *Drosophila melanogaster*. *Dis. Model. Mech.* **9,** 271–281 (2016).

18. Kuhbacher, T. & Fölsch, U. R. Practical guidelines for the treatment of inflammatory bowel disease. *World J. Gastroenterol.* **13,** 1149–55 (2007).
19. McKay, R. *et al. Controlling Localization of E. coli Populations Using a Two-Part Synthetic Motility Circuit: An Accelerator and Brake*. *Biotechnology and Bioengineering* (2017). doi:10.1002/bit.26391
20. Virgile, C. R. *et al.* Engineering bacterial motility towards hydrogen-peroxide. *PLoS One* **13,** 1–21 (2018).
21. Patel, R. & Dupont, H. L. New approaches for bacteriotherapy: Prebiotics, new-generation probiotics, and synbiotics. *Clin. Infect. Dis.* **60,** S108–S121 (2015).
22. Vieira, A. T., Fukumori, C. & Ferreira, C. M. New insights into therapeutic strategies for gut microbiota modulation in inflammatory diseases. *Clin. Transl. Immunol.* **5,** e87 (2016).
23. El Hage, R., Hernandez-Sanabria, E. & Van de Wiele, T. Emerging Trends in "Smart Probiotics": Functional Consideration for the Development of Novel Health and Industrial Applications. *Front. Microbiol.* **8,** 1889 (2017).
24. Fraser, A. G., ORchard, T. P. & Jewell, D. P. The efficacy of azathioprine for the treatment of inflammatory bowel disease: a 30 year review. *Gut* **50,** 485–489 (2002).
25. Noti, M., Corazza, N., Mueller, C., Berger, B. & Brunner, T. TNF suppresses acute intestinal inflammation by inducing local glucocorticoid synthesis. *J. Exp. Med.* **207,** 1057–1066 (2010).
26. Levin, A. D., Wildenberg, M. E. & van den Brink, G. R. Mechanism of Action of Anti-TNF Therapy in Inflammatory Bowel Disease. *J. Crohns. Colitis* **10,** 989–997 (2016).
27. Guarner, F. & Malagelada, J. R. Gut flora in health and disease. *Lancet* **361,** 512–519 (2003).
28. Deriu, E. *et al.* Probiotic Bacteria Reduce Salmonella Typhimurium Intestinal Colonization by Competing for Iron. *Cell Host Microbe* **14,** 26–37 (2013).
29. Wu, H. *et al.* Autonomous bacterial localization and gene expression based on nearby cell receptor density. *Mol. Syst. Biol.* **9,** 636 (2013).
30. Forbes, N. S. Engineering the perfect (bacterial) cancer therapy Neil. *Nat. Rev. Cancer* **10,** 785–794 (2010).
31. Thomas, C. M. & Versalovic, J. Probiotics-host communication: Modulation of signaling pathways in the intestine. *Gut Microbes* **1,** 148–163 (2010).
32. Quigley, E. M. M. & Flourie, B. Probiotics and irritable bowel syndrome: a rationale for their use and an assessment of the evidence to date. *Neurogastroenterol. Motil.* **19,** 166–172 (2007).
33. Jucker, M. The benefits and limitations of animal models for translational research in neurodegenerative diseases. *Nat. Med.* **16,** 1210–1214 (2010).
34. Moraes, C., Mehta, G., Lesher-Perez, S. C. & Takayama, S. Organs-on-a-Chip: A focus on compartmentalized microdevices. *Ann. Biomed. Eng.* **40,** 1211–1227 (2012).
35. Gavhane, Y. N. & Yadav, A. V. Loss of orally administered drugs in GI tract. *Saudi Pharm. J.* **20,** 331–344 (2012).

36. Villenave, R. *et al.* Human Gut-On-A-Chip Supports Polarized Infection of Coxsackie B1 Virus In Vitro. *PLoS One* **12,** e0169412 (2017).
37. Kim, H. J., Huh, D., Hamilton, G. & Ingber, D. E. Human gut-on-a-chip inhabited by microbial flora that experiences intestinal peristalsis-like motions and flow. *Lab Chip* **12,** 2165 (2012).
38. Tottey, W. *et al.* The Human Gut Chip ‘“ HuGChip ”’, an Explorative Phylogenetic Microarray for Determining Gut Microbiome Diversity at Family Level. *PLoS One* **8,** 1–12 (2013).
39. Kim, H. J., Lee, J., Choi, J.-H., Bahinski, A. & Ingber, D. E. Co-culture of Living Microbiome with Microengineered Human Intestinal Villi in a Gut-on-a-Chip Microfluidic Device. *J. Vis. Exp.* **114,** e54344 | (2016).
40. Kim, H. J., Li, H., Collins, J. J. & Ingber, D. E. Contributions of microbiome and mechanical deformation to intestinal bacterial overgrowth and inflammation in a human gut-on-a-chip. *PNAS* **113,** E7-15 (2015).
41. Shah, P. *et al.* A microfluidics-based in vitro model of the gastrointestinal human–microbe interface. *Nat. Commun.* **7,** 11535 (2016).
42. Gong, J. & Yang, C. Advances in the methods for studying gut microbiota and their relevance to the research of dietary fi ber functions. *Food Res. Int.* **48,** 916–929 (2012).
43. Abbeele, P. Van Den *et al.* Butyrate-producing Clostridium cluster XIVa species specifically colonize mucins in an in vitro gut model. *ISME J.* **7,** 949–961 (2012).
44. Choe, A., Ha, S. K., Choi, I. & Choi, N. Microfluidic Gut-liver chip for reproducing the first pass metabolism. *Biomed. Microdevices* **19,** 1–11 (2017).
45. Von Martels, J. Z. H. *et al.* The role of gut microbiota in health and disease : In vitro modeling of host-microbe interactions at the aerobe-anaerobe interphase of the human gut. *Anaerobe* **44,** 3–12 (2017).
46. Lim, S. M. *et al.* Improved biological half-life and anti-tumor activity of TNF-related apoptosis-inducing ligand (TRAIL) using PEG-exposed nanoparticles. *Biomaterials* **32,** 3538–3546 (2011).
47. Sung, J. H. *et al.* Microfabricated mammalian organ systems and their integration into models of whole animals and humans. *Lab Chip* **13,** 1201–1212 (2013).
48. Costello, C. M. *et al.* Synthetic small intestinal scaffolds for improved studies of intestinal differentiation. *Biotechnol. Bioeng.* **111,** 1222–1232 (2014).
49. Costello, C. M. *et al.* 3-D Intestinal Scaffolds for Evaluating the Therapeutic Potential of Probiotics. *Mol. Pharm.* **11,** 2030–2039 (2014).
50. Yu, J., Peng, S., Luo, D. & March, J. C. In vitro 3D human small intestinal villous model for drug permeability determination. *Biotechnol. Bioeng.* **109,** 2173–2178 (2012).
51. Yu, J., Carrier, R. L., March, J. C. & Griffith, L. G. Three dimensional human small intestine models for ADME-Tox studies. *Drug Discov. Today* **19,** 1587–1594 (2014).
52. Liu, Y. *et al.* Connecting Biology to Electronics: Molecular Communication via Redox Modality. *Adv. Healthc. Mater.* 1700789 (2017). doi:10.1002/adhm.201700789

53. Kim, E. *et al.* Chitosan to Connect Biology to Electronics: Fabricating the Bio-Device Interface and Communicating Across This Interface. *Polymers (Basel).* **7,** 1–46 (2014).
54. Kim, E., Liu, Y., Bentley, W. E. & Payne, G. F. Redox capacitor to establish bio-device redox-connectivity. *Adv. Funct. Mater.* **22,** 1409–1416 (2012).
55. Kim, E., Gordonov, T., Liu, Y., Bentley, W. E. & Payne, G. F. Reverse engineering to suggest biologically relevant redox activities of phenolic materials. *ACS Chem. Biol.* **8,** 716–724 (2013).
56. Kim, E. *et al.* Redox-capacitor to connect electrochemistry to redox-biology. *Analyst* **139,** 32–43 (2014).
57. Liba, B. D. *et al.* Biofabricated film with enzymatic and redox-capacitor functionalities to harvest and store electrons. *Biofabrication* **5,** 015008 (2013).
58. Kim, E., Gordonov, T., Bentley, W. E. & Payne, G. F. Amplified and in situ detection of redox-active metabolite using a biobased redox capacitor. *Anal. Chem.* **85,** 2102–2108 (2013).
59. Liu, Y., Kim, E., White, I. M., Bentley, W. E. & Payne, G. F. Information processing through a bio-based redox capacitor : Signatures for redox-cycling. *Bioelectrochemistry* **98,** 94–102 (2014).
60. Kim, E. *et al.* Redox-capacitor to connect electrochemistry to redox-biology. *Analyst* **139,** 32–43 (2014).
61. Bull, M. J. & Plummer, N. T. Part 1: The Human Gut Microbiome in Health and Disease. *Integr. Med. (Encinitas).* **13,** 17–22 (2014).
62. Shreiner, A. B., Kao, J. Y. & Young, V. B. The gut microbiome in health and in disease. *Curr Opin Gastroenterol.* **31,** 69–75 (2016).
63. Sung, J. H., Kam, C. & Shuler, M. L. A microfluidic device for a pharmacokinetic-pharmacodynamic (PK-PD) model on a chip. *Lab Chip* **10,** 446–455 (2010).
64. Kim, H. J. & Ingber, D. E. Gut-on-a-Chip microenvironment induces human intestinal cells to undergo villus differentiation. *Integr. Biol.* **5,** 1130–1140 (2013).
65. Bhatia, S. N. & Ingber, D. E. Microfluidic organs-on-chips. *Nat. Biotechnol.* **32,** 760–772 (2014).
66. Gunther, A. *et al.* A microfluidic platform for probing small artery structure and function. *Lab Chip* **10,** 2341–2349 (2010).
67. Wang, Z., Samanipour, R., Koo, K. & Kim, K. Organ-on-a-Chip Platforms for Drug Delivery and Cell Characterization : A Review. *Sensors Mater.* **27,** 487–506 (2015).
68. An, F., Qu, Y., Liu, X., Zhong, R. & Luo, Y. Organ-on-a-Chip : New Platform for Biological Analysis. 39–45 (2015). doi:10.4137/ACI.S28905.TYPE
69. Kimura, H., Yamamoto, T., Sakai, H., Sakai, Y. & Fujii, T. An integrated microfluidic system for long-term perfusion culture and on-line monitoring of intestinal tissue models. *Lab Chip* **8,** 741–6 (2008).
70. Gao, Y., Sun, J., Lin, W.-H., Webb, D. & Li, D. A compact microfluidic gradient generator using passive pumping. *Microfluid. Nanofluidics* **12,** 887–895 (2012).

71. Toh, A. G. G., Wang, Z. P., Yang, C. & Nguyen, N. T. Engineering microfluidic concentration gradient generators for biological applications. *Microfluidics and Nanofluidics* **16,** 1–18 (2014).
72. Weltin, A. *et al.* Cell culture monitoring for drug screening and cancer research: a transparent, microfluidic, multi-sensor microsystem. *Lab Chip* **14,** 138–146 (2014).
73. Luo, X., Vo, T., Jambi, F., Pham, P. & Choy, J. S. Microfluidic partition with in situ biofabricated semipermeable biopolymer membranes for static gradient generation. *Lab Chip* **16,** 3815–3823 (2016).
74. Sanderson, J. *et al.* High-throughput clone library analysis of the mucosa-associated microbiota reveals dysbiosis and differences between inflamed and non-inflamed regions of the intestine in inflammatory bowel disease. *BMC Microbiol.* **11,** 7 (2011).
75. Rajilic-Stojanovic, M. *et al.* Development and application of the human intestinal tract chip , a phylogenetic microarray : analysis of universally conserved phylotypes in the abundant microbiota of young and elderly adults. *Environ. Microbiol.* **11,** 1736–1751 (2009).
76. Perkel, J. M. The Internet of Things comes to the lab. *Nature* **542,** 125–126 (2017).
77. Gibney, E. The inside story on wearable electronics. *Nature* **528,** 26–28 (2015).
78. Deep, A., Chaudhary, U. & Gupta, V. Quorum sensing and bacterial pathogenicity: From molecules to disease. *J. Lab. Physicians* **3,** 4 (2011).
79. de Kievit, T. R., Iglewski, B. H., Kievit, T. R. De & Teresa, R. MINIREVIEW Bacterial Quorum Sensing in Pathogenic Relationships. *Infect. Immun.* **68,** 4839–4849 (2000).
80. Duan, F. & March, J. C. Engineered bacterial communication prevents Vibrio cholerae virulence in an infant mouse model. *PNAS* **107,** 1001294107 (2010).
81. Tschirhart, T. *et al.* Electronic control of gene expression and cell behavior in Escherichia coli through redox signaling. *Nat. Commun.* **8,** 14030 (2017).
82. Tschirhart, T. *et al.* Electrochemical Measurement of the β-Galactosidase Reporter from Live Cells: A Comparison to the Miller Assay. *ACS Synth. Biol.* **5,** 28–35 (2015).
83. Aurand, T. C. & March, J. C. Development of a Synthetic Receptor Protein for Sensing Inflammatory Mediators Interferon- g and Tumor Necrosis Factor- a. *Biotechnol. Bioeng.* **113,** 492–500 (2016).
84. Liu, Y. *et al.* Using a Redox Modality to Connect Synthetic Biology to Electronics : Hydrogel-Based Chemo-Electro Signal Transduction for Molecular Communication. *Adv. Healthc. Mater.* **6,** 1600908 (2017).
85. Meyer, W. L. *et al.* Chitosan-coated wires: Conferring electrical properties to chitosan fibers. *Biomacromolecules* **10,** 858–864 (2009).
86. Park, J. J. *et al.* Chitosan-mediated in situ biomolecule assembly in completely packaged microfluidic devices. *Lab Chip* **6,** 1315–1321 (2006).
87. Wang, Y. *et al.* Coupling electrodeposition with layer-by-layer assembly to address proteins within microfluidic channels. *Adv. Mater.* **23,** 5817–5821 (2011).

88. Gray, K. M. *et al.* Electrodeposition of a biopolymeric hydrogel: Potential for one-step protein electroaddressing. *Biomacromolecules* **13,** 1181–1189 (2012).
89. Cheng, Y. *et al.* Biocompatible multi-address 3D cell assembly in microfluidic devices using spatially programmable gel formation. *Lab Chip* **11,** 2316–2318 (2011).
90. Betz, J. F. *et al.* Optically clear alginate hydrogels for spatially controlled cell entrapment and culture at microfluidic electrode surfaces. *Lab Chip* **13,** 1854–8 (2013).
91. Servant, G. *et al.* Polarization of Chemoattractant Receptor Signaling During Neutrophil Chemotaxis. *Science (80-.).* **287,** 1037–1040 (2000).
92. Lin, F. *et al.* Neutrophil migration in opposing chemoattractant gradients using microfluidic chemotaxis devices. *Ann. Biomed. Eng.* **33,** 475–482 (2005).
93. Friedl, P. & Weigelin, B. Interstitial leukocyte migration and immune function. *Nat. Immunol.* **9,** 960–969 (2008).
94. O'Hayre, M., Salanga, C. L., Handel, T. M. & Allen, S. J. Chemokines and cancer : migration , intracellular signalling and intercellular communication in the microenvironment. *Biochem. J.* **409,** 635–649 (2008).
95. Yang, J. & Weinberg, R. A. Review Epithelial-Mesenchymal Transition : At the Crossroads of Development and Tumor Metastasis. *Cell Press* **14,** 818–829 (2008).
96. Stewart, P. S. & Franklin, M. J. Physiological heterogeneity in biofilms. *Nat. Rev. Microbiol.* **6,** 199–210 (2008).
97. Solano, C., Echeverz, M. & Lasa, I. Biofilm dispersion and quorum sensing. *Curr. Opin. Microbiol.* **18,** 96–104 (2014).
98. Diao, J. *et al.* A three-channel microfluidic device for generating static linear gradients and its application to the quantitative analysis of bacterial chemotaxis. *Lab Chip* **6,** 381–388 (2006).
99. Boyden, B. S. THE CHEMOTACTIC E F F E C T OF MIXTURES OF ANTIBODY AND ANTIGEN ON POLYMORPHONUCLEAR LEUCOCYTES (From the Department of Experimental Pathology , John Curtin School of Medical Research , Australian National University , Canberra) Materials and Methods. *J. Exp. Med.* 453–466 (1962).
100. Zicha, D., Dunn, G. A. & Brown, A. F. A new direct-viewing chemotaxis chamber. *J. Cell Sci.* **99,** 769–75 (1991).
101. Zigmond, S. H. ABILITY OF P O L Y M O R P H O N U C L E A R LEUKOCYTES TO ~ ' co ~ er slip t FmURE 1 Chamber used for visual assay . *J. Cell Biol.* **75,** 606–616 (1977).
102. Keenan, T. M., Hsu, C.-H. & Folch, A. Microfluidic "jets" for generating steady-state gradients of soluble molecules on open surfaces. *Appl. Phys. Lett.* **89,** 114103 (2006).
103. Amadi, O. C. *et al.* A low resistance microfluidic system for the creation of stable concentration gradients in a defined 3D microenvironment. *Biomed. Microdevices* **12,** 1027–1041 (2010).
104. Shin, Y. *et al.* Microfluidic assay for simultaneous culture of multiple cell types on surfaces or within hydrogels. *Nat. Protoc.* **7,** 1247–59 (2012).

105. Huang, Y., Agrawal, B., Sun, D., Kuo, J. S. & Williams, J. C. Microfluidics-based devices: New tools for studying cancer and cancer stem cell migration. *Biomicrofluidics* **5,** 013412 (2011).
106. Stroka, K. M. *et al.* Water permeation drives tumor cell migration in confined microenvironments. *Cell* **157,** 611–623 (2014).
107. Whitesides, G. M. The origins and the future of microfluidics. *Nature* **442,** 368–73 (2006).
108. Jeon, N. L. *et al.* Neutrophil chemotaxis in linear and complex gradients of interleukin-8 formed in a microfabricated device. *Nat. Biotechnol.* **20,** 826–830 (2002).
109. Mao, H., Cremer, P. S. & Manson, M. D. A sensitive , versatile microfluidic assay for bacterial chemotaxis. *j* **100,** 5449–5454 (2003).
110. Irimia, D. & Toner, M. Cell handling using microstructured membranes. *m* **6,** 345–352 (2006).
111. Saadi, W., Wang, S., Francis, L. & Jeon, N. L. A parallel-gradient microfluidic chamber for quantitative analysis of breast cancer cell chemotaxis. *Biomed Microdevices* **8,** 109–118 (2006).
112. Englert, D. L., Manson, M. D. & Jayaraman, A. A Microfluidic Device for Quantifying Bacterial Chemotaxis in Stable Concentration Gradients made by replica molding of PDMS from SU-8 master . *JOVE* **38,** e1779 (2010).
113. Seymour, J. R., Macros & Stocker, R. Resource Patch Formation and Exploitation throughout the. *Am. Nat.* **173,** 15–29 (2009).
114. Ahmed, T., Shimizu, T. S. & Stocker, R. Microfluidics for bacterial chemotaxis. *Integr. Biol.* **2,** 604 (2010).
115. Kim, K. P. *et al.* In situ monitoring of antibiotic susceptibility of bacterial biofilms in a microfluidic device. *Lab Chip* **10,** 3296–3299 (2010).
116. Cheng, S.-Y. *et al.* A hydrogel-based microfluidic device for the studies of directed cell migration. *Lab Chip* **7,** 763–769 (2007).
117. Zhang, C. *et al.* A sensitive chemotaxis assay using a novel microfluidic device. *Biomed Res. Int.* **2013,** (2013).
118. García, S. *et al.* Generation of stable orthogonal gradients of chemical concentration and substrate stiffness in a microfluidic device. *Lab Chip* **15,** 2606–2614 (2015).
119. Abhyankar, V. V, Lokuta, M. a, Huttenlocher, A. & Beebe, D. J. Characterization of a membrane-based gradient generator for use in cell-signaling studies. *Lab Chip* **6,** 389–93 (2006).
120. Kim, T., Pinelis, M. & Maharbiz, M. M. Generating steep, shear-free gradients of small molecules for cell culture. *Biomed. Microdevices* **11,** 65–73 (2009).
121. Mosadegh, B. *et al.* Uniform cell seeding and generation of overlapping gradient profiles in a multiplexed microchamber device with normally-closed valves. *Lab Chip* **10,** 2959–64 (2010).
122. Cate, D. M., Sip, C. G. & Folch, A. A microfluidic platform for generation of sharp gradients in open-access culture. *Biomicrofluidics* **4,** 44105 (2010).
123. Sip, C., Nirveek, B. & Albert, F. Microfluidic transwell inserts for generation of tissue culture-friendly gradients in well plates. *Lab Chip* **14,** 302–314 (2015).

124. Ahmed, T., Shimizu, T. S. & Stocker, R. Bacterial Chemotaxis in Linear and Nonlinear Steady Microfluidic Gradients. *Nano Lett.* **10,** 3379–3385 (2010).
125. Mohari, B. *et al.* Novel pseudotaxis mechanisms improve migration of straight- swimming bacterial mutants through a porous environment. *MBio* **6,** 1–12 (2015).
126. Irimia, D., Charras, G., Agrawal, N., Mitchison, T. & Toner, M. Polar stimulation and constrained cell migration in microfluidic channels. *Lab Chip* **7,** 1783–1790 (2007).
127. Adler, J., Hazelbauer, G. L. & Dahl, M. M. Chemotaxis toward sugars in *Escherichia coli*. *J. Bacteriol.* **115,** 824–847 (1973).
128. Yan, J., Pedrosa, V. A., Enomoto, J. & Simonian, A. L. Electrochemical biosensors for on-chip detection of oxidative stress from immune cells. *Biomicrofluidics* **5,** 1–11 (2011).
129. Dumitrescu, I., Yancey, D. F. & Crooks, R. M. Dual-electrode microfluidic cell for characterizing electrocatalysts. *Lab Chip* **12,** 986 (2012).
130. Luka, G. *et al.* Microfluidics integrated biosensors: A leading technology towards lab-on-A-chip and sensing applications. *Sensors (Switzerland)* **15,** 30011–30031 (2015).
131. Li, Q. & Yuan, Y. J. Application of vertical electrodes in microfluidic channels for impedance analysis. *Micromachines* **7,** (2016).
132. Lee, G. H. *et al.* Single Microfluidic Electrochemical Sensor System for Simultaneous Multi-Pulmonary Hypertension Biomarker Analyses. *Sci. Rep.* **7,** 1–8 (2017).
133. Shin, S. R. *et al.* Aptamer-Based Microfluidic Electrochemical Biosensor for Monitoring Cell-Secreted Trace Cardiac Biomarkers. *Anal. Chem.* **88,** 10019–10027 (2016).
134. Bavli, D. *et al.* Real-time monitoring of metabolic function in liver-on- chip microdevices tracks the dynamics of mitochondrial dysfunction. *PNAS* **113,** E2231-2240 (2016).
135. Zhang, Y. S. *et al.* Multisensor-integrated organs-on-chips platform for automated and continual in situ monitoring of organoid behaviors. *Proc. Natl. Acad. Sci.* **114,** E2293–E2302 (2017).
136. Ali, M. A. *et al.* Highly efficient bienzyme functionalized nanocomposite-based microfluidics biosensor platform for biomedical application. *Sci. Rep.* **3,** 1–9 (2013).
137. Esteves-Villanueva, J. O., Trzeciakiewicz, H. & Martic, S. A protein-based electrochemical biosensor for detection of tau protein, a neurodegenerative disease biomarker. *Analyst* **139,** 2823–31 (2014).
138. Wu, L. Q. & Payne, G. F. Biofabrication: Using biological materials and biocatalysts to construct nanostructured assemblies. *Trends Biotechnol.* **22,** 593–599 (2004).
139. Yi, H. *et al.* Signal-Directed Sequential Assembly of Biomolecules on Patterned Surfaces. *Langmuir* **21,** 2104–2107 (2005).
140. Park, J. J., Luo, X., Yi, H., Ghodssi, R. & Rubloff, G. W. In situ biomolecule assembly and activity within completely packaged microfluidic devices. *Lab Chip* **1,** 1315–1321 (2006).

141. Liu, Y. *et al.* Biofabrication to build the biology – device. *Biofabrication* **2,** 022002 (2010).
142. Koev, S. T. *et al.* Chitosan : an integrative biomaterial for lab-on-a-chip devices. *Lab Chip* **10,** 3026–3042 (2010).
143. Wu, L. Q. *et al.* Voltage-dependent assembly of the polysaccharide chitosan onto an electrode surface. *Langmuir* **18,** 8620–8625 (2002).
144. Redepenning, J., Venkataraman, G., Chen, J. & Stafford, N. Electrochemical preparation of chitosan/hydroxyapatite composite coatings on titanium substrates. *J. Biomed. Mater. Res.* **66A,** 411–416 (2003).
145. Ladet, S., David, L. & Domard, A. Multi-membrane hydrogels. *Nature* **452,** 76–79 (2008).
146. Cheng, Y. *et al.* In situ quantitative visualization and characterization of chitosan electrodeposition with paired sidewall electrodes. *Soft Matter* **6,** 3177 (2010).
147. Wu, L. Q., Ghodssi, R., Elabd, Y. A. & Payne, G. F. Biomimetic pattern transfer. *Adv. Funct. Mater.* **15,** 189–195 (2005).
148. Wu, L. Q., McDermott, M. K., Zhu, C., Ghodssi, R. & Payne, G. F. Mimicking biological phenol reaction cascades to confer mechanical function. *Adv. Funct. Mater.* **16,** 1967–1974 (2006).
149. Kim, E. *et al.* Biomimetic Approach to Confer Redox Activity to Thin Chitosan Films. *Adv. Funct. Mater.* **20,** 2683–2694 (2010).
150. Luo, X. *et al.* Programmable assembly of a metabolic pathway enzyme in a pre-packaged reusable bioMEMS device. *Lab Chip* **8,** 420 (2008).
151. Lau, G. W., Hassett, D. J., Ran, H. & Kong, F. The role of pyocyanin in Pseudomonas aeruginosa infection. *Trends Mol. Med.* **10,** 599–606 (2004).
152. Jacob, C., Jamier, V. & Ba, L. A. Redox active secondary metabolites. *Curr. Opin. Chem. Biol.* **15,** 149–155 (2011).
153. Okegbe, C., Sakhtah, H., Sekedat, M. D., Price-Whelan, A. & Dietrich, L. E. P. Redox Eustress: Roles for Redox-Active Metabolites in Bacterial Signaling and Behavior. *Antioxid. Redox Signal.* **16,** 658–667 (2012).
154. Racher, A. J., Looby, D. & Griffiths, J. B. Use of lactate dehydrogenase release to assess changes in culture viability. *Cytotechnology* **3,** 301–307 (1990).
155. Haslam, G., Wyatt, D. & Kitos, P. A. Estimating the number of viable animal cells in multi-well cultures based on their lactate dehydrogenase activities. *Cytotechnology* **32,** 63–75 (2000).
156. Wolterbeek, H. T. & van der Meer, A. J. G. M. Optimization, application, and interpretation of lactate dehydrogenase measurements in microwell determination of cell number and toxicity. *Assay Drug Dev. Technol.* **3,** 675–682 (2005).
157. Bosetti, M. *et al.* Cell behaviour on phospholipids-coated surfaces. *J. Mater. Sci. Mater. Med.* **18,** 611–617 (2007).
158. Soares-Bezerra, R. J. *et al.* An improved method for P2X7R antagonist screening. *PLoS One* **10,** (2015).
159. Liu, Z., Liu, Y., Kim, E., Bentley, W. E. & Payne, G. F. Electrochemical Probing through a Redox Capacitor To Acquire Chemical Information on Biothiols. *Anal. Chem.* **88,** 7213–7221 (2016).

160. Kim, E. *et al.* Redox-cycling and H2O2generation by fabricated catecholic films in the absence of enzymes. *Biomacromolecules* **12,** 880–888 (2011).
161. Rathee, K., Dhull, V., Dhull, R. & Singh, S. Biosensors based on electrochemical lactate detection : A comprehensive review. *Biochem. Biophys. Reports* **5,** 35–54 (2016).
162. Decker, T. & Lohmann-Matthes, M.-L. A quick and simple method for the quantitation of lactate dehydrogenase release in measurements of cellular cytotoxicity and tumor necrosis factor (TNF) activity. *J. Immunol. Methods* **115,** 61–69 (1988).
163. Borner, M. M. *et al.* The detergent Triton X-100 induces a death pattern in human carcinoma cell lines that resembles cytotoxic lymphocyte-induced apoptosis. *FEBS Lett.* **353,** 129–132 (1994).
164. Meunier, V., Bourrie, M., Berger, Y. & Fabre, G. The human intestinal epithelial cell line Caco-2; pharmacological and pharmacokinetic applications. *Cell Biol. Toxicol.* **11,** 187–194 (1995).
165. Borchardt, R. T. Hidalgo, I. J., Raub, T. J., and Borchardt, R. T.: Characterization of the Human Colon Carcinoma Cell Line (Caco-2) as a Model System for Intestinal Epithelial Permeability, Gastroenterology, 96, 736–749, 1989—The Backstory. *AAPS J.* **13,** 323–327 (2011).
166. Oleaga, C. *et al.* Multi-Organ toxicity demonstration in a functional human in vitro system composed of four organs. *Sci. Rep.* **6,** 20030 (2016).
167. Zheng, F. *et al.* Organ-on-a-Chip Systems : Microengineering to Biomimic Living Systems. *Biomaterials* **12,** 2253–2282 (2016).
168. Damiati, S., Kompella, U., Damiati, S. & Kodzius, R. Microfluidic Devices for Drug Delivery Systems and Drug Screening. *Genes (Basel).* **9,** 103 (2018).
169. Zervantonakis, I. K. *et al.* Three-dimensional microfluidic model for tumor cell intravasation and endothelial barrier function. *PNAS* **109,** 13515–20 (2012).
170. Pagano, G. *et al.* Optimizing design and fabrication of microfluidic devices for cell cultures: An effective approach to control cell microenvironment in three dimensions. *Biomicrofluidics* **8,** (2014).
171. Zhang, B. *et al.* Biodegradable scaffold with built-in vasculature for organ-on-a-chip engineering and direct surgical anastomosis. *Nat. Mater.* **15,** 669–680 (2016).
172. Chi, M., Yi, B., Oh, S., Park, D. & Sung, J. H. A microfluidic cell culture device (μFCCD) to culture epithelial cells with physiological and morphological properties that mimic those of the human intestine. *Biomed Microdevices* **17,** 58 (2015).
173. Douville, N. J. *et al.* Fabrication of Two-Layered Channel System with Embedded Electrodes to Measure Resistance Across Epithelial and Endothelial Barriers. *Anal. Chem.* **82,** 2505–2511 (2010).
174. Nguyen, T. A., Yin, T., Reyes, D. & Urban, G. A. Micro fluidic Chip with Integrated Electrical Cell-Impedance Sensing for Monitoring Single Cancer Cell Migration in Three-Dimensional Matrixes. *Anal. Chem.* **85,** 11068–11076 (2013).

175. Liu, M. *et al.* Electrofluidic pressure sensor embedded microfluidic device: a study of endothelial cells under hydrostatic pressure and shear stress combinations. *Lab Chip* **13,** 1743–1753 (2013).
176. Kieninger, J., Aravindalochanan, K., Sandvik, J. A., Pettersen, E. O. & Urban, G. A. Pericellular oxygen monitoring with integrated sensor chips for reproducible cell culture experiments. *Cell Prolif.* **47,** 180–188 (2014).
177. Weltin, A. *et al.* Cell culture monitoring for drug screening and cancer research: a transparent, microfluidic, multi-sensor microsystem. *Lab Chip* **14,** 138–146 (2014).
178. Weltin, A. *et al.* Polymer-based , flexible glutamate and lactate microsensors for in vivo applications. *Biosens. Bioelectron.* **61,** 192–199 (2014).
179. Lima, E. *et al.* Multichamber Multipotentiostat System for Cellular Microphysiometry. *Sensors Actuators B Chem.* **204,** 536–543 (2014).
180. Eklund, S. E. *et al.* Metabolic Discrimination of Select List Agents by Monitoring Cellular Responses in a Multianalyte Microphysiometer. *Sensors* **9,** 2117–2133 (2009).
181. Weltin, A., Kieninger, J. & Urban, G. A. Microfabricated, amperometric, enzyme-based biosensors for in vivo applications. *Anal. Bioanal. Chem.* **408,** 4503–4521 (2016).
182. Weltin, A. *et al.* Biosensors and Bioelectronics Accessing 3D microtissue metabolism : Lactate and oxygen monitoring in hepatocyte spheroids. *Biosens. Bioelectron.* **87,** 941–948 (2017).
183. Kim, E. *et al.* Redox Probing for Chemical Information of Oxidative Stress. *Anal. Chem.* **89,** 1583–1592 (2017).
184. Cruz, H. J., Rosa, C. C. & Oliva, A. G. Immunosensors for diagnostic applications. *Parasitol. Res.* **88,** 4–7 (2002).
185. Ogi, H. *et al.* Nonspecific-adsorption behavior of polyethylenglycol and bovine serum albumin studied by 55-MHz wireless-electrodeless quartz crystal microbalance. *Biosens. Bioelectron.* **24,** 3148–3152 (2009).
186. Lao, M. & Toth, D. Effects of Ammonium and Lactate on Growth and Metabolism of a recombinant chinese hamster ovary cell culture. *Biotechnol. Prog* **13,** 688–691 (1997).
187. Lampe, K. J., Namba, R. M., Silverman, T. R. & Bjugstad, K. B. Impact of Lactic Acid on Cell Proliferation and Free Radical Induced Cell Death in Monolayer Cultures of Neural Precursor Cells. *Biotechnol. Bioeng.* **103,** 1214–1223 (2010).
188. Li, J., Wong, C. L., Vijayasankaran, N., Hudson, T. & Amanullah, A. Feeding lactate for CHO cell culture processes: Impact on culture metabolism and performance. *Biotechnol. Bioeng.* **109,** 1173–1186 (2012).
189. Matsuki, T. *et al.* Epithelial Cell Proliferation Arrest Induced by Lactate and Acetate from Lactobacillus casei and Bifidobacterium breve. *PLoS One* **8,** 2–9 (2013).
190. de Oliveira, D. *et al.* Catechol cytotoxicity in vitro: Induction of glioblastoma cell death by apoptosis. *Hum. Exp. Toxicol.* **29,** 199–212 (2010).

191. Schweigert, N., Zehnder, A. J. B. & Eggen, R. I. L. Chemical properties of catechols and their molecular modes of toxic action in cells, from microorganisms to mammals. *Environ. Microbiol.* **3,** 81–91 (2001).
192. Winkler, T. E. *et al.* Electrochemical study of the catechol-modified chitosan system for clozapine treatment monitoring. *Langmuir* **30,** 14686–14693 (2014).
193. Rover, L. *et al.* Study of NADH stability using ultraviolet-visible spectrophotometric analysis and factorial design. *Anal. Biochem.* **260,** 50–55 (1998).
194. Haumeil, J. C. C. & Rnaud, P. A. Evaluation of the Cytotoxicity Effect of Dimethyl Sulfoxide (DMSO) on Caco2 / TC7 Colon Tumor Cell Cultures. *Biol. Pharm. Bull.* **25,** 1600–1603 (2002).
195. Aurand, T. C., Russell, M. S. & March, J. C. Synthetic signaling networks for therapeutic applications. *Curr. Opin. Biotechnol.* **23,** 773–779 (2012).
196. Kanthakumar, K. *et al.* Mechanisms of action of Pseudomonas aeruginosa pyocyanin on human ciliary beat in vitro. *Infect. Immun.* **61,** 2848–2853 (1993).
197. Hebert, C. G. *et al.* Biological Nanofactories Target and Modulating Bacterial Quorum Sensing. *ACS NA* **4,** 6923–6931 (2010).
198. Zargar, A. *et al.* Bacterial Secretions of Nonpathogenic Escherichia coli Elicit Inflammatory Pathways : a Closer Investigation of Interkingdom. *MBio* **6,** 1–10 (2015).
199. Koyama, S. & Podolsky, D. K. Rapid Publication Differential Expression of Transforming Growth Factors a and ft in Rat Intestinal Epithelial Cells. *J Clin Invest* **83,** 1768–1773 (1989).
200. Ward, J. B. J., Keely, S. J. & Keely, S. J. Oxygen in the regulation of intestinal epithelial transport. *J Physiol* **12,** 2473–2489 (2014).